5-7-2005

CORRECTION OF TRANSIENT SOLID-EMBEDDED THERMOCOUPLE DATA WITH APPLICATION TO INVERSE HEAT CONDUCTION

August N.F. Johnson

Follow this and additional works at: https://scholarsjunction.msstate.edu/td

CORRECTION OF TRANSIENT SOLID-EMBEDDED THERMOCOUPLE DATA

WITH APPLICATION TO INVERSE HEAT CONDUCTION

By

August Nathan Fletcher Johnson

A Thesis
Submitted to the Faculty of
Mississippi State University
in Partial Fulfillment of the Requirements
for the Degree of Master of Science
in Mechanical Engineering
in the Department of Mechanical Engineering

Mississippi State, Mississippi

May 2005

Copyright by

August Nathan Fletcher Johnson

2005

CORRECTION OF TRANSIENT SOLID-EMBEDDED THERMOCOUPLE DATA

WITH APPLICATION TO INVERSE HEAT CONDUCTION

By

August Nathan Fletcher Johnson

Approved:

_____   _____
Rogelio Luck   John T. Berry
Associate Professor of Mechanical   Professor of Mechanical Engineering
Engineering   (Committee Member)
(Director of Thesis)

_____   _____
Steven R. Daniewicz   Kirk H. Schulz
Professor of Mechanical Engineering   Dean of the College of Engineering
and Director of Graduate Studies in
Mechanical Engineering
(Committee Member)

Name: August Nathan Fletcher Johnson

Date of Degree: May 7, 2005

Institution: Mississippi State University

Major Field: Mechanical Engineering

Major Professor: Dr. Rogelio Luck

Title of Study: CORRECTION OF TRANSIENT SOLID-EMBEDDED THERMOCOUPLE DATA WITH APPLICATION TO INVERSE HEAT CONDUCTION

Pages in Study: 135

Candidate for Degree of Master of Science

The current research investigates the use of solid-embedded thermocouples for determining accurate transient temperature measurements within a solid medium, with emphasis on measurements intended for use in inverse heat conduction problems. Metal casting experiments have been conducted to collect internal mold temperatures to be used, through inverse conduction methods, to estimate the heat exchange between a casting and mold. Inverse conduction methods require accurate temperature measurements for valid boundary estimates. Therefore, various sources of thermocouple measurement uncertainty are examined and some suggestions for uncertainty reduction are presented. Thermocouple installation induced bias uncertainties in experimental temperature data are dynamically corrected through the development and implementation of an embedded thermocouple correction (ETC) transfer function. Comparisons of experimental data to dynamically adjusted data, as well as the inverse conduction estimates for heat flux from each data set, are presented and discussed.

DEDICATION

I would like to dedicate this research to my family, who raised me to know that…

I can do all things through Christ which strengtheneth me.

- Philippians 4:13

ACKNOWLEDGEMENTS

TABLE OF CONTENTS

LIST OF TABLES

LIST OF FIGURES

ABBREVIATIONS, NOMENCLATURE, AND SYMBOLS

Abbreviations

RTD	Resistance Temperature Device
IHC	Inverse Heat Conduction
IHTC	Interface Heat Transfer Coefficient
B.C.	Boundary Condition
I.C.	Initial Condition
DAQ	Data Acquisition
MSU	Mississippi State University
PC	Personal Computer
ETC	Embedded Thermocouple Correction
TF	Transfer Function
C.V.	Control Volume
K	Kelvin (Temperature)

Nomenclature and Symbols

k	Thermal Conductivity (generic)
ρ	Density (generic)
c	Specific Heat (generic)
α	Thermal Diffusivity (generic)
T	Temperature (generic)

t	Time (generic)
x	Spatial Coordinate (generic)
q	Heat Flux (generic)
Q	Heat Flux (Laplace domain)
T_u	Undisturbed Temperature
$G_u(s)$	Undisturbed Transfer Function
T_d	Disturbed Temperature
$G_d(s)$	Disturbed Transfer Function
$G(s)$	Embedded Thermocouple Correction Transfer Function
T_p	Temperature at Node P
n	Number of Control Volumes (Undisturbed Model)
Δx	Control Volume Spacing
δx	Nodal spacing
ntc	Number of Control Volumes (Sensor Sub-model)
Δr	Radial Distance Between C.V. Faces
δr	Radial Distance Between Nodes
$\Delta \theta$	Angular Distance Between C.V. Faces
$\delta \theta$	Angular Distance Between Nodes
σ	Standard Deviation

CHAPTER I

INTRODUCTION

Temperature measurement is one of the most common of all engineering tasks, but that does not mean that it is a simple one. There are literally countless situations found throughout industry where a solution is realized through a temperature measurement, which most assuredly led to the wide variety of methods currently available for obtaining temperature measurements. Among these are the use of thermocouples, resistance temperature devices (RTDs), thermistors, bimetallic devices, fluid-expansion devices, optical pyrometers, and infrared systems. The decision of which method to use depends on a variety of factors such as cost, required measurement accuracy, measurement environment, and expected temperature range.

Thermocouples are likely the most widely used type of temperature measurement device in industry, due to their relatively low cost, high accuracy, and wide range of measurement application. The broad variety of industrial applications in which thermocouples are employed to monitor and/or collect temperature data speaks for their popularity in industry. One such use for thermocouples, the focus of the current research, is in solid-embedded applications.

Solid-embedded thermocouples are thermocouples that are installed within a solid medium to track the temperature sensor history inside the medium at the thermocouple location.   More specifically, embedded thermocouples are often utilized in industrial

1

applications for the sole purpose of attaining accurate temperature data for the implementation of inverse heat conduction (IHC) problems. The results produced from these inverse problems can be used to establish estimates of the critical boundary information used in the mathematical modeling and simulation of various thermal systems in industry.

In order to clearly understand the implication of the term "inverse" problem, the "forward" problem must first be explained. In a typical "forward" heat conduction problem, the governing differential equations, material properties, and all boundary and initial conditions are known. Assuming this information is available, it is possible to determine the temperature at any location within the medium of interest as a function of time. However, in most real life situations, there is some piece of this required information that is missing or unattainable. The missing component usually occurs in the form of a boundary condition, such as a heat flux or a heat transfer coefficient. Without this crucial information, the heat conduction problem cannot be solved in the forward fashion. This is why the inverse problem has proven to be of great utility. In an inverse heat conduction problem, experimental temperature data collected from discrete locations within the domain is utilized to recover an approximation of the boundary conditions. However there are limitations of the usefulness, as the experimental data must be as accurate and "clean" as possible because any error, especially high frequency noise, in the temperature data tends to be greatly amplified in the estimates for the boundary conditions obtained through inverse methods. Figure 1.1 shows a graphical comparison of the forward and inverse conduction problems.
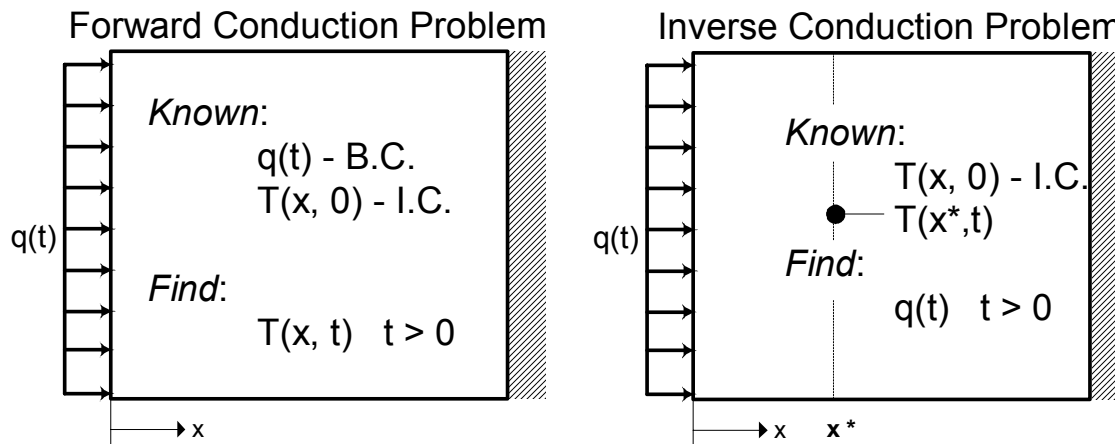
Figure 1.1 - Forward & Inverse Conduction Problems

IHC boundary estimates prove useful in modeling a wide variety of scientific and engineering fields, such as billet, strip, and shape casting, metal working, heat treating, and welding. As illustrated in the casting industry, temperature data can be collected within a mold during a pour, and through inverse methods, the boundary heat fluxes and resulting heat transfer coefficients at the mold-metal interface can be approximated. Additionally, other operations involving chemical, aerospace, nuclear engineering, food science, medical, and other fields also employ inverse methods to obtain similar information.

Goals for the Current Research

The current research investigates the use of embedded thermocouples within a permanent mold during a casting process to obtain internal temperature data for estimating metal-mold interface boundary conditions. It has been stated in the literature that the interface heat transfer coefficient is one of the most dominant parameters when considering the mathematical modeling or computer simulation of metal casting processes [1-4]. The more accurately the heat transfer coefficient value is known in time, the better a casting simulation driven by that information can be. Typically, heat transfer coefficient values must be determined using inverse conduction methods which employ an internal mold temperature collected by an embedded thermocouple during laboratory experiments. It is widely known and shown in the literature that inverse conduction solutions are highly sensitive to error in the experimental temperature data [5-8]. Therefore, it is obvious that the validity of a computational casting simulation can ultimately depend on the quality of the collected temperature data used to calculate the heat transfer coefficient utilized in the simulation.

The motivation for investigation of embedded thermocouples comes from the need to acquire very accurate internal mold temperatures for inverse solution estimates of the boundary condition at the mold-metal interface during metal casting process, but other analogous applications also exist. Accurate transient thermocouple measurements are needed in order produce valid inverse conduction solutions. Therefore, it is important for experimenters involved in these types of data acquisition situations to understand the

sources of errors for their thermocouple measurements and the challenges involved in minimizing the total uncertainty in the temperature data.

This thesis work is presented as three key sections. The first section discusses the many sources of uncertainty contained in an embedded thermocouple measurement during transient measurement periods; the familiar static components, as well as some dynamic components that might not be quite as familiar. Both random and systematic uncertainties are considered, with particular emphasis on the systematic uncertainties due to installation effects of the thermocouple sensor. The second part presents and discusses an inverse conduction project pertaining to the solidification of aluminum A356 in a mild steel permanent mold performed at Mississippi State University (MSU) through funding by the U. S. Department of Energy and the Cast Metals Coalition. The purpose of the project was to execute a controlled experiment in which accurate temperature measurements would be collected within a permanent mold near the mold-metal interface during a casting process, and utilized through inverse methods, to estimate the heat transfer coefficients at the interface. The processes and procedures will be discussed and the lessons learned will be presented. The third section of the thesis presents a potential method for correcting for some of the installation effects caused by the intrusion of the sensor into the system, which can be a significant contributor to the total systematic error in some cases.

CHAPTER II

EMBEDDED THERMOCOUPLE ERROR EXAMINED

Introduction to Solid-embedded Thermocouples

A thermocouple is a thermoelectric sensor used to measure temperatures. A typical thermocouple consists of two dissimilar metal wires joined together to form a junction. Heating and cooling of the junction produces a voltage that can be measured across the free ends of the thermocouple, which is known as the Seebeck effect [9]. This voltage can then be directly correlated to the temperature of the junction. The four most common calibrations of thermocouples and their compositions are shown in Table 2.1 [10].

Table 2.1 - Common Thermocouple Calibrations

Thermocouple Type	Composition	
	Positive Lead (+)	Negative Lead (-)
K	Nickel-Chromium	Nickel-Aluminum
J	Iron	Copper-Nickel
T	Copper	Copper-Nickel
E	Nickel-Chromium	Copper-Nickel

Solid-embedded thermocouples are thermocouples that are inserted into a solid medium to track the temperature history within the medium at the thermocouple location. Embedded thermocouples are used in a wide variety of industrial and research oriented applications, for example gathering thermal history data of a workpiece during a welding

6

or machining operation [11, 12] or collection of thermal effects associated with stress waves in a solid [13]. This type of thermocouple installation is of particular interest for the work of this thesis.

Industrial Applications

Internal temperature measurements obtained by embedded thermocouples are frequently used in industry applications in which the temperature measurement is collected for use in an inverse conduction problem solution. These inverse conduction problem solutions can aid engineers in understanding a variety of interfacial situations, including applications such as determining boundary conditions of gas turbine blades and gun barrels [14], thermal deformation of machine tools [15], and the heat transfer at the mold-metal interface during a casting solidification process [1, 3, 4, 8, 16-18].

As previously mentioned, inverse conduction solutions are very sensitive to thermocouple measurement error. A relatively small uncertainty in measured temperature can result in a much larger uncertainty in the inverse conduction estimates for boundary conditions. Therefore, obtaining quality thermocouple data is a high priority when the data is intended for use in IHC problem solutions.

Design of Experiments Employing Solid-embedded Thermocouples

Any experimentally measured signal will inevitably include some amount of uncertainty. The uncertainty can never be completely eliminated, but there are a variety of measures that can be taken to reduce the total amount of uncertainty in a signal [19]. Before uncertainty can be reduced, however, it must first be recognized. Therefore, the

initial step in uncertainty reduction is to gain a thorough understanding of the various sources that make up the total uncertainty in a signal.

In the design of an experiment, an imperative initial action is to perform a preliminary uncertainty analysis in order to better understand the system under investigation. This step is important in order to identify specific sources of uncertainty, estimate the contribution of each source component, and implement methods for the reduction of these uncertainty components.

For this thesis research, the various categories of the uncertainty will be discussed in a manner relative to experimentation involving solid embedded thermocouples in order to provide some basic guidelines to consider when collecting temperature data. These guidelines will focus primarily on the embedding of thermocouples within permanent molds in the casting industry to obtain time histories of temperature at specific locations within the molds for use in inverse methods to estimate mold-metal interface heat flux.

Types of Temperature Measurement Uncertainty

The uncertainty in a measuring device can be divided into two major categories: systematic uncertainty and random uncertainty. Systematic, or bias, uncertainties are the fixed or constant components of the total error [19]. These types of uncertainties are usually contributed by limitations in the manufacturing, calibration, installation, or perhaps modeling of the sensors. Random, or precision, uncertainty is the portion of the total uncertainty that is typically associated with measurement noise and usually, but not always, follows some type of statistical distribution [9]. Random uncertainty, or the signal noise, is usually due to electrical interference, either external or within the data

acquisition circuitry. The systematic and random components sum to yield the total uncertainty component for any measured signal.

Static and Dynamic Measurements

When using an embedded thermocouple to obtain temperature measurements, the type of measurement could either be static or dynamic, depending on the state of the system. It is important to understand the type of measurement required of an experiment in order to design the experiment with appropriate measures to meet its purpose. Static measurements are those types that are obtained after the entire system in consideration, both the measured material and the thermocouple sensor, has been allowed adequate time to "thermally settle" after any boundary condition changes. In other words, the temperature to be measured is not changing with time. However, many practical situations exist in which a temperature within a solid medium is to be obtained during a period when the boundary condition is changing with time [1, 3, 4, 8, 14-18].

Dynamic measurements are measurements that are intended to obtain temperature at a location as it changes with time. Dynamic, or transient, measurement capabilities would be considered necessary to measure temperature during a time prior to a system reaching its steady-state response, or perhaps if the system exhibited a time varying steady response. Uncertainties for dynamic measurements include all the components found in a static measurement, as well as some additional uncertainty components that are specific to dynamic measurements, such as phase errors. For a metal casting process, when considering temperature collection within a permanent mold after molten aluminum

is poured into the mold cavity, the necessity for accurate transient temperature measurements is evident.

Systematic Uncertainty Components – Static and Dynamic Measurements

The purpose of this section of the current research is to discuss several systematic sources of uncertainty for dynamic measurements using embedded thermocouples. As previously stated, any static measurement uncertainty component would also contribute in the case of a dynamic measurement; therefore components common to both will be discussed first, followed by additional uncertainty sources unique to dynamic measurements.

Manufacturer's Uncertainty and Calibration

All measurement sensors come from the manufacturer with a specified systematic component of measurement uncertainty. This component is commonly referred to as manufacturer's uncertainty, and can either be specified as an absolute value or as a percentage of the measured scale. This portion of the systematic uncertainty is due to limitations prescribed by the manufacturing operations to produce and assemble the sensor. Thermocouples that are typically used in industry are purchased as prefabricated units from a supplier or as rolls of industry standard thermocouple wire. In either case, the manufacturer would specify a level of accuracy to which the sensor is certified. Typically, the manufacturer's uncertainty can be reduced through the process of calibrating the thermocouple to a well known standard, such as the boiling point of water [9, 19]. However, no standard itself is perfect; therefore calibration can never completely

eliminate the manufacturer's uncertainty, only reduce it to the level of uncertainty of the calibration standard.

Data Acquisition and Data Reduction Uncertainties

Data acquisition and reduction errors are another category of systematic errors [19]. This category concerns the biases associated with the data acquisition (DAQ) system that acquires, possibly conditions, and stores the output of the sensor. Uncertainties of this type would include those relating to round-off, truncation, or sampling errors when transferring thermocouple voltage outputs to the digital domain of data acquisition hardware and the personal computer used to control the DAQ devices. Once the voltage values from a thermocouple sensor are obtained, they must be correlated to a corresponding thermocouple junction temperature for each voltage value. This process is accomplished using experimentally determined correlation curves for temperature values. These empirical curves also have a certain levels of uncertainty associated with them as well.

Uncertainty from Conceptual Errors

Systematic uncertainties can also arrive from conceptual errors, such as when a measured value is taken to be a point value for a specific location in space when it is, in realistically, an average temperature over a larger region. For embedded thermocouples, this error might arise from the assumption that a thermocouple is measuring the temperature at a point location within the medium of interest. In actuality, the thermocouple is likely registering an average temperature over the entire junction bead

[8, 10]. This type of error can be reduced most obviously by reducing the thermocouple junction size.

Installation Uncertainty

Another type of elemental systematic error source, and the one that is of key interest for this thesis research, is that of the installation error. Installation errors for measurements include uncertainties that are due to the intrusive nature of an embedded thermocouple installation and the inhomogeneity subsequently caused. Geometric tolerances involved in pinpointing the location of a thermocouple bead embedded within the solid medium, as well as effects due to heat loss through the thermocouple leads are also considered as types of possible installation uncertainties [8, 15, 20-25].

The contributions from installation uncertainties have been shown in various sources throughout the literature to be of sufficient magnitude to merit efforts to recognize and, if possible, reduce them [8, 13, 15, 20-27]. These types of errors for a static measurement occur as typical bias offsets in magnitude from the "true" temperature value. However, when considering installation errors for a transient measurement, more consideration must be exercised because the presence of the embedded sensor within the medium completely alters the dynamic response of both the measured medium and the measurement sensor from what they would be independent of each other [11, 23, 26].

Additional Systematic Uncertainty for Dynamic Measurements

Dynamic, or transient, temperature measurements can be described as measurements collected while the temperature at the sensor location is still varying as a function of time. Transient measurements can incorporate additional sources of error due to the dynamic response characteristics of the embedded thermocouple and the measured medium, as well as the dynamic interaction between them. These sources can cause errors not only as biases in magnitude of the signal, but also as a phase shift of the signal in time [11, 13, 23, 26, 28]. These additional distortions in magnitude and phase can further increase the total uncertainty of the temperature measurements.

During a transient period, a thermal system is dynamically responding to changes in the boundary conditions, such as a change in the heat flux or surface temperature, resulting in the temperature field varying with time. A previously discussed example that is the practical interest to this research is the pouring of molten aluminum into a preheated steel mold. The mold is subjected to a rapid change in heat flux at the mold-metal interface as the molten aluminum enters the mold cavity. It is during this period that boundary heat flux identification is desired, and therefore it is when transient temperature data is collected to assist in determining these unknown, unsteady boundary conditions.

Distortion of the Localized Thermal Field

In order to determine a temperature within a solid body, such as a metal mold, a hole must be machined into the solid in order to provide access to the point of interest by the sensor. A major concern when collecting transient temperature data is the localized

distortion experienced in portions of the thermal field surrounding the installed sensor. The presence of a cavity within a solid body, whose contents have differing material properties than the surrounding medium, has been shown in the literature to induce distortions in the local thermal field around the cavity [15, 20-22]. Isotherms in the measured solid near the sensor installation can actually "bend" and distort due to several factors relating to the presence of the sensor in an otherwise homogeneous medium. The distortion can be attributed to several factors, such as the thermocouple installation cavity dimensions and orientation, differences in thermal properties of the medium, thermocouple, and filler material in the cavity, and heat loss conducted through the thermocouple leads.

Chen et. al [14, 25] performed a number of laboratory experiments several years ago to investigate the transient temperature errors due to the embedded installation of type K thermocouples parallel to an applied heat flux. They ascertained that the degree of distortion depended largely on the differing properties of the parent material and the materials which filled the cavity (air and thermocouple) and the diameter and depth of the installation hole. As is consistent with expectations, they showed that the temperature measurement error decreased with a decrease in the size of the installation cavity and embedded thermocouple.

More recently, Attia et. al [15, 20-22] have published several comprehensive studies investigating the thermal distortions induced by the insertion of an embedded thermocouple into a solid material, as well as the effects of heat loss through the thermocouple leads. Multiple in-depth studies were conducted to determine the effects of

varying the thermal conductivity of the parent material, the thermocouple, and the cavity filler material, as well as geometric placement of the thermocouple bead in the cavity base on thermocouple measurement error. It was concluded that distortion within the local thermal field around the embedded thermocouple was highly dependant upon the ratio of the thermal conductivities of the cavity filler material to the parent material. Also, a local "hot" and "cold" zone was discovered to form at the perimeter of the thermocouple installation cavity due to the disturbance to the local thermal field. The size and location of the zones varied depending upon the ratio of material properties considered. Studies investigating the effect of positioning of the thermocouple bead within the cavity on thermocouple measurement error showed significant amounts of deviation from the expected value, as both temperature overestimation and underestimation, depending upon which zone at the cavity base the bead was in contact with. It was also shown that reduction of the thermal gradient across the parent material allowed for a significant increase of heat flow into the thermocouple leads and that this heat loss through the leads will generally result in an overall underestimation of the "true" temperature. Temperature measurement errors as much as 20 percent of the temperature drop over a distance equal to the cavity radius were shown to be possible.

Woodbury and Gupta [8] recently investigated the impact of deterministic thermocouple errors in sand molds on inverse heat conduction problems. They showed through finite element modeling how four typical thermocouple sizes, AWG 24, 30, 36, and 44, with glass braid and alumina sheathing can cause distortion to the thermal field around the thermocouple. They reported that for a typical 24 AWG size thermocouple

embedded in a sand mold, transient errors of up to 35 C were possible, which led to errors of up to 40 percent for the estimated boundary heat flux.

In conduction systems with multiple types of materials involved, it is important to note that the temperature drop across the interface may be significant [29]. The temperature drop is caused by what is known as a thermal contact resistance. The thermal contact resistance usually arises when two solids are butted together and heat is conducted across their interface. The contact resistance usually occurs as an additional resistance to heat travel due primarily to surface roughness of each surface in contact.

For embedded thermocouple installations, a thermal contact resistance could exist between the thermocouple junction and the surrounding parent material due to the fact that they will most likely be in less than perfect contact. There may be air, filler cement, etc. between the two materials which will cause additional resistance to heat flow to the point of interest over the same geometrical location in a solid block of parent material with no thermocouple installed. Incropera and DeWitt [29] suggest that increasing contact pressure or reducing the surface roughness can lead to greater contact area therefore reducing the contact resistance. They also mention that using filler materials to bond two surfaces of interest can decrease the contact resistance, assuming the filler material has a higher conductivity than that of air.

Heat Loss through Thermocouple Leads

Another thermocouple error contributor that must be recognized is the possibility of conduction of heat away from the point of interest via the thermocouple leads. Through the insertion of the measurement device, a path has been created for heat to

escape, leading to a bias error that could, depending upon other error sources, lead to the underestimation of the desired temperature value. This source of error has also been investigated and discussed in the literature [15, 20-22, 27, 30].

According to Weathers et. al. [27], the amount of heat dissipated through the thermocouple leads depends greatly on the orientation of the leads with respect to the predominant direction of the heat flux. They conducted a three dimensional finite element study of the effects of installation orientation of solid embedded thermocouple within permanent (steel) and sand molds. Horizontally (perpendicular) and vertically (parallel) positioned thermocouples, with respect to the isotherms across the temperature gradient, were examined. For permanent (steel) molds, it was shown that horizontal installation, perpendicular to the isotherms, proved to produce more accurate transient temperature data and allow for more geometrical control of the thermocouple junction with regards to the distance from the metal-mold interface. For sand molds, the vertical installation, parallel to the isotherms, was shown to be preferable due to the reduction in the amount of heat conducted and lost through the thermocouple leads.

Embedded Thermocouple Positioning

In preparation for temperature history logging for use in inverse problems, thermocouples are usually embedded very near to the surface where the boundary conditions are applied so that the thermocouple will be more sensitive to the abrupt changes at the mold-metal interface. However, it is important to realize that if the sensor is installed too near to the interface, the previously discussed distortion due to the presence of the probe could extend into the interface surface, disturbing the surface

condition and boundary heat flux as stated by Chen et. al. in [31]. Because the installation of a thermocouple in a solid medium produces a local region of thermal distortion around the installation cavity, it is crucial to understand the relative size of this distorted region in relation to the cavity size. If the "reach" of the distortion effects is known, the sensor can be placed at the optimal distance from the boundary of interest, without being so close as to disturb the thermal field at the boundary surface. This critical distance from the boundary surface is suggested to depend upon the cavity dimensions, as well as the material properties of the parent material and cavity contents.

Chen and Li [14] created an idealized finite element model of a type K thermocouple embedded in a flat circular steel disc in which a large steady heat flux was applied to one surface. They presented graphical plots demonstrating the dependence of thermocouple measurement errors on a variety of the thermocouple installation geometrical parameters, such as cavity diameter, thermocouple diameter, distance from the interface, etc. They suggest, for best sensitivity to boundary changes, the distance from the interface should be as small as possible. In Chen and Thomson's work [31], however, a reminder is given suggesting that a sensor at the surface will disturb the surface conditions and heat flow at the interface. Therefore, an optimal sensor distance from the interface surface must exist to provide as accurate a representation of the dynamics of the surface conditions as possible without disturbing them.

In [25], Chen and Danh revisited the presence of a cylindrical cavity in a flat slab through a well controlled laboratory experiment. The thermocouples in their experiments were mounted in steel blocks parallel to the direction of the boundary heat flux

application. Included in their work is a summary of the typical maximum errors observed for the prescribed variations of the thermocouple cavity geometry and the boundary condition application time. They stated through their findings that the distortion in temperature response was much more sensitive to cavity diameter than depth of the thermocouple hole.

Elphick et. al [24] discuss how thermocouple assemblies installed in solids can create changes in the heat flux distributions therefore resulting in steady-state or transient temperature measurements that are quite different from the expected temperature. They conducted numerical simulations to assess the error involved in using several sheathed thermocouple configurations to obtain a temperature history within a solid. They found that through the selection of a filler, or plug material, with an appropriate thermal conductivity to "balance" the dynamics between the parent and thermocouple material properties, the thermocouple error could be minimized. Thermocouple cavity diameter, distance from the cavity tip to boundary interface of interest, and the magnitude of the surface boundary conditions were presented as some of the most important factors contributing to the amount of error for a thermocouple signal.

Phase Errors

In addition to errors in magnitude, for transient temperature measurements, errors can also occur as shifts in the phase of a signal, commonly observed as delays in sensor response in time. Rittel [28] investigated the use of embedded thermocouples for transient temperature measurements in polymer discs undergoing dynamic deformation and straining. He shows that through using a theoretically derived impulse response of

the system, the experimental data can be deconvolved to an estimated signal that occurs a bit earlier, faster, and with higher values of observed temperature. Rabin and Rittel [13] follow the investigation of transient temperature measurement using solid-embedded thermocouples with a model for the time response of the thermocouple. They discuss the idea of the existence of a "thermal inertia" effect that can cause undesired delay in the response of an embedded thermocouple. This "thermal inertia" effect is shown to be due to the rate of change of temperature of the measured material, the differing thermophysical properties of the thermocouple and the measured material, and the geometry of the thermocouple installation. They examined thermocouple response with respect to the ratios of the thermal diffusivity of the thermocouple material to the domain material. Thermal diffusivity ratios of one or less were reported to be inadequate for transient measurement situations. Also, for locations within the measured domain greater than three times the thermocouple radius, the presence of the thermocouple was shown to have no significant effects.

In his analyses of transient measurements, W. G. Alwang [26] suggests that a transient measurement consists of two pieces of information: the value measured and the time at which it was measured. He proceeds to state that transient measurements depend on all error sources which depend on the dynamic response of the measurement system, and therefore also the time behavior of the quantity being measured.

Modeling Errors

In [23], Alwang approaches the problem of uncertainty estimation and reduction in transient measurements through modeling of the systems under investigation and

deconvolution of the experimental signals. Two extremes of the effects of time-dependant uncertainty are presented: the case where additional uncertainty due to transient measurement is negligible and the case where these additional uncertainties are large. He shows that through a process of time-dependant calibration of the system, a measured response can be corrected for many of the inherent transient measurement errors encountered.

Analytical approaches [32] and a variety of modeling efforts [11, 26] have been made to characterize and aid in the reduction of experimental temperature measurement installation errors. However, as no model will ever exactly duplicate a real life situation, differences between the model and the real process it simulates will result in modeling uncertainties being present in the signal. For embedded thermocouples, errors could exist due to inadequacies of the model to represent the dynamics of the real process or perhaps uncertainty as to the exact location of the thermocouple bead in the cavity once installed. Still, if the model sufficiently represents the real process, the total uncertainty can be reduced.

Random Uncertainty

Random uncertainty, or the signal noise, is usually due to electrical interference, either from external devices or within the data acquisition circuitry. As stated previously, the random uncertainty components for a set of collected data typically follow a statistical distribution. For a transient temperature measurement, at each instant in time that a temperature value is measured, a component of random, or precision, uncertainty

will be included within the signal. These components should be comparable to the random uncertainty within a static measurement with the same physical sensor setup.

Summary of Solid-embedded Thermocouple Error

This chapter has presented a detailed overview of several categories of uncertainty that can be anticipated when using embedded thermocouples for transient temperature measurements.   This information was offered as evidence of the presence of a variety of errors in measured temperature data, and to illustrate the necessity to improve embedded temperature measurements, especially when considering temperature data collected for highly sensitive inverse processes. The key point of this chapter is to emphasize that, in addition to common sensor uncertainties (manufacturer's, data acquisition, etc.), the installation of a temperature sensor within a solid domain changes the dynamic behavior of the domain in the region surrounding the sensor. This results in experimental data that does not accurately reflect what the theoretical temperature within the domain would have been were the sensor not installed. Therefore, with all the sources of error in temperature measurement presented in this chapter, opportunities for improvement of the measurement will always exist.

CHAPTER III

OBTAINING EXPERIMENTAL TEMPERATURE DATA

Introduction to Experimental Setup

Inverse conduction solutions are often employed in the metal casting industry in order to estimate unknown boundary conditions during the casting solidification process. Temperature measurements are recorded during the casting process using thermocouples that are embedded within the mold. The temperature values observed by the thermocouples may then be used, through inverse processes, to recover boundary condition estimates over time at the metal-mold interface. These estimates of the boundary conditions can then be utilized in computational casting simulations to more accurately represent real life casting processes. It has been shown extensively in the literature concerning inverse problems, that small errors in temperature data can be amplified greatly in estimates for boundary conditions [5-7]. Therefore, it is critical to minimize error in temperature data when intended for use in inverse methods, so that the resulting estimated boundary conditions, and ultimately computational simulations in which they are used, will be as representative of real world processes as possible.

Through funding by the U. S. Department of Energy and the Cast Metals Coalition, Mississippi State University was able to plan and perform an inverse conduction project pertaining to the solidification of aluminum A356 in a mild steel permanent mold. The purpose of the project was to execute a controlled experiment in

23

which accurate temperature measurements would be collected within a permanent mold near the mold-metal interface during a casting process, and utilized through inverse methods, to estimate the heat transfer coefficients at the interface. The two key objectives for this project were to develop and maintain good practices for obtaining accurate temperature data from the thermocouples embedded in the mold and to use the temperature data obtained to estimate, through inverse analysis, the mold-metal interface heat transfer coefficients. The content of this thesis focuses primarily on the first objective, the collection of quality embedded thermocouple data. The interface heat transfer coefficient estimation portion of the project was performed and reported by fellow graduate student, Mr. Jeff Weathers, in his written master's thesis [33].

Description of the Current Research Experiments

The foundry facilities located in the basement of the Carpenter Mechanical Engineering building at Mississippi State University were used to conduct all of the metal pouring experiments. Aluminum A356 was chosen as the casting alloy for use because it was readily available, suitable for the MSU facilities, and due to its wide commercial use in areas such as the automotive industry. The permanent mold employed for the study was a three-piece low carbon steel mold with a simple, rectangular slab plate geometry. The mold was designed to accept one of four interchangeable center inserts having thicknesses of 1/8", 1/4", 1/2", and 1" respectively. The 1/2" insert was selected to be used for the entirety of the project. Photographs of the three piece steel mold in its disassembled and partially assembled form are shown in Figure 3.1 and Figure 3.2. A dimensioned drawing of the mold is presented in Figure 3.3.

Figure 3.1 - Three-piece Steel Mold (disassembled)

Figure 3.2 - Three-piece Steel Mold (partially assembled)
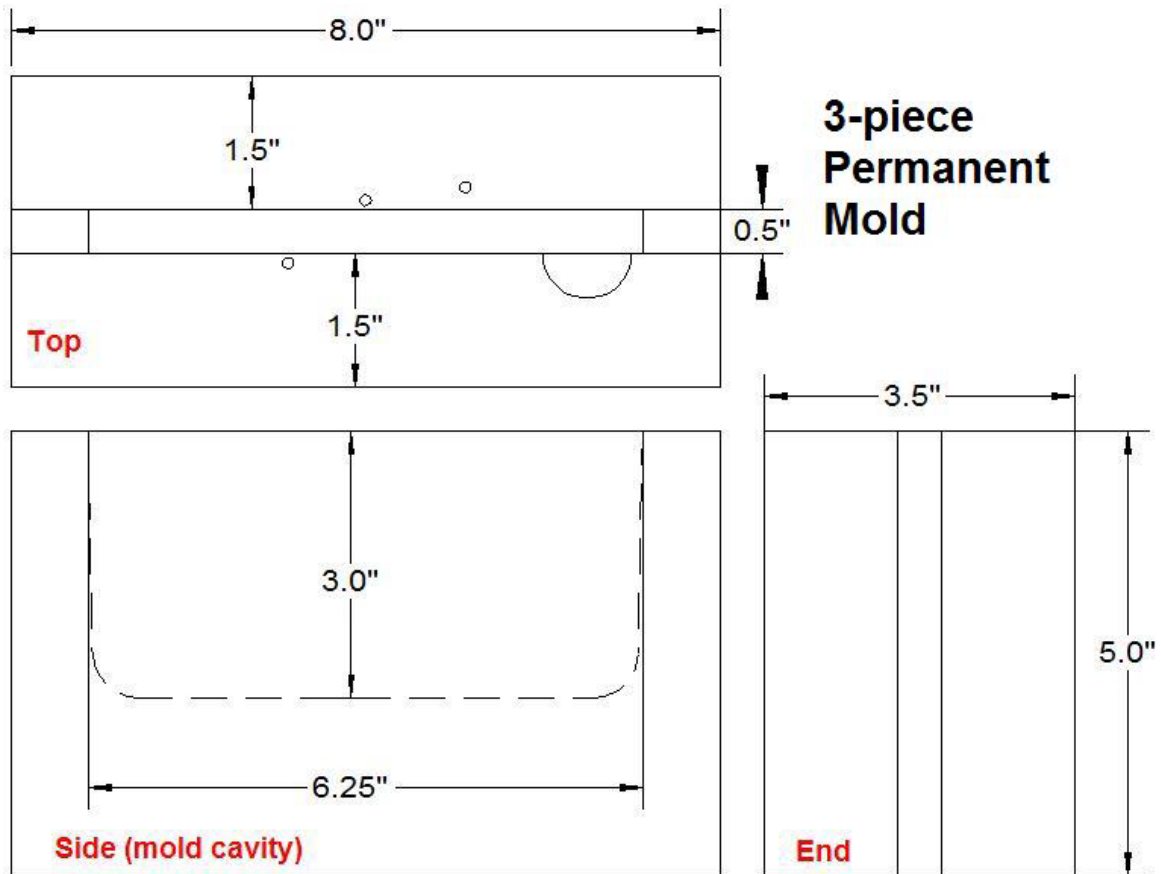
Figure 3.3 - Permanent Mold Dimensions

Although not all castings are exceedingly complicated geometrically, a recognized benefit of metal casting is that it can be used to create complex geometries that would normally prove difficult or even unattainable to produce by other processes, such as machining. Nonetheless, this program's goals focus on the methodology and procedure of obtaining "good" temperature data for the prediction of heat transfer coefficients through inverse methods. Therefore, it was considered best to begin the study with a very basic, understandable geometry, and leave more complex casting geometries to be considered in the future.

A particular interest is often shown in the metal casting community for the study of solidification control of thin section castings or portions of castings, which can be very difficult. Therefore, the thin slab casting geometry chosen was to some extent representative of this area of interest. Also, the simple geometry of the permanent mold selected allowed for the simplifying assumption that heat flow was predominant in one dimension only (the thickness direction of the mold). This assumption reduced some of the complexity involved in modeling for this initial research effort.

Thermocouple Construction and Installation

The mold was instrumented with thermocouples within the interior of the mold halves to measure internal temperatures during the casting process. The preparation and fixturing of the mold was performed with the intention of being able to reuse the same experimental setup for multiple experimental trials. Consideration of the expected temperature range led to the selection of standard Type K wire for thermocouples in the experimentation. Type K is known for its wide temperature range, -200 to 1250 C (-328 to 2282 F), and common use in industry for similar applications.
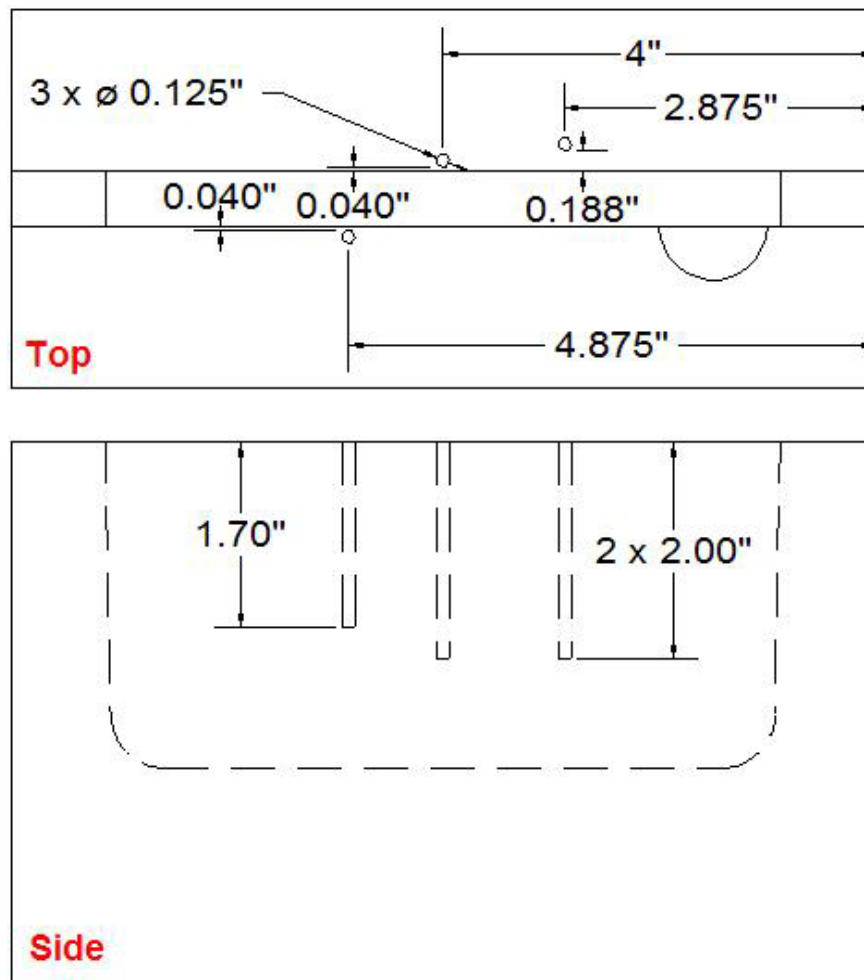
Figure 3.4 - Solid-embedded Thermocouple Cavity Locations

Three 1/8" diameter pilot holes were machined in the mold halves to the depths and geometric locations shown in Figure 3.4. The holes were placed relatively close to the mold-metal interface in order to be as sensitive to the change in boundary conditions as possible. In retrospect, some of the holes may have been machined too close to the interface surface when considering the attempt to keep the distortion caused by the thermocouple installation from "protruding" into the boundary surface and disturbing the boundary conditions.

Three thermocouples were used to collect the temperature data within the mold, and one additional thermocouple was centrally positioned in the mold cavity to collect the casting temperature. The thermocouples were beaded junction type made in-house from standard Omega brand 24-gauge K-type thermocouple wire using a capacitive discharge through the thermocouple leads against a carbon block. The bead sizes were typically slightly larger than one millimeter (0.041" – 0.049").

OMEGATITE 200 twin bore alumina insulators sleeves with 1/8" outside diameters were used to electrically insulate the portion of the thermocouple leads that were to be inserted into the depth of the drilled pilot holes. The sleeves helped to prevent any short circuit of the thermocouple leads within the pilot hole above the bead junction and created a rigid assembly that could be easily inserted into the thermocouple cavity. The sleeves were cut to lengths matching the depths of the holes using a diamond blade circular saw. They were inserted onto the thermocouple toward the beaded junction until only about 1/4" – 3/8" of thermocouple wire was left exposed as shown in Figure 3.5.
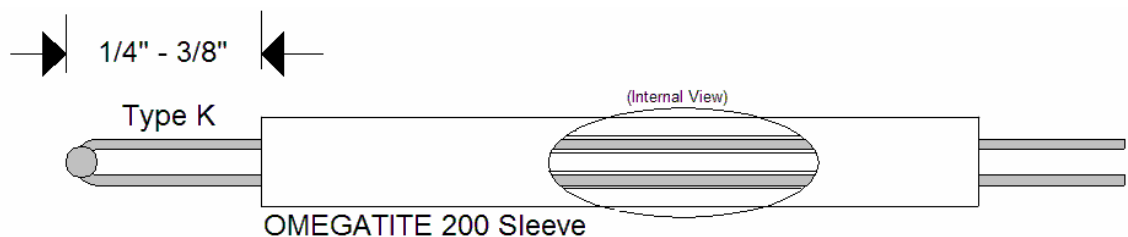
Figure 3.5 - Embedded Thermocouple Sleeve Assembly

After construction, each of the three thermocouple-sleeve assemblies was inserted into a pilot hole in the mold halves until the bead bottomed out. A small portion of the

sleeve protruded out of the top of the thermocouple cavity.   To be certain of the contact between the thermocouple bead and the cavity base, a standard Fluke multi-meter was used to check for continuity by attaching one probe to the exterior of the mold and the other probe to one of the thermocouple leads. After an initial continuity check, high temperature cement, OMEGABOND 400, was used to affix the protruding portion of the alumina sleeve to the mold. The cement was allowed to dry for several hours and then a post installation continuity check was performed to ensure bead to metal contact within the cavity. The leads from the three installed thermocouples were then connected to the three OMEGA ceramic ultra high temperature type K connectors as shown in Figure 3.6. The connectors were then affixed on the side of the mold carrier, as seen in Figure 3.7.
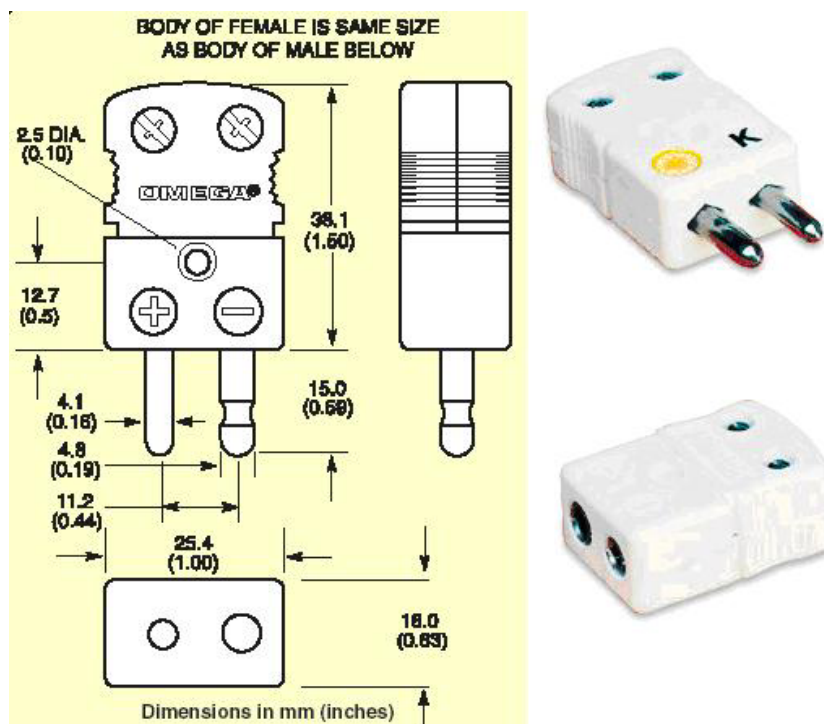
Figure 3.6 - OMEGA Ceramic Connectors
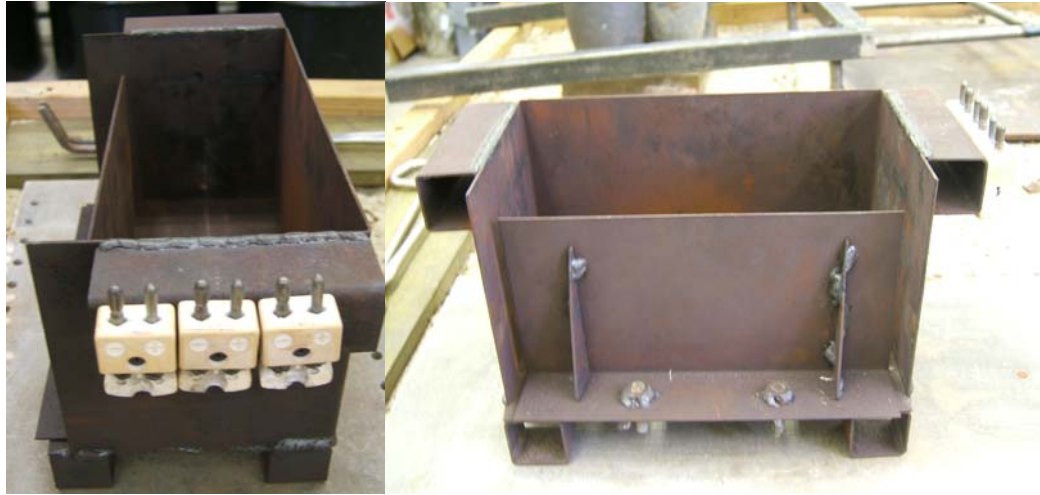
Figure 3.7 - Mold Carrier with Mounted Ceramic Thermocouple Connectors

Mold Preparation and Coating

Many industrial casting processes utilize spray on mold coatings in an attempt to manage solidification at specified locations within a casting, such as gates, runners, or feed paths. These coatings add a heat resistive layer on the mold cavity surface to slow solidification, and in some instances, improve the casting surface finish [34]. Because the same thin or narrow section areas in castings which receive coatings are often the critical areas of interest in casting simulations, mold coatings can bear an important role [4]. Therefore, multiple experiments were performed at Mississippi State to collect sets of experimental temperature data for a variety of typical industry standard mold coating configurations, with the intention of calculating interface heat transfer coefficients for each configuration.

An industry standard base coating media and insulating media, Foseco Dycote 39ESS (base coat) and Foseco Dycote 34 (insulating coat), were donated for use in the

experimentation. Prior to each coating application, the application contact surfaces of the mold were sand blasted at about 80 psi with 25 -70 mesh size aluminum oxide. These coatings were then applied per the coating procedure in configurations and thicknesses shown in Table 3.1. An experimental run was performed and temperature data was collected for each configuration.

Table 3.1 - Mold Coating Configurations

ID	Number of Replications	Coating Configuration	Pours/ Replication
1	1	No Coating	2 – 4
2,3	2	Base Coating @ 2 mils	2 – 4
4,5	2	Base Coating @ 2 mils + Release Coat BN	2 – 4
6,7	2	Base Coating @ 2 mils + Insulating Coating @ 2 mils (light)	2 – 4
8,9	2	Base Coating @ 2 mils + Insulating Coating @ 4 mils (heavy)	2 – 4

Multiple replications of each configuration were run, and several castings were produced per coating application. The temperature data collected from each run was used to determine, through inverse methods, the heat flux at the mold-metal interface, and subsequently a time dependant interface heat transfer coefficient for each configuration which are reported and discussed in detail in [33].
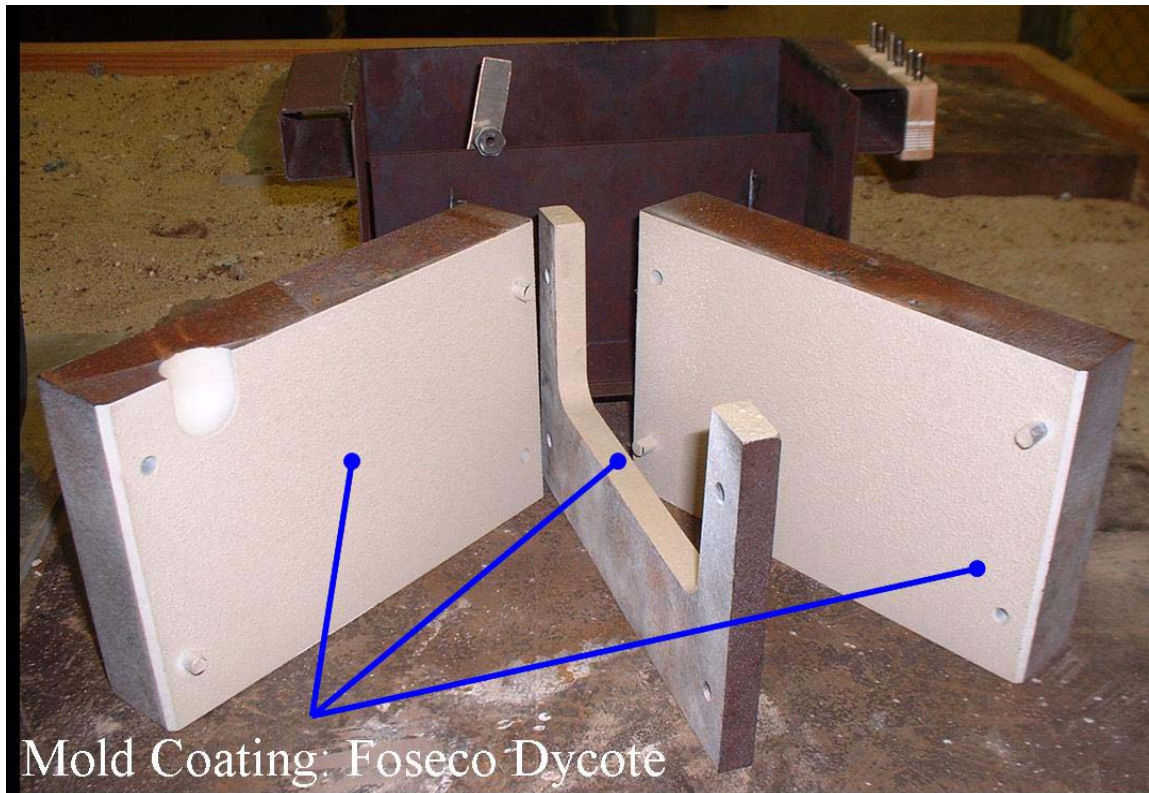
Figure 3.8 - Permanent Steel Mold with Coating Applied

The mold coatings are applied by pressurized spraying of the coating mix on the contact surfaces of the heated mold. The mold with a typical coating applied is shown in Figure 3.8. The procedure employed at MSU for coating the steel mold halves and center insert contact surfaces are as follows:

Mold Preparation

1. Ensure steel is clean of rust and has a rough (preferably grit blasted) surface. (Sand blasted at 80 psi with 25 -70 mesh size aluminum oxide before each coating variation application)

2. Heat entire tool (mold) to approximately 500 deg F (450 – 500 F).

3. Mix coatings thoroughly with appropriate ratio of added water to insure that the coatings are dispersed. Mixing ratios are specified on coating containers.

Coating Application

4. Remove mold from oven and let it cool to approximately 400 deg F.

5. Spray surface to be coated lightly with a fine mist of water. (This promotes oxidation which aids the coating adhesion)

6. Fill spray gun with coating, adjust air pressure to around 40 psi.

7. Adjust gun so spray is dispersed and uniform.
    a. Clear nozzle on cardboard or other surface before beginning spraying sequence.

8. Spray the coating on uniformly across the entire surface, using an Elcometer 456 coating thickness gauge intermediately after several passes to measure the coating thickness.
    a. If coating bubbles, the mold is too hot.
    b. If the water suspension does not vaporize immediately, the mold is too cold.
    c. Ideal coating temperatures are between 350 and 400 degrees F

9. Once desired thickness is achieved, dump unused coating back into container, rinse spray gun thoroughly with water.

10. Let mold air cool or continue with next layer of coating if specified (mold may require an intermediate re-heating for 10 – 15 minutes for multiple coating type configurations if mold temperature has dropped below ideal spraying temperature).

Data Acquisition Equipment

Initial pilot experiments were conducted with departmental equipment, including a 12-bit PCMIA DAQ Card 6024E, to investigate data acquisition performance requirements for the project. A simple DAQ card bit analysis, included in Appendix A, revealed that a 16-bit card could improve the machine precision to 1.5 microvolts (0.038 C) versus about 24 microvolts (0.612 C) for a 12-bit card. Therefore, a desktop computer was purchased and equipped with a 16-bit National Instruments PCI DAQ Card 6036E. A 16-channel National Instruments (NI) shielded connector block, SCB-68, and a two meter shielded cable were also purchased in order to help protect the data signal from external electrical noise.
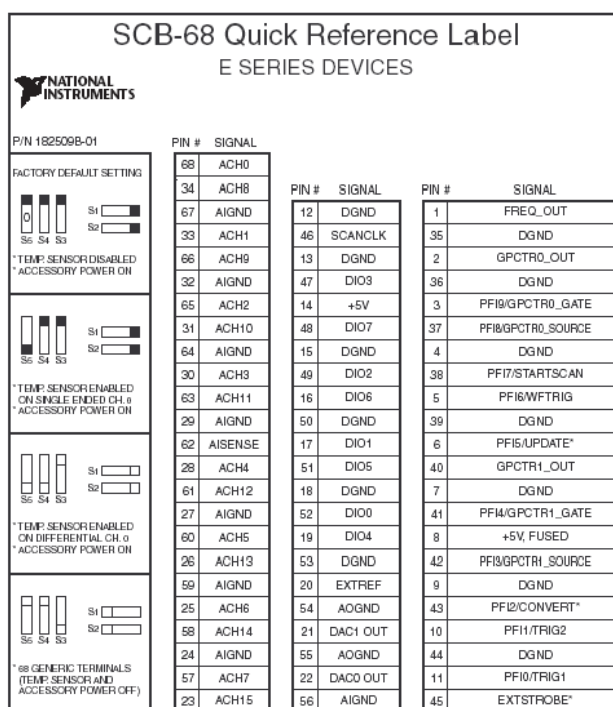
Figure 3.9 - National Instruments SCB-68 Connector Block Pinout Diagram

Thermocouple Circuit Construction

The three embedded thermocouples and the single casting thermocouple were connected to the connector block and all were referenced to a common cold junction. The quick reference diagram for the NI SCB-68 is shown in Figure 3.9 [35].

The four data acquisition thermocouples and the cold junction reference thermocouple were arranged within the data acquisition connector block, NI SCB-68, in the configuration as shown in Figure 3.10. The cold junction was constructed using a Styrofoam insulated container filled with ice water to construct a traditional ice bath.
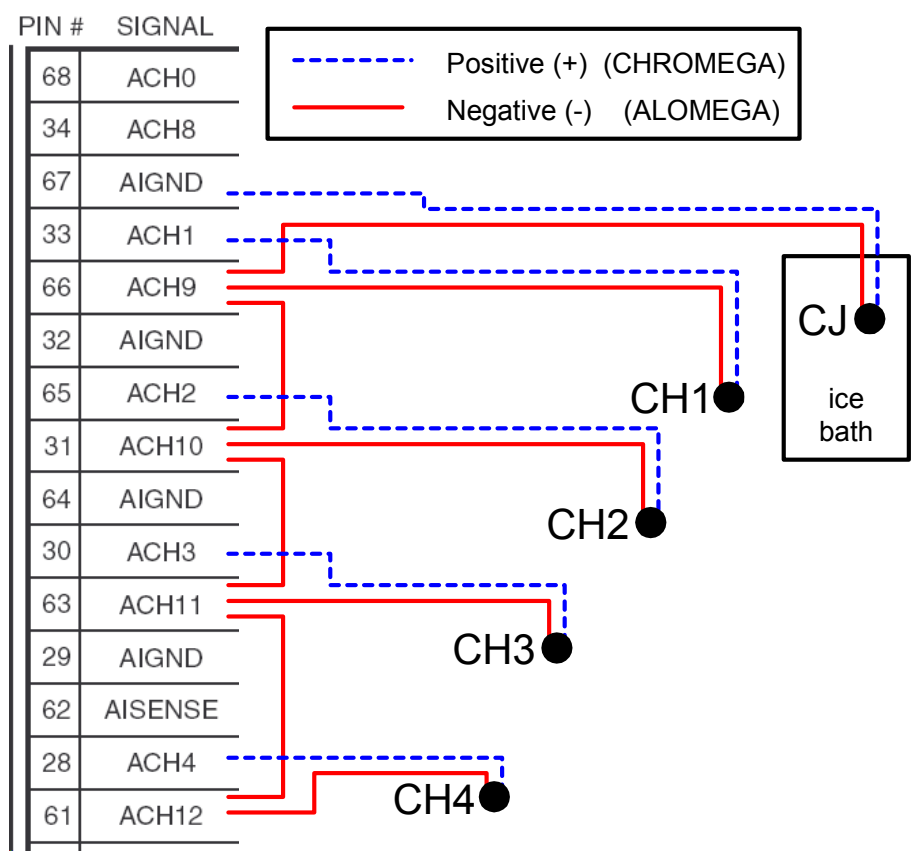
Figure 3.10 - Thermocouple Circuit

Labview Data Acquisition .vi Construction

     A Labview .vi was created specifically for the acquisition of up to eight channels of data. The .vi was designed with the capability of sampling at high rates (100+ samples/second) if necessary. User defined channels, sampling rates, and sampling duration were required prior to running the .vi to collect temperature data. Channel outputs, in voltage, were displayed graphically on the PC screen and prompted for storage in a data file after the completion of each data acquisition session.   Figure 3.11 - Figure 3.13 show the front panel and block diagram for the .vi used to obtain the data.
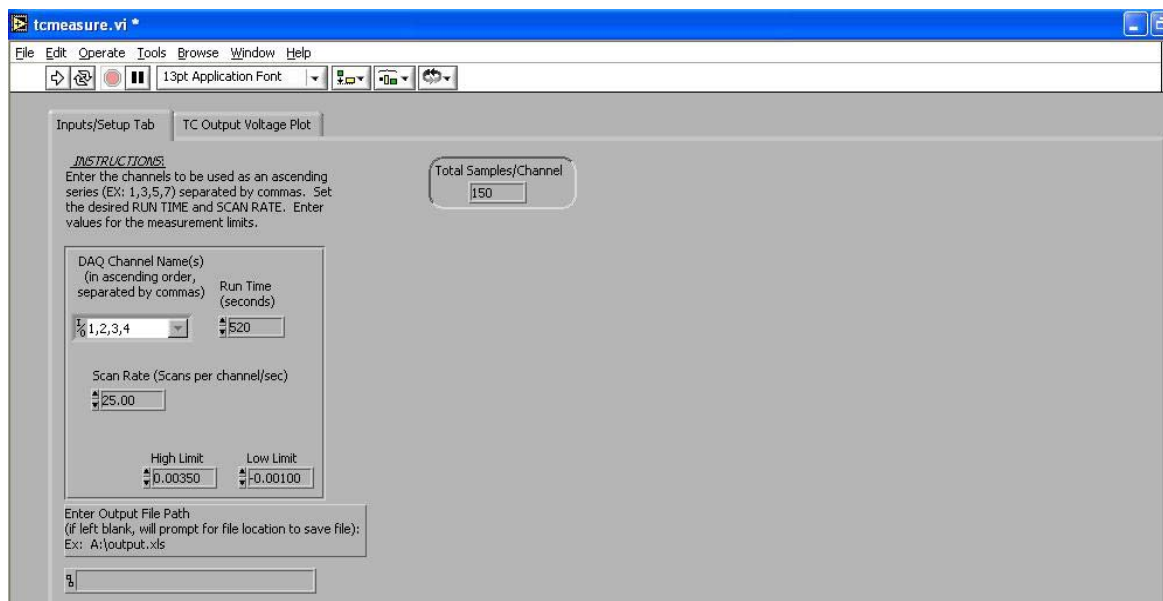
Figure 3.11 - Labview .vi Front Panel (Input Screen)
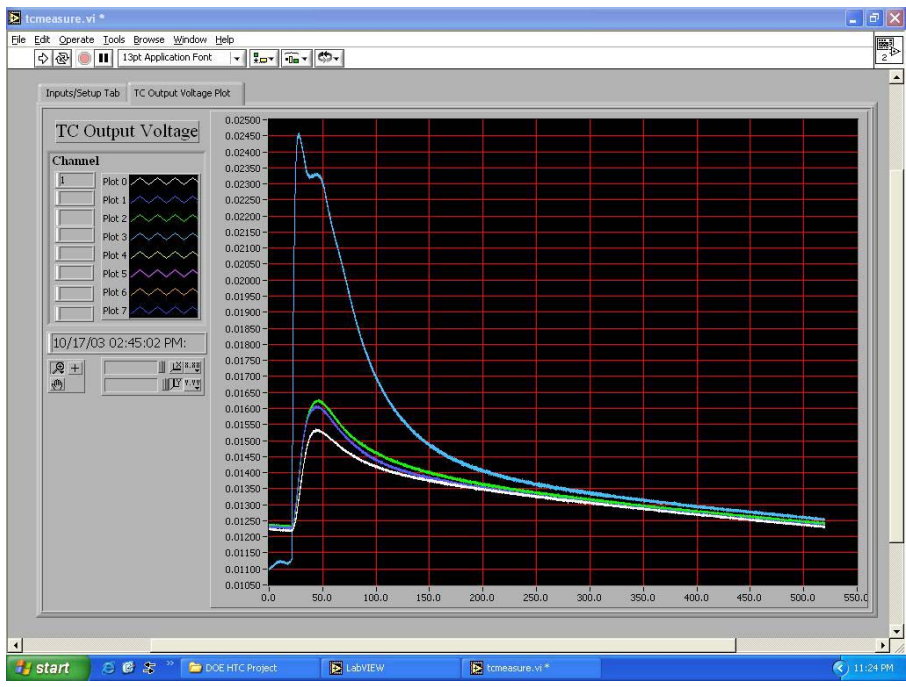
Figure 3.12 - Labview .vi Front Panel (Output Screen)
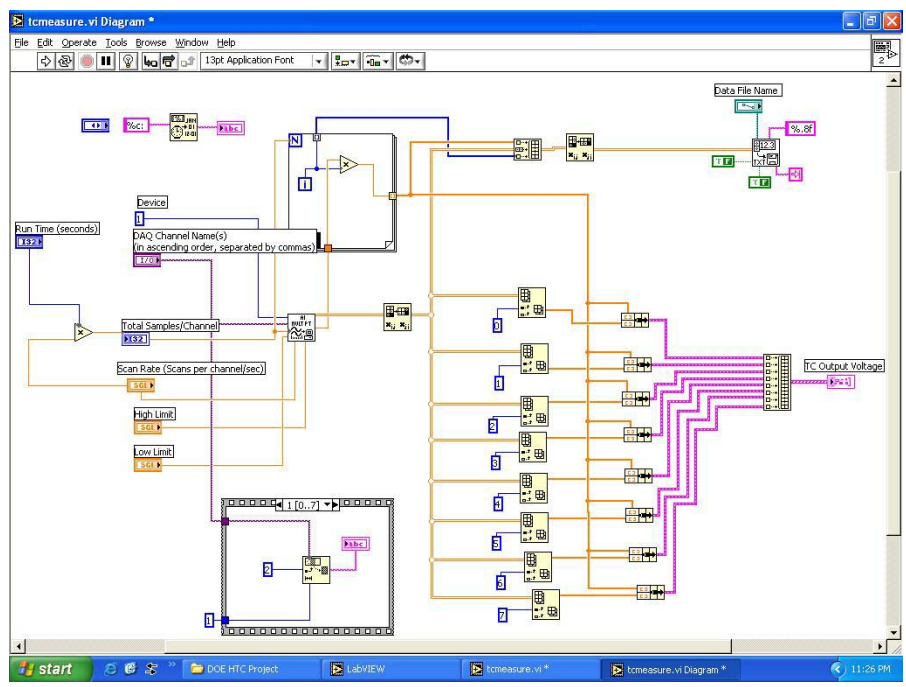
Figure 3.13 - Labview .vi Wiring Diagram

A356 Aluminum Pour Experimental Summary

A total of 12 separate experimental runs were conducted at Mississippi State University, producing three sets of temperature data for each run. Although only one internal mold temperature signal is necessary to estimate the boundary conditions, data from all three embedded thermocouples were recorded as backup data in the case of a channel malfunction or extreme error. The same basic procedure was followed for each experimental run and can be best described by a pre-pour and pour routine.

Pre-Pour Routine

An experimental run begins by placing the coated and instrumented mold into the mold carrier and connecting the thermocouple leads to the ceramic connectors on the side of the carrier. After checking thermocouple continuity, the mold is preheated to 315 C (600 F) in the resistance heated muffle furnace. Typical preheat duration is approximately 4 – 5 hours, with periodic monitoring of the mold temperature using a K-type thermocouple reader coupled to one of the three ceramic connectors on the mold carrier side. After initiating the mold preheat, A356 aluminum stock was removed from storage supply and placed into the melting furnace set at 800 C (1472 F) . A single casting required approximately 450 grams of A356, and enough metal was typically melted to pour 2 – 3 castings. While waiting for the mold to reach preheat temperature and the aluminum to melt, the sacrificial thermocouples for measuring the temperature within the casting were made for insertion into the casting cavity. The ice bath was prepared by filling the Styrofoam container with ice and water, the cold junction thermocouple was mounted in the center of the bath, and the lid was sealed. The PC and

DAQ system were then set up and a check run was conducted for each of the four thermocouple channels using a temporary test thermocouple to ensure that the system was functioning properly.

Pour Routine and Typical Temperature Data Set Produced

Figure 3.14 - Mold Carrier Removal Process (staged)

Once the aluminum is melted and the mold has reached the desired preheat, everything is ready to continue with the pour. The pre-heated mold is removed from the oven by two individuals using the welded leverage bar and placed in the metal pouring sand box as shown in Figure 3.14. As quick as possible, the four thermocouples are connected to the data acquisition system via the K-type ceramic connectors. All electrical equipment operating within the casting area, such as the oven, melting furnace, ventilation fan, and lights, is turned off in order to reduce the electrical noise in the data acquisition environment. The Labview .vi is then employed to collect about ten seconds

of internal mold temperature data. This short run provides a good idea of the preheat

temperature and a last check to ensure proper thermocouple function. Upon completion

of this short data collection segment, the molten aluminum is poured in a refractory ladle

and the melt temperature is collected using a hand held K-type digital thermocouple

reader. The target melt temperature for pouring is 699 – 704 C (1290 - 1300 F). Finally,

the Labview .vi is started, the molten aluminum is poured into the mold cavity, and data

is collected from 5 – 7 minutes, depending on user input. Once data collection has

completed, the cast plate is removed from the mold, and one or two additional castings

are poured in the same manner, replacing the sacrificial casting thermocouple with each

run. In the event that the mold preheat temperature is no longer sufficient, the mold can

be reheated in the oven for a short duration to obtain an adequate preheat temperature

before beginning the next run. A typical data set resulting from one experimental run is

shown as Figure 3.15.
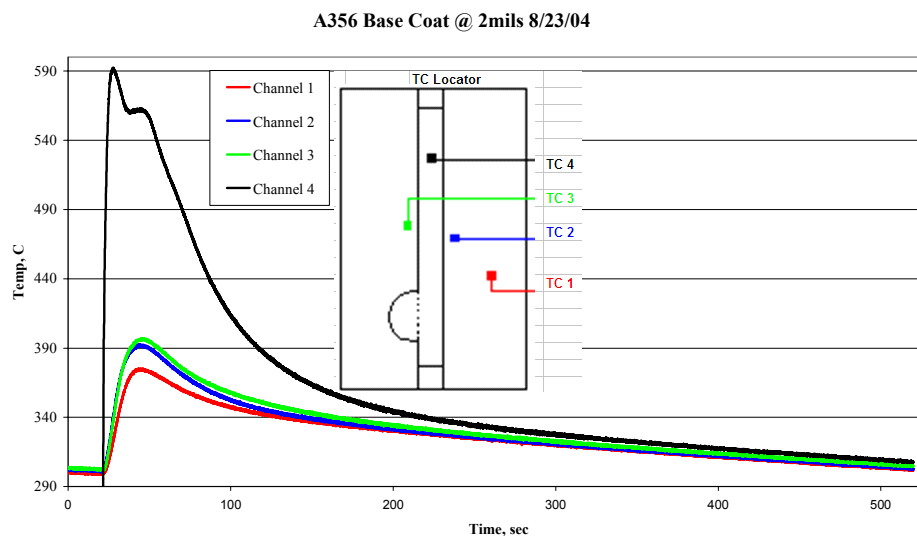
Figure 3.15 - Typical Temperature Data Set (8/23/2004)

CHAPTER IV

CORRECTING THERMOCOUPLE INSTALLATION INDUCED ERRORS

In Chapter II, a number of uncertainty components attributed to the installation of

an embedded thermocouple for steady-state as well as transient temperature measurement

were discussed.   The installation of an embedded thermocouple in a solid material was

shown to have the potential to induce significant errors in both magnitude and phase

(time) for transient temperature measurements. These errors tend to be of particular

significance when very accurate transient temperature measurements are required, such

as the type of measurement needed for accurate solution of an inverse conduction

problem.   These installation induced errors can be managed, however, if an appropriate

mathematical model representing the dynamic behavior of the measurement domain, as

well as the installed sensor, is developed. This type of method basically provides a

process through which the model of the system can be employed to "undo" the signal

deviation caused by the presence of the thermocouple sensor in the solid domain. The

accuracy of the reconstructed temperature data, therefore, depends greatly on how well

the model used in the reconstruction process represents the dynamic behavior of the real

life system, a solid medium surrounding an embedded thermocouple. It is important to

recognize that, since most models do not precisely replicate their real life counterpart,

some amount of uncertainty will remain in the reconstructed temperature data. The

objective of this procedure is to perform, in a sense, a calibration of the experimental

42

temperature data, so that afterward, the original uncertainty due to the installation effects of the embedded thermocouple are reduced to a much smaller model uncertainty. The goal of this chapter is to explain the method used in creating a heat conduction model to examine and adjust experimental temperature data for the measurement error associated with the presence of an embedded thermocouple within the solid medium.

Discussion of Intended Application

The application being examined for this thesis work is the permanent steel mold used in casting 1/2" thick aluminum plates described in detail in Chapter III. Due to the relatively large width and height of the mold cavity compared to the thickness, heat transfer is assumed to be predominant in the thickness direction, therefore one-dimensional heat transfer is assumed. Figure 4.1 shows a representative picture of the three-piece steel permanent mold and the assumed unidirectional heat transfer.

Due to symmetry in this heat transfer process, only one mold half, with and without an embedded thermocouple sensor, need be considered for modeling the system. Although obtaining a temperature history within a permanent mold is the application of motivation for the current research, other applications that behave as transient, one-dimensional systems as described above could also be investigated using similar methods.
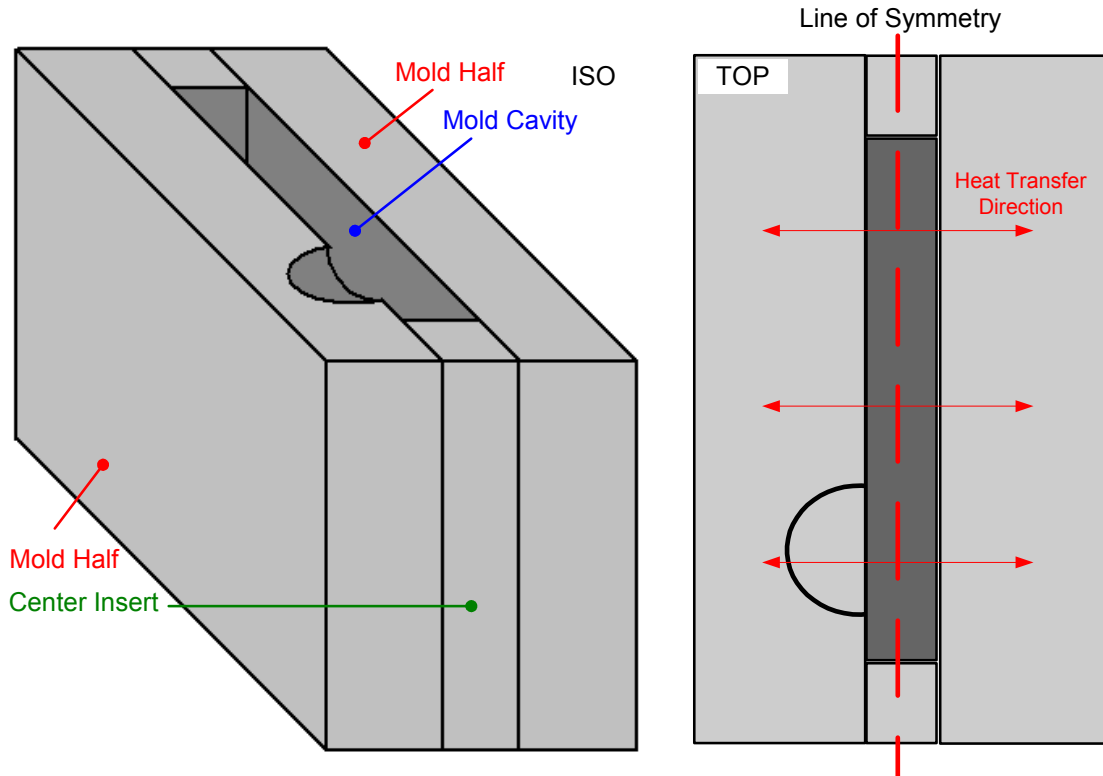
Figure 4.1 - Mold Showing Direction of Predominant Heat Flow

The system, without the temperature sensor yet installed, is basically a solid,

homogeneous block of material. It can be modeled as a basic, one-dimensional transient

heat conduction system with known initial condition. The boundary conditions are

specified as a time dependant heat flux on one surface and an insulated boundary (q_{out} =

0) on the back surface. The time dependent heat flux boundary condition is the result of

the semi-instantaneous pouring of molten aluminum into the mold cavity. The exterior

boundary condition is assumed as insulated, which is a good approximation when the

inside surface is exposed to a large heat flux while the outside surface is in contact with

air at rest [14]. The material properties for thermal conductivity (k), density (ρ), and

specific heat (c) are assumed to be temperature independent and the thermal diffusivity, α, is given as $\alpha = k/\rho \cdot c$. Figure 4.2 shows a graphical representation of the basic system. Equations (4.1) - (4.4) are the differential equation and initial/boundary conditions for this system.
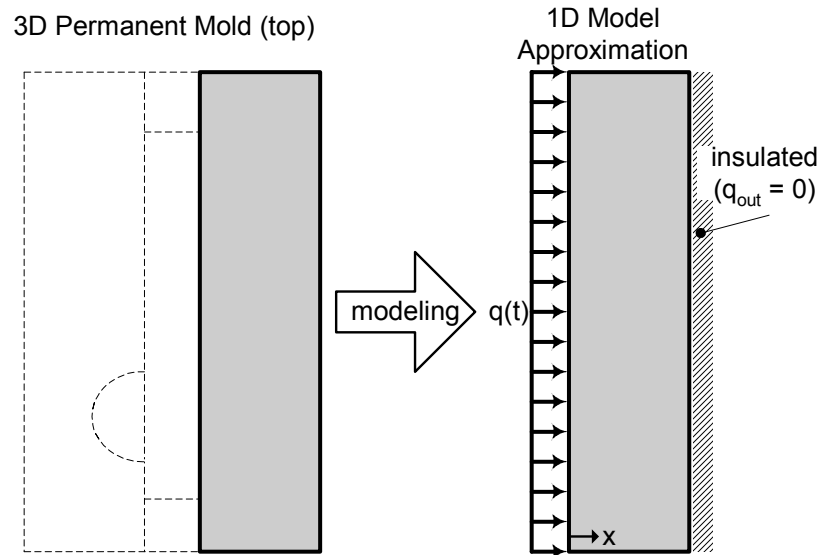
Figure 4.2 - Mold Half Model Description

$$\frac{1}{\alpha} \cdot \frac{\partial T}{\partial t} = \frac{\partial^2 T}{\partial x^2} \tag{4.1}$$

$$\begin{aligned} T(0, x) &= T_{initial} \\ 0 &\le x \le L \end{aligned} \tag{4.2}$$

$$-k\frac{\partial T}{\partial x}\bigg|_{x=0} = q(t) \quad t > 0 \tag{4.3}$$

$$\frac{\partial T}{\partial x}\bigg|_{x=L} = 0 \quad t > 0 \tag{4.4}$$

General Explanation of Current Modeling Research

The initial objective is to develop models that provide a good representation of the dynamic behavior of the system before and after the temperature sensor has been installed in the mold half. These models are referred to as the undisturbed and disturbed models, with respect to the temperature measurement errors at a point of interest induced by the installation of an embedded thermocouple. The first model constructed is the undisturbed model, where the thermocouple has not been installed. This model is able to predict an undisturbed temperature, considered as the "true" or theoretical temperature, at the location of interest. The second model, the disturbed model, is similar to the first model except that it also includes the dynamics of an embedded thermocouple installation at the location of interest. It is important to remember, as was discussed in Chapter II, the temperature registered by the embedded thermocouple is in error from the "true" temperature that should have been measured at the point of interest due to measurement uncertainty, of which a major contributor is the presence of the thermocouple sensor in the system. The reduction of the sensor installation induced uncertainty component in experimental temperature data, or the disturbed data, is accomplished through the use of a specific transfer function developed through the combination of the undisturbed and disturbed models, relating an estimated undisturbed temperature to an experimentally measured disturbed temperature.

The undisturbed model is used to determine the relationship between the "true" temperature at the point of interest and the applied boundary heat flux. The dynamics of a linear transient heat conduction system can be represented by its Laplace transform [5].

Therefore, a transfer function can be developed that captures the dynamics between the input heat flux and the output temperature at the point of interest. A simple graphical representation is shown in Figure 4.3.
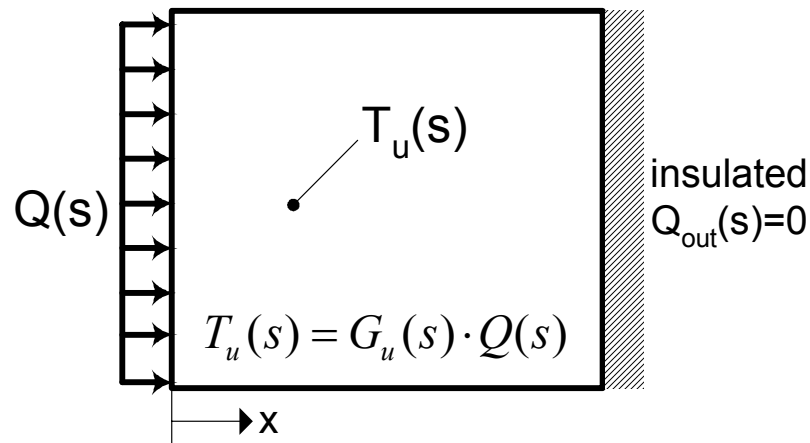
Figure 4.3 - Undisturbed System Transfer Function

The disturbed model is similar to the undisturbed model, with the addition of an embedded thermocouple installation. It is used, in turn, to determine the relationship between the temperature the thermocouple registers and the input boundary heat flux. The disturbed transfer function not only captures the characteristics of the domain medium, but also the additional response changes due to the thermocouple, thermocouple cavity, and any filler material. A simple graphical representation of the disturbed system is shown in Figure 4.4.
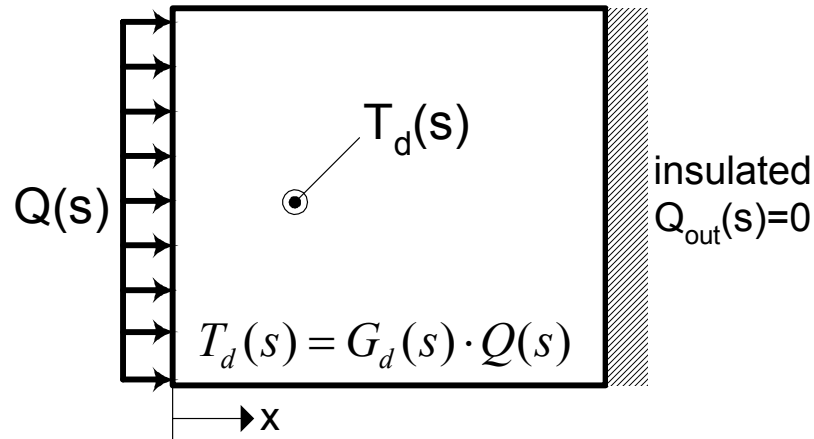
Figure 4.4 - Disturbed System Transfer Function

Once the undisturbed and disturbed transfer functions have been developed, a relationship can be derived relating a disturbed temperature to an undisturbed temperature for a common heat flux input. A new transfer function can be developed to describe this relationship as shown in Equations (4.5) - (4.7).

$$T_u(s) = \frac{G_u(s)}{G_d(s)} \cdot T_d(s) \tag{4.5}$$

$$\therefore \quad T_u(s) = G(s) \cdot T_d(s) \tag{4.6}$$

where
$$G(s) = {G_u(s)} \big/ {G_d(s)} \tag{4.7}$$

Equation (4.6) summarizes the general concept of being able to collect experimental temperature data, and then filter that data through the transfer function of Equation (4.7) to recover predicted temperature data that has been relieved of much of the uncertainty due to the thermocouple installation. This embedded thermocouple correction (ETC) transfer function takes into account the changes in system dynamics

caused by the presence of the thermocouple in the solid medium. It accepts as an input experimentally measured temperature data and adjusts it to reflect predicted temperature values that likely would have been collected were it not for the disturbances caused by the sensor installation.

Development of Control Volume Type Models for the Current Research

To begin the process of developing the transfer function relations mentioned above, models for the undisturbed and disturbed cases were first developed. Numerical Heat Transfer and Fluid Flow by S. V. Patankar [36] was the key reference used to discretize each model into a partitioned, control volume type heat transfer system. Both the undisturbed and disturbed system models were divided into non-overlapping, finite control volumes over their entire domain. Using the structuring in Patankar [36], a state variable equation was developed for each control volume describing the interaction with, and contribution to, the surrounding neighbor control volumes. The result is a set of first order differential equations in time of the temperature state for each control volume. The temperature state for a particular control volume is assumed to be constant over that control volume for each instant in time. The undisturbed model is a simple model of the entire conducting medium of interest with no thermocouple embedded within the medium at the point of interest. The disturbed model is essentially the undisturbed model linked to an additional senor sub-model that simulates the effects of the installation of an embedded thermocouple at a specified geometric location.

Undisturbed Model Development

The embedded thermocouple application under investigation for this thesis is the determination of the temperature history at a specific location within a mold half after metal pouring. This process was assumed to be a one-dimensional transient heat conduction process and Figure 4.2 visually explained the approximation of the three-dimensional mold half as a one-dimensional model. Therefore, the undisturbed model is created as a conducting medium with one-dimensional transient heat transfer capabilities. The differential equation describing the undisturbed system is same shown as Equation (4.1) with the specified boundary and initial conditions in Equations (4.2) - (4.4).

The one-dimensional undisturbed model is converted to a discretized system of control volumes following Patankar [36] as a guide. Each control volume in the discretized system has a node positioned at its center that is assigned a temperature state. The control volumes are Δx units thick and considered to have identical, constant cross-sectional areas normal to each of them. The distance between adjacent temperature nodes is given as δx, and for the current research, a uniform grid was instated, in effect equating Δx to δx. Boundary nodes are considered to be located at the geometric center of zero-thickness control volumes, $\Delta x = 0$, adjacent to the discretized domain. Therefore, the distance between a boundary node and the adjacent temperature node becomes half the distance δx.

Procedure for the Discretization of the Undisturbed Model

In an effort to explain the method used in developing the state equations for the undisturbed model, a simplified example is presented with a time dependant heat flux at

one boundary and an insulated boundary at the other. Figure 4.5 illustrates the example

case where the domain is divided uniformly into four, equally spaced control volumes of

Δx thickness. The example contains four temperature nodes located at the geometric

centers of the control volumes and two additional boundary condition nodes located at

the boundary surfaces.   Dotted lines represent the control volume boundaries.
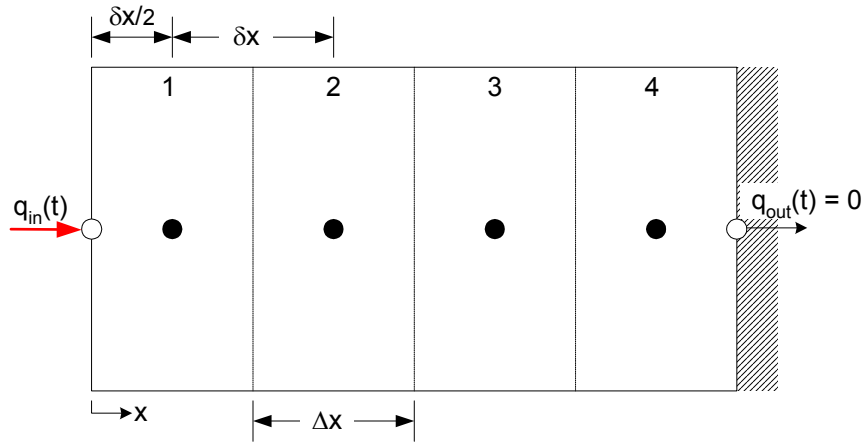
Figure 4.5 - Sample Discretization Scheme: Undisturbed Model

An energy balance can be performed for each control volume in the system to develop a

set of four state equations, one for each temperature node. To begin, the energy balance

is executed on control volume one as follows:

$$E_{in} - E_{out} = E_{stored} \tag{4.8}$$

where
$$E_{in} = q(t) \cdot A \tag{4.9}$$

and
$$E_{out} = -kA\frac{\partial T}{\partial x} = \frac{kA}{\delta x}(T_1 - T_2) \tag{4.10}$$

and
$$E_{stored} = \rho c V \frac{dT_1}{dt} = \rho c A \Delta x \cdot \dot{T}_1 \tag{4.11}$$

Substituting Equations (4.9) - (4.11) into Equation (4.8) and simplifying yields

$$\dot{T}_1 = \left(\frac{k}{\rho c \, \delta x \Delta x} \right) \cdot (T_2 - T_1) + \frac{q(t)}{\rho c \Delta x} \tag{4.12}$$

Control volumes two and three are internal and therefore have a slightly different form from the control volumes at the boundary. The energy balance for control volume two is conducted as follows:

$$E_{in} - E_{out} = E_{stored} \tag{4.13}$$

where

$$E_{in} = kA \frac{\partial T}{\partial x} = \frac{kA}{\delta x}(T_1 - T_2) \tag{4.14}$$

and

$$E_{out} = -kA \frac{\partial T}{\partial x} = -\frac{kA}{\delta x}(T_2 - T_3) \tag{4.15}$$

and

$$E_{stored} = \rho c V \frac{dT_2}{dt} = \rho c A \Delta x \cdot \dot{T}_2 \tag{4.16}$$

Substituting Equations (4.14) - (4.16) into Equation (4.13) and simplifying yields:

$$\dot{T}_2 = \left(\frac{k}{\rho c \, \delta x \Delta x} \right) \cdot (T_1 - 2T_2 + T_3) \tag{4.17}$$

And similarly for control volume three, the form would be developed as:

$$\dot{T}_3 = \left(\frac{k}{\rho c \, \delta x \Delta x} \right) \cdot (T_2 - 2T_3 + T_4) \tag{4.18}$$

Therefore, a generalized state equation for any internal control volume, n, could be shown as follows:

$$\dot{T}_n = \left(\frac{k}{\rho c \, \delta x \Delta x} \right) \cdot (T_{n-1} - 2T_n + T_{n+1}) \tag{4.19}$$

The fourth control volume for the example includes the second boundary condition. It will have a state equation similar to that of the first, except that it is bounded by an insulated exterior face, meaning that the heat flux out of the control volume is zero, resulting in the following state equation:

$$\dot{T}_4 = \left(\frac{k}{\rho c \, \delta x \Delta x} \right) \cdot (T_3 - T_4) \tag{4.20}$$

The four resulting state equations can be combined and written in matrix form as follows:

$$\begin{bmatrix} \dot{T}_1 \\ \dot{T}_2 \\ \dot{T}_3 \\ \dot{T}_4 \end{bmatrix} = \left(\frac{a}{b} \right) \cdot \begin{bmatrix} -1 & 1 & 0 & 0 \\ 1 & -2 & 1 & 0 \\ 0 & 1 & -2 & 1 \\ 0 & 0 & 1 & -1 \end{bmatrix} \begin{bmatrix} T_1 \\ T_2 \\ T_3 \\ T_4 \end{bmatrix} + \left(\frac{1}{b} \right) \cdot \begin{bmatrix} 1 & 0 \\ 0 & 0 \\ 0 & 0 \\ 0 & 1 \end{bmatrix} \cdot \begin{bmatrix} q_{in}(t) \\ q_{out}(t) = 0 \end{bmatrix} \tag{4.21}$$

where $\qquad a = \dfrac{k}{\delta x} \quad$ and $\quad b = \rho \cdot c \cdot \Delta x \tag{4.22}$

Equation (4.21) can be written in the more concise form of Equation (4.23) as shown.

$$\dot{T} = A \cdot T + B \cdot Q \tag{4.23}$$

The system matrix developed exhibits a tri-diagonal pattern that is easily extendable to any number of desired control volumes. For the current research, a simple code was developed within MATLAB to construct the system matrix, A, according to user defined material properties, number of control volumes, n, and control volume thickness Δx.

Disturbed Model Development

The disturbed model is developed to simulate the heat transfer through the mold half as in the undisturbed model, with the addition of a simulated embedded thermocouple installation. As discussed in Chapter II, the installation of a thermocouple into a solid material causes localized distortions in the temperature field around the

installation site. For that reason, an "extended thermocouple sensor" sub-model was created that includes the thermocouple, thermocouple cavity, and a localized region of the medium of interest where the temperature field is affected by the presence of the thermocouple. Because the distortion caused by the thermocouple installation only occurs in a localized region around the cavity, the sensor sub-model only characterizes a small part of the total domain. The thermal field is undistorted for the remainder of the domain sufficiently distant from the installation location [15, 20-22, 28]. Thus, the majority of the system behaves just as it did previously in the undisturbed case, and can continue to be represented by the undisturbed model. As a result, the model of the disturbed system is constructed through a controlled combination of the sensor sub-model with the undisturbed model.

Sensor Sub-model Development

The sensor sub-model was developed to approximate the distortion imparted on the system due to the thermocouple installation. In practice, the actual thermocouple cavity is a cylindrical hole drilled to a depth from the top of the mold half. Ideally the thermocouple bead is in contact with the base of the cavity, where it should obtain a temperature measurement. In Chapter II, disturbances to the local thermal field around the cavity due to differing thermal properties of the thermocouple and filler material in the cavity, as well as heat loss through the thermocouple leads were discussed. For the sensor sub-model, the errors induced by the differences in material properties were the focal point, and any heat lost through the leads was neglected. Due to the radial attributes of a thermocouple installation, the sensor sub-model is designed to represent a circular

region of a specified area including the thermocouple cavity contents and the area of parent material where the thermal field is disturbed. This plane on which the sensor sub-model lies is assumed to pass through the base of the thermocouple bead and cavity. As discussed by Attia et. al [15, 20-22], there are end effects associated with cylindrical cavities in solids. However, for this model the distortion was assumed be two dimensional, and therefore end effects were not considered.

The sensor sub-model was constructed in two-dimensional polar coordinates to represent the heat conduction in the thermally disturbed region centered about the thermocouple installation site. The governing differential equation for two-dimensional transient heat conduction in polar coordinates is shown as Equation (4.24).

$$\rho c \cdot \frac{\partial T}{\partial t} = \frac{1}{r} \cdot \frac{\partial}{\partial r}\left(rk \cdot \frac{\partial T}{\partial r}\right) + \frac{1}{r} \cdot \frac{\partial}{\partial \theta}\left(\frac{k}{r} \cdot \frac{\partial T}{\partial \theta}\right) \tag{4.24}$$

$$T(0, r, \theta) = T_{initial} \tag{4.25}$$

$$T(t, r_{max}, \theta) = T_{boundary} \tag{4.26}$$

The two dimensions are seen to be r, the radial distance from the origin at the center, and θ, the angular distance. This equation can be discretized in a manner similar to the energy balance methods used for the undisturbed model in Cartesian coordinates.

Figure 4.6 displays a discretized polar coordinate system in r and θ, where the control volume around temperature node P is considered. The control volumes are specified and then a temperature node is assigned at the geometric center of each control volume. Neighboring nodes and control surfaces are labeled with the compass directions

of north, south, east, and west with respect to the node of interest, P. Uppercase letters

represent nodes and lowercase the control volume boundary surfaces.
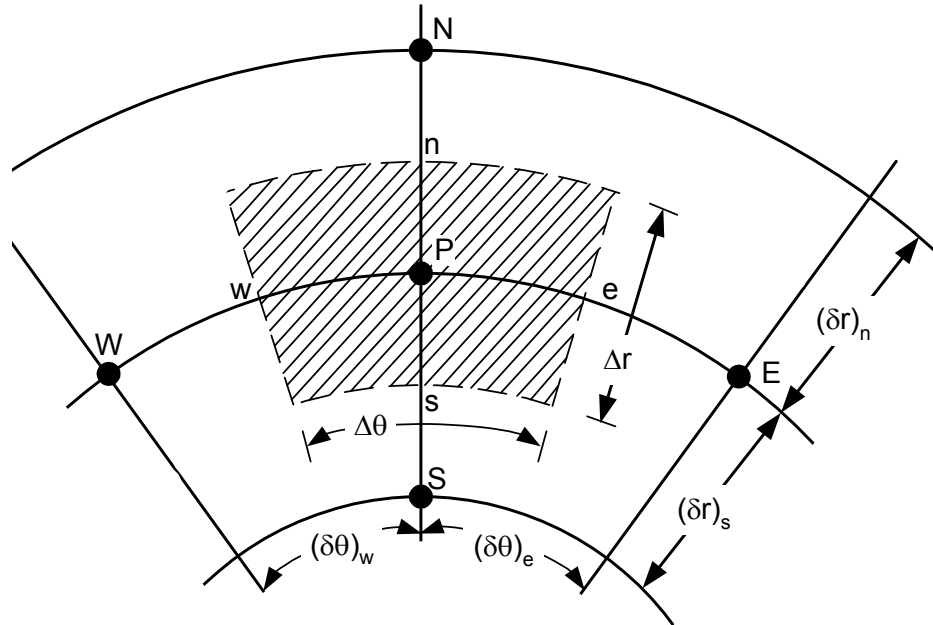
Figure 4.6 - Discretization Scheme: Sensor Sub-model Interior Nodes

Equation (4.27) presents the discretized form of Equation (4.24), presented by

Patankar [36], for a control volume surrounding node P, where T_x is the temperature of

the control volume containing node x.

$$a_P \cdot T_P = a_N T_N + a_S T_S + a_E T_E + a_W T_W + a_P^0 T_P^0 \qquad (4.27)$$

T_p is the control volume under consideration and the superscript of zero is a time index

representing the previous time step (with regard to the non-superscripted temperatures).

The other terms are geometrical and material property driven parameters for the

neighboring nodes given by Equations (4.28) - (4.33).

$$a_N = \frac{k_n r_n \Delta\theta}{\delta r_n} \qquad (4.28)$$

$$a_S = \frac{k_s r_s \Delta\theta}{\delta r_s} \qquad (4.29)$$

$$a_E = \frac{k_e \Delta r}{r_e \cdot \delta\theta_e} \qquad (4.30)$$

$$a_W = \frac{k_w \Delta r}{r_w \cdot \delta\theta_w} \qquad (4.31)$$

$$a_P^0 = \frac{\rho c \Delta V}{\Delta t} \qquad (4.32)$$

$$a_P = a_N + a_S + a_E + a_W + a_P^0 \qquad (4.33)$$

Substituting the above equations into the Equation (4.27) and performing some minor manipulation results in the rate equation for the control volume around node P as shown as Equation (4.34).

$$\frac{(T_P - T_p^0)}{\Delta t} = \frac{1}{\rho c \Delta V}\left[-(a_N + a_S + a_E + a_W)\cdot T_P + a_N T_N + a_S T_S + a_E T_E + a_W T_W\right] \qquad (4.34)$$

Rewriting the time derivative and re-casting several variables for simpler presentation yields the following state equation, (4.35), for the control volume containing node P.

$$\dot{T}_P = \frac{1}{\Gamma}\cdot(\Theta \cdot T_P + a_N T_N + a_S T_S + a_E T_E + a_W T_W) \qquad (4.35)$$

where $$\Theta = -(a_N + a_S + a_E + a_W) \qquad (4.36)$$

and $$\Gamma = 1/\rho c \Delta V \qquad (4.37)$$

This procedure was used to develop the state equation for each of the interior control volumes contained in the sensor sub-model.
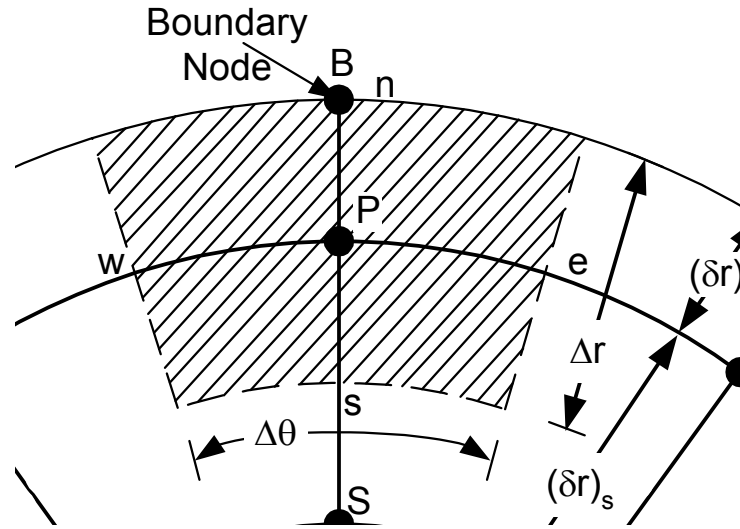
Figure 4.7 - Discretization Scheme: Sensor Sub-model Boundary Nodes

Development of rate equations for the boundary control volumes is only slightly different from that of interior control volumes. Figure 4.7 presents a graphic displaying a control volume at the boundary of the sensor sub-model. Boundary inputs are controlled through the assignment of a "zero-volume" control volume containing a boundary node B at the boundary. The temperature at node B, T_B, is a known sub-model input at a "northern" control volume face. Similar boundary input nodes will occur radially around the sub-model for each control volume at the boundary. The state equation for a control volume at temperature T_P at is shown as Equation (4.38).

$$\dot{T}_P = \frac{1}{\Gamma}(\Theta_B \cdot T_P + a_B T_B + a_S T_S + a_E T_E + a_W T_W) \tag{4.38}$$

$$\Theta_B = -(a_B + a_S + a_E + a_W) \tag{4.39}$$

$$\Gamma = 1/\rho c \Delta V \tag{4.40}$$

$$a_B = \frac{k_b r_b \Delta\theta}{\delta r_b} \qquad (4.41)$$

Comparing the state equation for an internal control volume to the one for a boundary control volume, it is seen that the parameters for a typical internal neighboring control volume to the "north" shown in (4.35) are simply replaced the with the parameters for the boundary node in (4.38).

A system of first order differential equations is developed through the determination of the state equation for each control volume within the sensor sub-model. As was done for the undisturbed model, this set of differential equations can also be written in matrix form where $\dot{T}$ is a vector of temperature rates, T is a vector of temperature states, T_B is a vector of input boundary temperatures, and A_s and B_s are the sensor sub-model system and input location matrices, respectively, shown as Equation (4.42).

$$\dot{T} = A_s \cdot T + B_s \cdot T_B \qquad (4.42)$$

The form of the system matrix A_s will depend on the numbering scheme used for labeling the control volumes, which determines how the equations are combined into matrix form. A MathCAD worksheet, included in the Appendix B.1, was developed to determine a sensor sub-model system matrix, A_s, and input location matrix, B_s, based on user defined parameters for importation into MATLAB.

"Installing" the Sensor Sub-model to Create the Disturbed Model

To create the disturbed model, the sensor sub-model is "installed" onto the undisturbed model. This "installation" occurs through the linking of the sensor sub-model boundary temperature nodes to user specified temperature nodes within the undisturbed model. In this way, the boundary nodes of the sub-model assume the temperature of the node in the undisturbed model to which they are linked. As a result, the sensor sub-model can be driven by a heat flux input applied to the undisturbed model. The disturbed model construction is finalized through this linking of the two models as described. The input to the disturbed model is the same heat flux as to the undisturbed model. The output is the temperature at the center node of the sensor sub-model, which through the linking, is position in the same geometric location as the undisturbed output temperature. The advantage of having a separate sensor sub-model is that the "thermocouple installation" can be simulated at any user defined distance from the boundary where the heat flux is applied by simply altering the nodes where the sensor sub-model is linked. Figure 4.1 shows a graphical illustration of the undisturbed and disturbed models lying in the plane cut through the mold half in which they simulate the heat diffusion process.
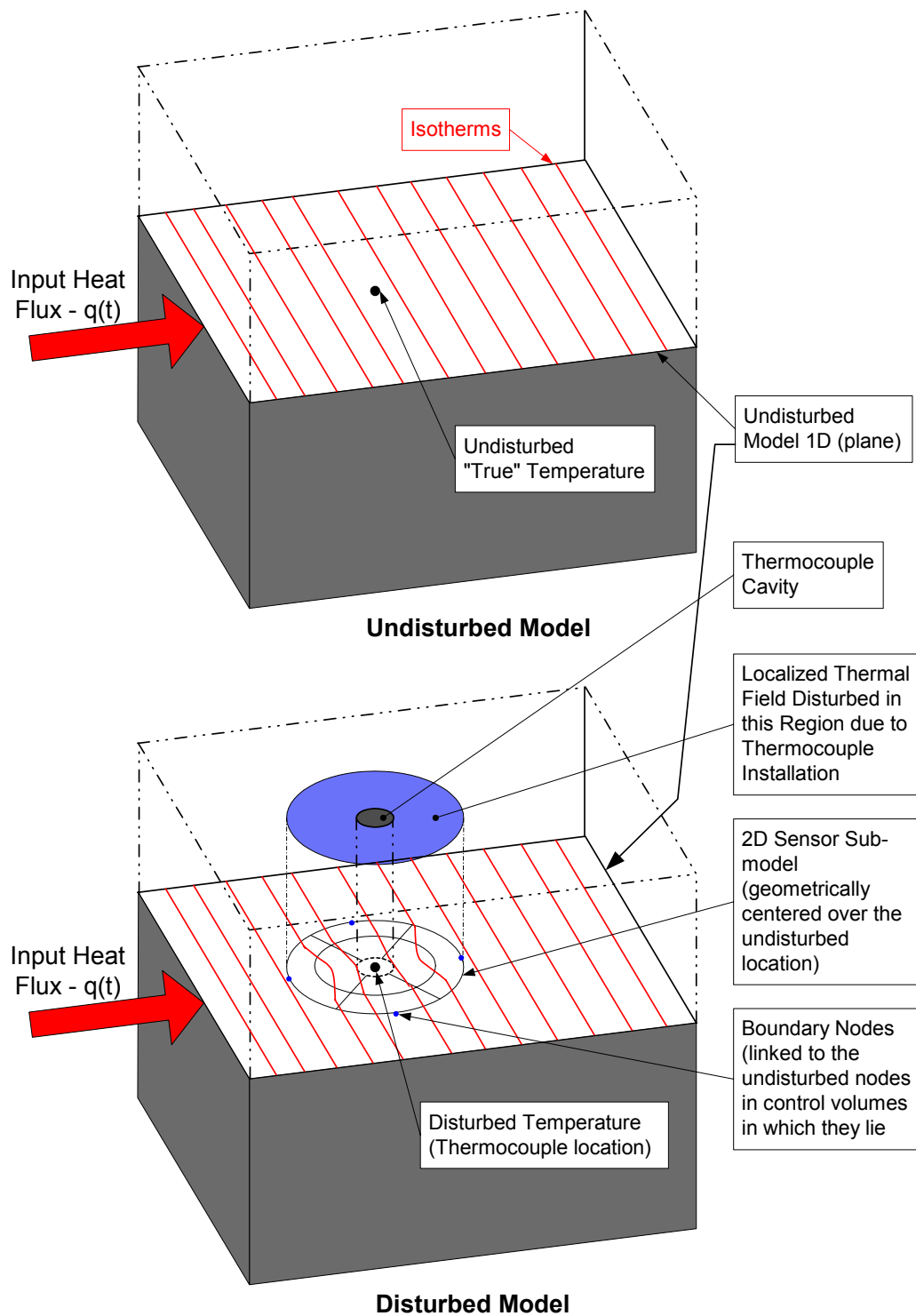
Figure 4.8 - Undisturbed and Disturbed Model Visualizations

Development of the Required Transfer Functions using MATLAB

Dynamic System Modeling Capabilities of MATLAB

MATLAB, a software package by The Mathworks Inc., was employed as the computational tool for developing and manipulating the various mathematical models described for the current research. MATLAB's Control System Toolbox was particularly valuable during model development because of the variety of system modeling and analysis functions that are readily available within it. This toolbox is specifically designed for the construction of models of linear time-invariant dynamical systems in a variety of model representations, with the ability to painlessly translate from one model representation to the next. The two model representations that were utilized for the current research were the state-space (SS) and transfer function (TF) representations. State-space models for MATLAB are presented as Equations (4.43) and (4.44).

$$\frac{dx}{dt} = A \cdot x + B \cdot u \qquad (4.43)$$

$$y = C \cdot x + D \cdot u \qquad (4.44)$$

A and B are system matrices of appropriate dimension, C and D are the output selection matrices of appropriate dimension, x is the state vector, and y and u are the output and input vectors, respectively. Transfer function representations in MATLAB take a form of

the Laplace transform of the system, represented by Equation (4.45), where num(s) and den(s) are the numerator and denominator polynomials of the transfer function respectively.

$$G(s) = \frac{num(s)}{den(s)} \qquad (4.45)$$

The undisturbed model and sensor sub-model were both developed as control volume type models with systems of state equations describing each model. The system matrices for each of these models are developed through expressing the defining sets of state equations in matrix form. The system matrices correspond to the A and B matrices in Equation (4.43) above are required for creation of a MATLAB state-space system. The observer vector, C, for the undisturbed model is a vector that selects the user defined temperature node (state) of interest within the modeled domain as the output. For the sensor sub-model, the C_s vector selects the center node, taken as the position of the thermocouple within the sub-model. For both models, the D matrix is zero. The MATLAB program created performs the various calculations necessary for the development of the system matrices necessary for the creation of the undisturbed and disturbed models. This MATLAB program is presented in line by line form in the Appendix B.2.

Creating the Undisturbed System using MATLAB

Using the MATLAB program developed, the undisturbed model and transfer function can be easily developed. Upon running the program in MATLAB with the user

supplied output temperature node, material properties and geometric parameters, state-space and transfer function representations for the undisturbed system are developed.

Creating the Disturbed System using MATLAB

The disturbed model development is slightly less straight-forward than that of the undisturbed. First, the system matrices, A_s and B_s, for the sensor sub-model must be assembled according to the user prescribed material properties and control volume size parameters. The MathCad worksheet shown in the Appendix B.1 performs the assembly of the sensor sub-model system matrices. After assembly in MathCad, the matrices can be imported into the MATLAB program. This one program contains the code necessary for the construction of not only the disturbed model, but the undisturbed model as well. To generate the disturbed model, the undisturbed model and sensor sub-model must be linked. This is accomplished through the combination of several intermediate transfer functions to achieve the final disturbed system transfer function.

For the current configuration, six intermediate transfer functions are required to link the sensor sub-model to the undisturbed model and develop the disturbed system transfer function. The first three transfer functions relate three distinct nodal temperatures within the undisturbed model to the input heat flux. The three temperature nodes are the undisturbed temperature of interest, T_u, and two other nodes that will be linked to the sensor sub-model. For convenience, the two additional nodes are labeled T_{up} and T_{dwn}, the "upstream" and "downstream" nodes with respect to the heat flow through the node of interest.   Equations (4.46) - (4.48) are the first three intermediate

transfer functions that are developed. Figure 4.9 is a graphical representation presenting

block diagrams for the first three transfer functions obtained from the undisturbed model.

$$T_u(s) = G_u(s) \cdot Q(s) \tag{4.46}$$

$$T_{up}(s) = G_{upq}(s) \cdot Q(s) \tag{4.47}$$

$$T_{dwn}(s) = G_{dwnq}(s) \cdot Q(s) \tag{4.48}$$
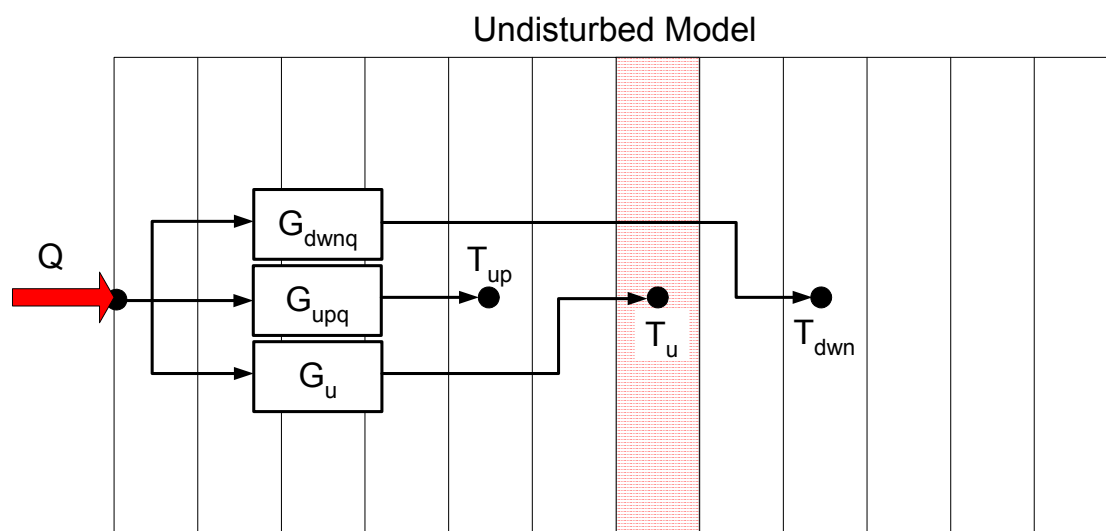
Undisturbed Model

Figure 4.9 - Undisturbed Model Transfer Functions
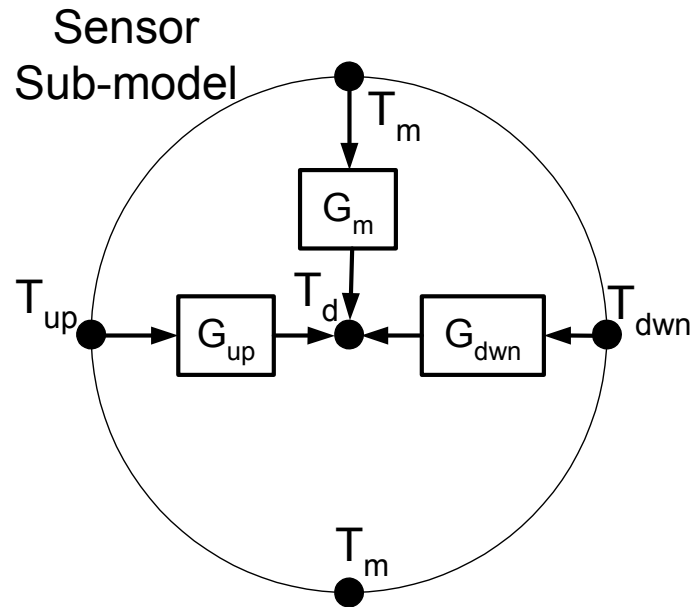
Figure 4.10 - Sensor Sub-model Transfer Functions

The three remaining transfer functions necessary to form the undisturbed model are obtained from the sensor sub-model as shown in Figure 4.10. Although, there are four boundary nodes, only three are distinct temperature input nodes because both the nodes labeled as T_m, for "middle", will be driven by the undisturbed temperature, T_u. This is because, when superimposed over the undisturbed model, both T_m nodes will lie within the same control volume, the one in which the undisturbed temperature node lies. Equations (4.49) - (4.51) show the three transfer functions developed that relate an input boundary temperature to a output disturbed temperature, T_d, in the sensor sub-model.

$$T_m(s) = G_m(s) \cdot T_d(s) \tag{4.49}$$

$$T_{up}(s) = G_{up}(s) \cdot T_d(s) \tag{4.50}$$

$$T_{dwn}(s) = G_{dwn}(s) \cdot T_d(s) \tag{4.51}$$
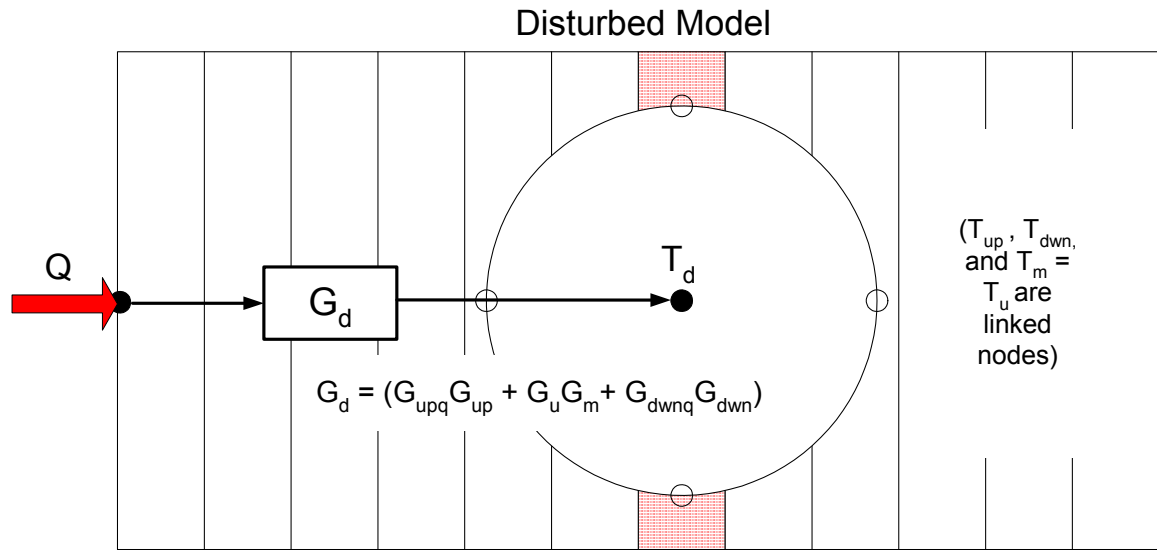
Figure 4.11 - Disturbed Model Transfer Function

Figure 4.11 displays a graphic depicting the "installation" of the sensor sub-model into the undisturbed model to create the disturbed model. Equations (4.46) - (4.51) are combined to develop the expression for the disturbed system transfer function relating a disturbed temperature to an input heat flux, shown as Equation (4.52).

$$T_d(s) = G_d(s) \cdot Q(s) \tag{4.52}$$

where the disturbed transfer function, $G_d(s)$, in its expanded form is Equation (4.53).

$$G_d(s) = G_{upq}(s) \cdot G_{up}(s) + G_u(s) \cdot G_m(s) + G_{dwnq}(s) \cdot G_{dwn}(s) \tag{4.53}$$

The development and combination of the six intermediate transfer functions, Equations (4.46) - (4.51), to obtain the disturbed system transfer function, as well as the development of the undisturbed transfer function is performed conveniently by same single program created in MATLAB.

Developing the Embedded Thermocouple Correction (ETC) Transfer Function

After the undisturbed and disturbed transfer functions are developed, one additional transfer function is necessary. The embedded thermocouple data correction (ETC) transfer function can be found by combining Equations (4.46) and (4.52) for the undisturbed and disturbed systems. Solving for the common heat flux input and equating the two yields a transfer function, G(s). The last transfer function created is shown as Equation (4.54).

$$T_u(s) = G(s) \cdot T_d(s) \qquad (4.54)$$

This transfer function describes the final desired system, where an input of disturbed temperature produces an output of undisturbed temperature. This data correction transfer function can now be used in MATLAB to dynamically adjust experimentally measured temperature data to recover estimated temperature data in which the effects of embedded thermocouple installation have been removed.

CHAPTER V

ADJUSTING DATA FOR EMBEDDED THERMOCOUPLE INDUCED ERRORS:
RESULTS AND DISCUSSION

The MATLAB program (in Appendix B.2) creates the embedded thermocouple correction (ETC) transfer function, G(s), from basic user defined material properties and geometries through the methodology described in Chapter IV. Once the ETC transfer function is obtained for a given system, embedded thermocouple data from that system can be adjusted to remove the portion of the error due to the difference of sensor installation material properties. The motivating problem for the current research is that of embedded temperature measurements within a low carbon steel mold during a casting process, but other similar transient conduction processes could also be handled in the same manner.

Required User Inputs

Sensor Sub-model Inputs (from MathCAD Worksheet)	
ntc	# of control volumes (#)
A_s	System Matrix
B_s	Input Location Matrix
nu	Node upstream (#)
nd	Node downstream (#)
Undisturbed Model Inputs	
k	thermal conductivity (W/m-K)
rho (ρ)	density (kg/m^3)
cp	specific heat (J/kg-K)
n	# of control volumes (#)
Dx (Δx)	Control volume thickness (m)
dx (δx)	Distance between nodes (m)
node	Node of interest (#)

INPUT

MATLAB Program

OUTPUT

Embedded Thermocouple Data Correction TF

G(s)

Figure 5.1 - Input/Output Diagram for MATLAB ETC Program

Example Cases for Embedded Thermocouple Data Correction

Figure 5.1 shows a block diagram outlining the user inputs required in order to

determine a ETC transfer function, G(s), for a system. In addition to this data correction

transfer function, the MATLAB program also creates the transfer functions that contain

the dynamic characteristics of the undisturbed and disturbed systems as defined in

Chapter IV. Several examples will now be presented and discussed to demonstrate the

usefulness of the embedded thermocouple data correction procedure. Results will be

presented in graphical form and discussed. The four example cases presented are

described in Table 5.1.

Table 5.1 - Example Cases Using ETC Process

Case		Description	Purpose
1		Comparison of undisturbed model to semi-infinite analytical solution	Validation of Undisturbed Model
2		Comparison of undisturbed & disturbed responses when no dissimilar materials are used in sensor sub-model	Validation of Disturbed Model
3	a	Correction of generated disturbed thermocouple data (noiseless) with G(s)	Validation of ETC Transfer Function (low diffusivity filler)
	b	Correction of generated disturbed thermocouple data (noiseless) with G(s)	Validation of ETC Transfer Function
	c	Correction of generated disturbed thermocouple data (noisy) with G(s)	Validation of ETC Transfer Function for use with noisy data
	d		
4		Comparison of estimated boundary heat flux from generated disturbed and recovered temperature responses using SVD [7, 37] model reduction methods	Confirmation of the necessity for correction of temperature data

For all the example cases, a block of low carbon steel was considered as the

undisturbed model (and as the parent material for the disturbed model). The block was

specified to have a thickness of approximately 1.5 inches, except as noted in Case 1.

Case 3a presents a scenario in which a low diffusivity material, paraffin wax, is used as

the filler in the thermocouple cavity. Non-moving air was assumed to fill the

thermocouple cavity for the simulations presented in Cases 3b – 3d and Case 4. The

undisturbed temperature of interest within the block for all cases was taken as node 7,

which is approximately 5 mm from the boundary surface where the heat flux is applied.

A constant input heat flux of 30 W/m^2 was used for Case 1 and Figure 5.2 shows the time

dependant input heat flux that was used for Cases 2, 3, and 4. The back boundary surface

was insulated for all cases. For each case where it was utilized, an outer diameter of 9

mm and thermocouple cavity diameter of 3 mm were specified for the sensor sub-model.

The material properties and geometrical parameters used throughout the example cases

are shown in Table 5.2 as they apply.
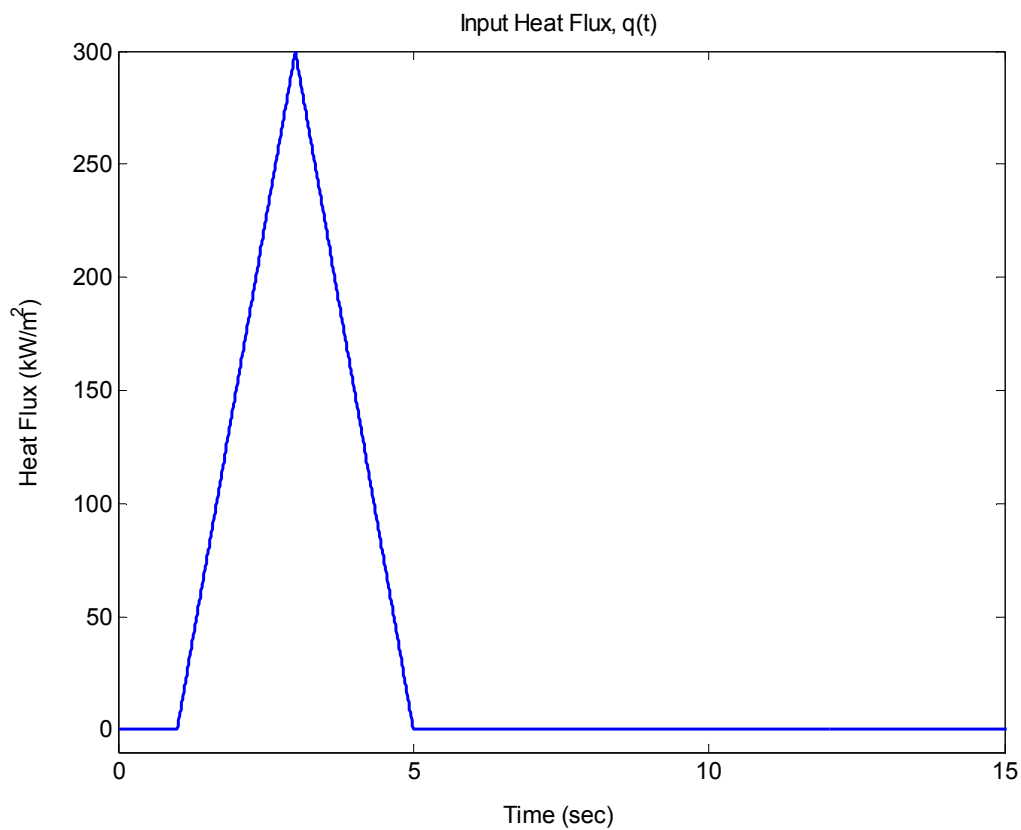
Figure 5.2 - Heat Flux Input for Case 2, 3, and 4

Table 5.2 - Material Properties, Geometries, and Other Parameters Used for Cases

Parameter	Description	Value	Case Used
Undisturbed Model Geometry			
n	Number of control volumes (undisturbed)	51	2 - 4
node	Node of interest number	7	All
nu	Upstream node number	1	2 - 4
nd	Downstream node number	13	2 - 4
Dx	Control volume spacing	0.75 mm	All
dx	Nodal spacing	0.75 mm	All
Sensor Sub-model Geometry			
ntc	Number of control volumes (sensor)	17	2 - 4
Δr	Radial distance between c.v. faces	0.5 mm	2 - 4
δr	Radial distance between nodes	0.5 mm	2 - 4
$\Delta\theta$	Angular distance between c.v. faces	90 deg	2 - 4
$\delta\theta$	Angular distance between nodes	90 deg	2 - 4
Material Properties			
AISI 1010 Low Carbon Steel @ 300K - "parent material"			
k	Thermal conductivity of low carbon steel	63.9 W/m-K	3a
rho	Density of low carbon steel	7832 kg/m^3	3a
cp	Specific heat of low carbon steel	434 J/kg-K	3a
Paraffin Wax @ 300K – "thermocouple cavity filler")			
kp	Thermal conductivity of paraffin	0.24 W/m-K	3a
rhop	Density of paraffin	900 kg/m^3	3a
cpp	Specific heat of paraffin	2890 J/kg-K	3a
AISI 1010 Low Carbon Steel @ 600K - "parent material"			
k	Thermal conductivity of low carbon steel	48.8 W/m-K	All (less 3a)
rho	Density of low carbon steel	7832 kg/m^3	All (less 3a)
cp	Specific heat of low carbon steel	559 J/kg-K	All (less 3a)
Air @ 600K – "thermocouple cavity filler"			
ka	Thermal conductivity of air	44 W/m-K	3b – 3d, 4
rhoa	Density of air	7250 kg/m^3	3b – 3d, 4
cpa	Specific heat of air	459 J/kg-K	3b – 3d, 4
Properties obtained from Appendix A of Incropera and DeWitt [29]			

Case 1: Validation of the Undisturbed Model

To demonstrate the ability of the undisturbed model to produce an accurate temperature profile for a given input heat flux, the model is compared to the analytical, one-dimensional solution for a semi-infinite solid with a constant surface heat flux given by Equation (5.1) [38].

$$T(x,t) = T_i + 2 \cdot \frac{q}{k} \cdot \left(\frac{\alpha \cdot t}{\pi} \right)^{\frac{1}{2}} \cdot e^{\left(-\frac{x^2}{4 \cdot \alpha \cdot t} \right)} - \left(\frac{q \cdot x}{k} \right) \cdot erfc \left(\frac{x}{2 \cdot (\alpha \cdot t)^{\frac{1}{2}}} \right) \qquad (5.1)$$

Figure 5.3 shows how the undisturbed model response compares to the semi-infinite analytical solution for an increasing number of control volumes in the undisturbed model. Since the model is a finite thickness, however, the undisturbed model will only accurately approximate the semi-infinite analytical solution for an initial period of time before it deviates from the analytical solution. However, by increasing the number of control volumes in the undisturbed model, n, it will behave ever more like a semi-infinite system. With each additional control volume, the period of time is extended in which the undisturbed model accurately approximates the analytical solution. Because the undisturbed model's temperature response compares well to the semi-infinite analytical solution's response at x = 5 mm during the initial time period, it confirms the proper functioning of the undisturbed model and its ability to accurately replicate the temperature response for a finite system.
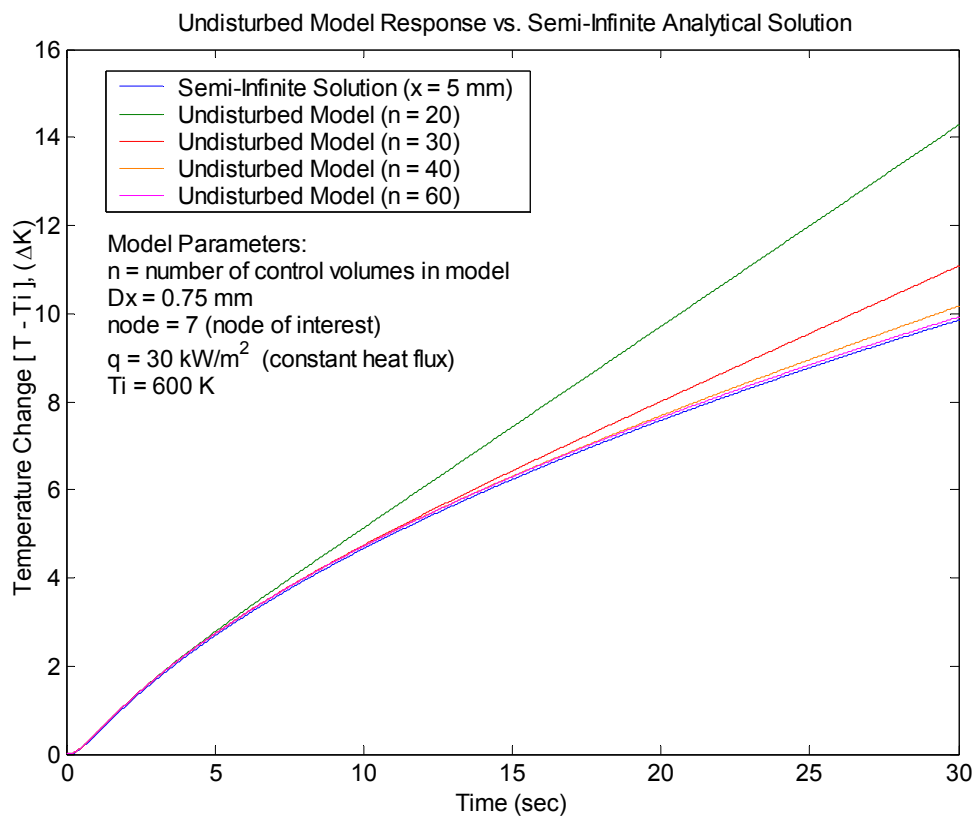
Figure 5.3 - Undisturbed Model Results vs. Semi-Infinite Analytical Solution

*Case 2: Validation of the Disturbed Model*
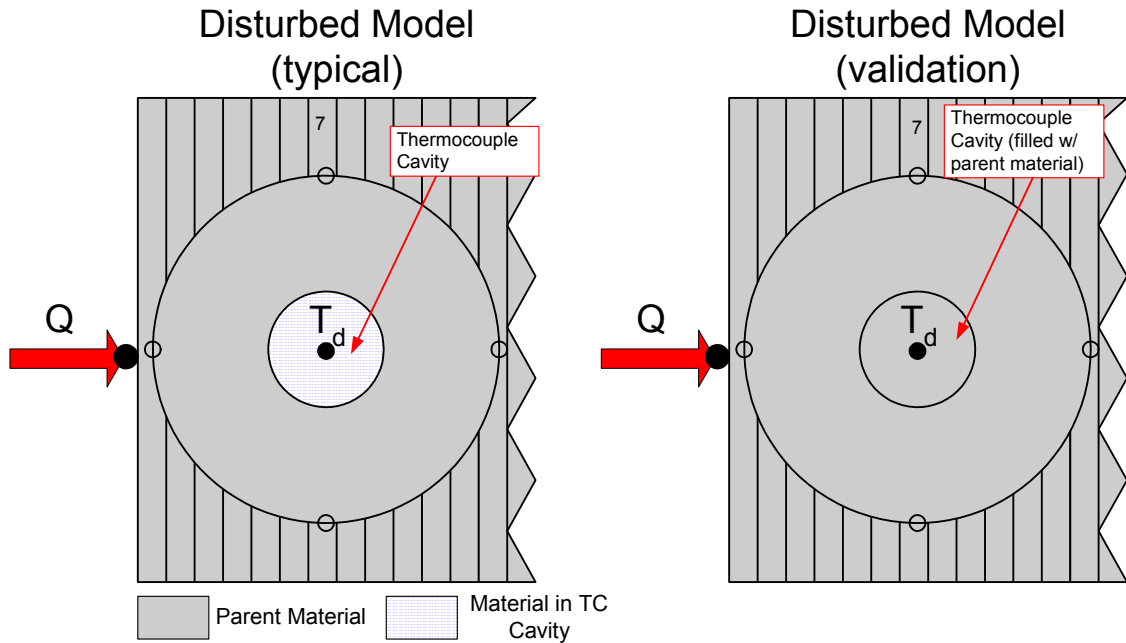
Figure 5.4 - Disturbed Model Validation Configuration

Verification of the disturbed model's accuracy can be accomplished by comparing the undisturbed model temperature response to a disturbed temperature response when the thermocouple cavity contains the parent material. This is accomplished by setting all the sensor sub-model control volumes, including those volumes representing the cavity, to be the parent material as shown in Figure 5.4. In this configuration, the disturbed model will ideally produce the same response as the undisturbed model. Any remaining response differences are strictly modeling errors, due to control volume spacing or improper assumptions in the linking of the senor sub-model. Figure 5.5 displays the

similarity between the disturbed and undisturbed responses for this case. Figure 5.6 is a

plot providing evidence that the difference between the two responses is negligible, at

most about 0.08 K, which confirms the accuracy of the disturbed model.
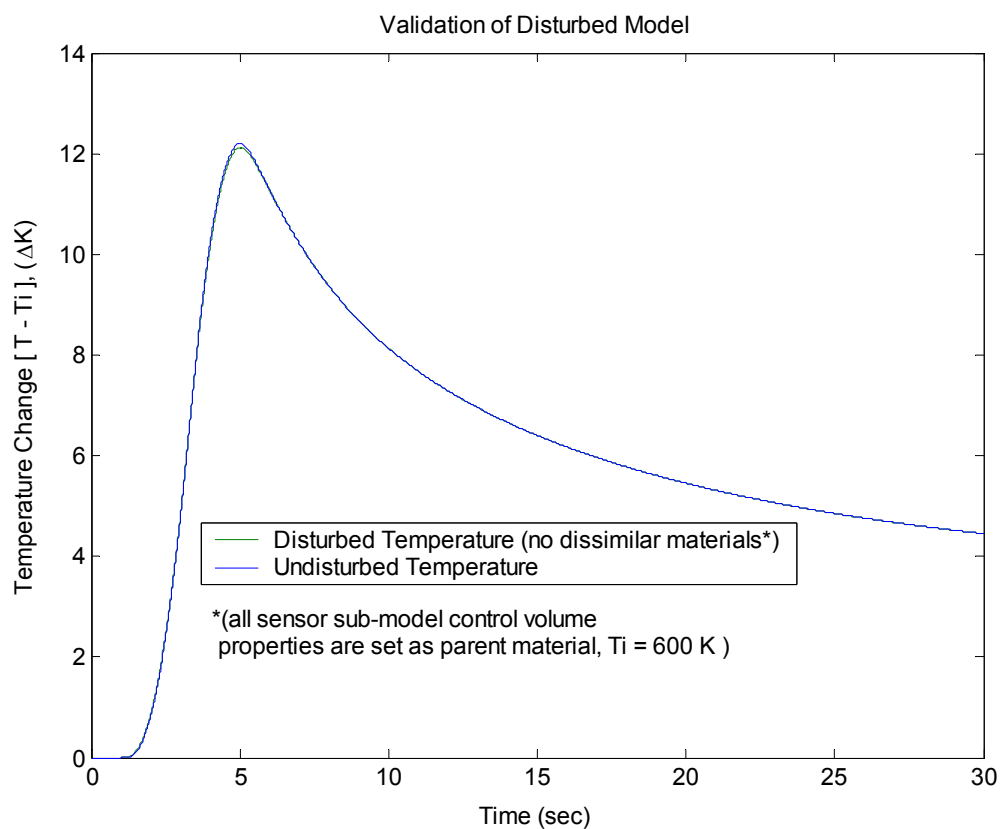
Figure 5.5 - Disturbed Model Validation: Disturbed Model vs. Undisturbed Model
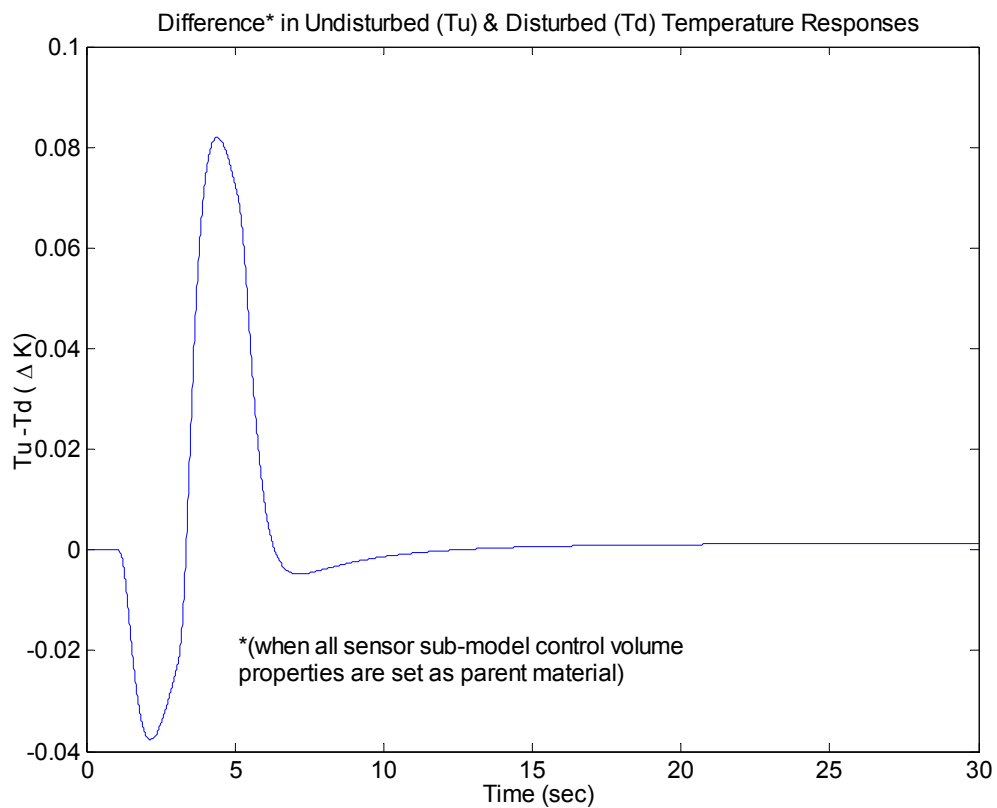
Figure 5.6 - Disturbed Model Validation: Error in Disturbed Response

Case 3: Validation of the Embedded Thermocouple Correction Transfer Function, G(s)
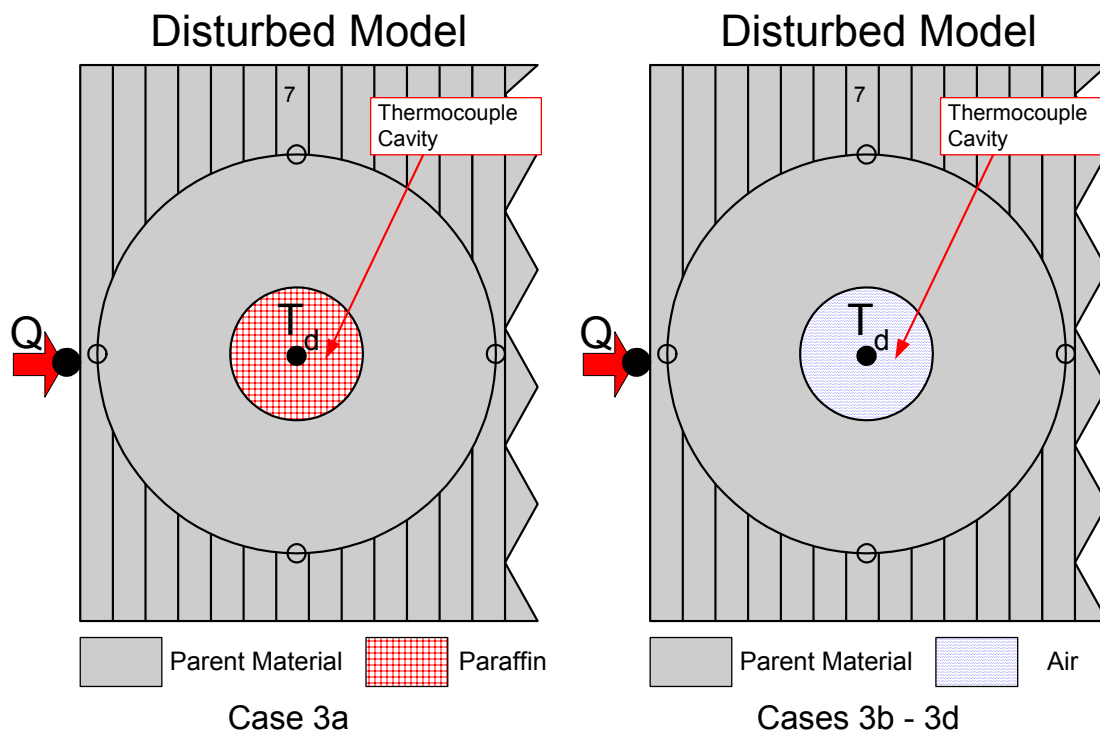
Figure 5.7 - Disturbed Model Configuration: ETC Transfer Function Validation

With both the undisturbed and disturbed model validated, the subsequent

objective is to verify the ability of the ETC transfer function to adjust embedded

thermocouple data to remove the error due to the sensor installation. Figure 5.7 is an

illustration depicting the disturbed model setup in two configurations, with low

diffusivity paraffin wax filling the thermocouple cavity and with non-moving air filling

the thermocouple cavity. Each of these disturbed model setups is used to generate a set

of "measured" temperature data, representative of what a similar experimental setup

would produce. The generated data is created with somewhat of a "worst case" scenario,

assuming the thermocouple is not even in contact with the parent material at the cavity base, thus causing it to register the paraffin or air temperature at the center of the thermocouple cavity. The "measured" data was generated with MATLAB as if it were sampled for 30 seconds at 100 Hz. Case 3 is presented as four sub-cases, differing in the material filling the thermocouple cavity and the amount of noise which was added to the generated "measured" data. This added noise simulates the random uncertainty typically present in actual experimental data. The noise was created as random normal values with zero mean and user defined standard deviation. Descriptions of the sub-cases are shown in Table 5.3.

Table 5.3 - Sub-cases of Case 3

Case	Standard Deviation of Noise (Kelvin)
3a	- no noise added (paraffin filler) -
3b	- no noise added (air filler) -
3c	0.1 K (air filler)
3d	0.5 K (air filler)

Case 3a: Noiseless Temperature Data - Paraffin TC Cavity Filler

Figure 5.8 displays the obvious difference between the disturbed "measured" data for the paraffin filled cavity and the undisturbed temperature response. Figure 5.9 is representative of the error contained in the "measured" data or its difference from the "true" undisturbed response. The maximum error is approximately 6 K for the current system and boundary input.
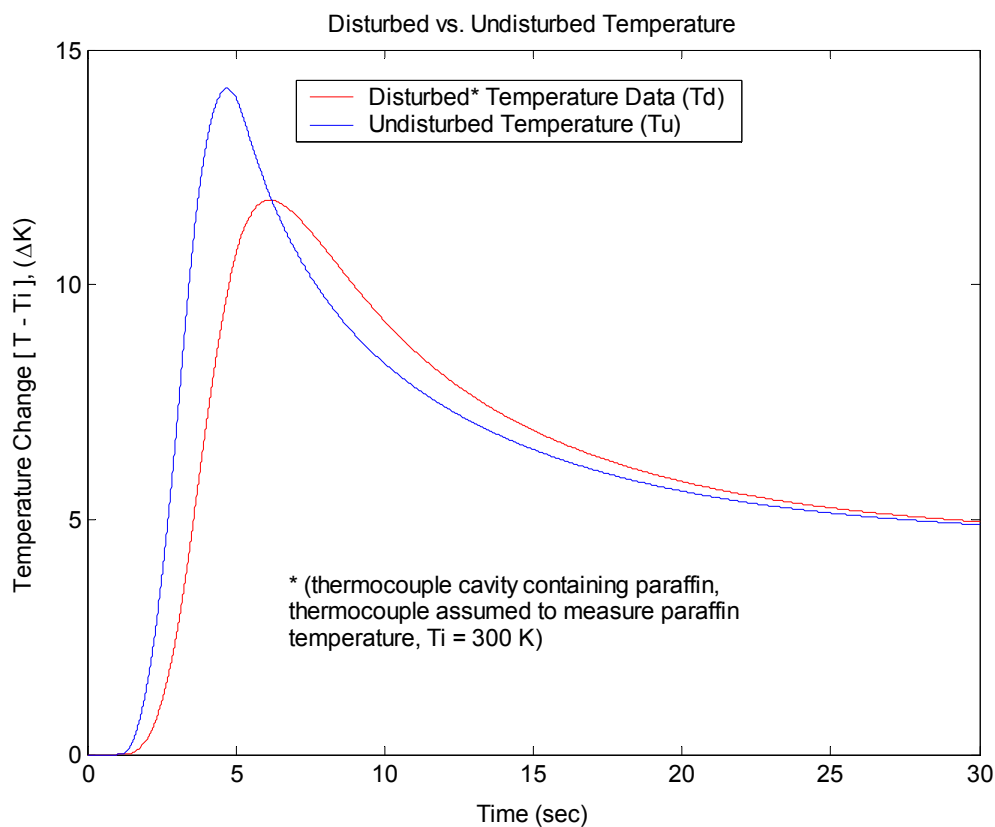

Figure 5.8 - Case 3a: Disturbed vs. Undisturbed Temperature Responses
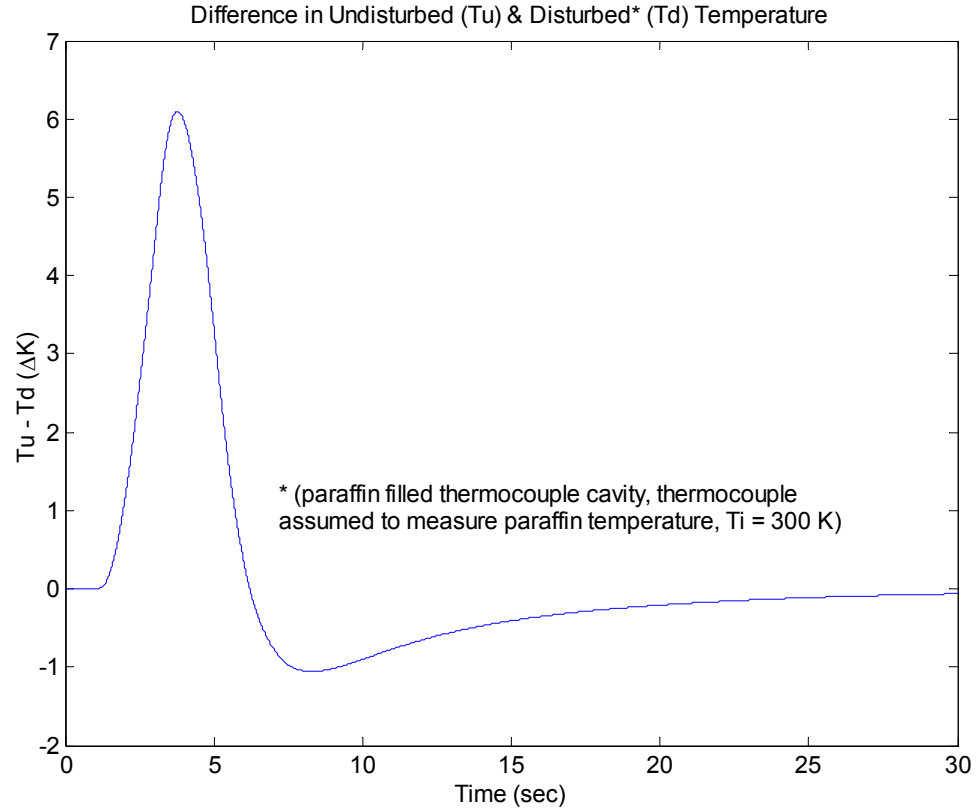
Figure 5.9 - Case 3a: Error in Disturbed Response

Using the MATLAB program developed, the generated "measured" data can be used as the input to the ETC transfer function to recover an adjusted set of temperature data in which the effects of the sensor installation have been removed. Figure 5.10 shows the ability of the ETC transfer function to accurately filter the "measured" data to produce a set of recovered temperature data that closely approximates the undisturbed response. Figure 5.11 displays the error in the reconstructed data with respect to the undisturbed response, which is seen to be minimal.
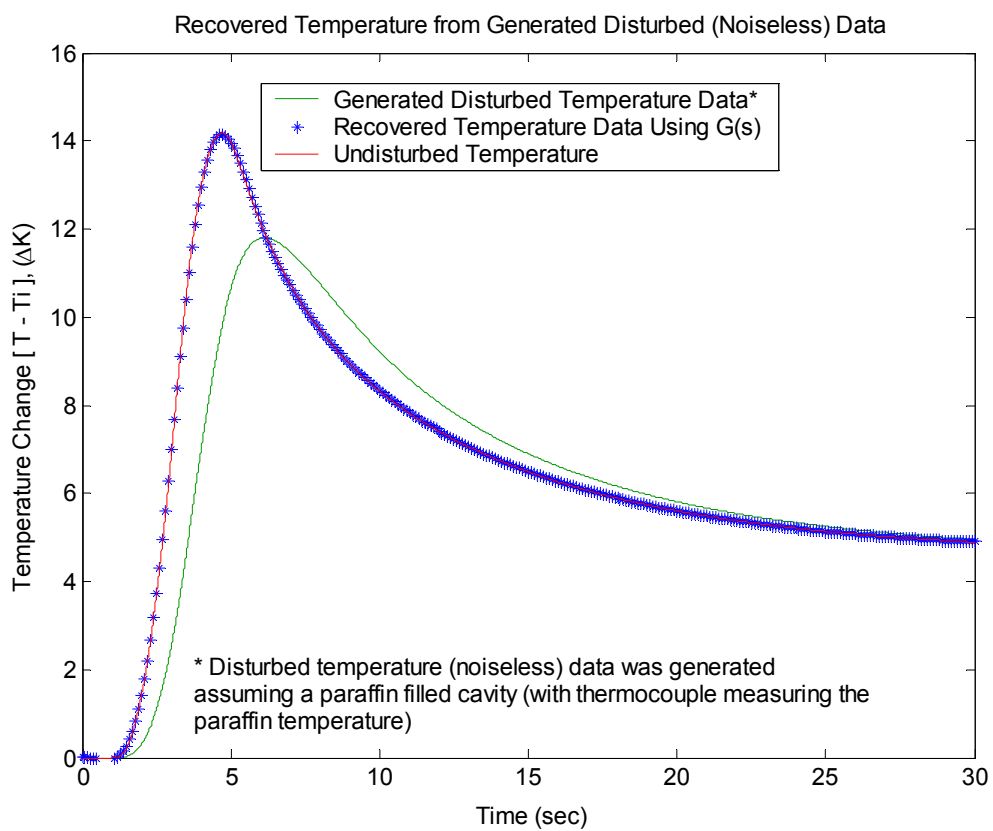
Figure 5.10 - Case 3a: Recovered Temperature Response
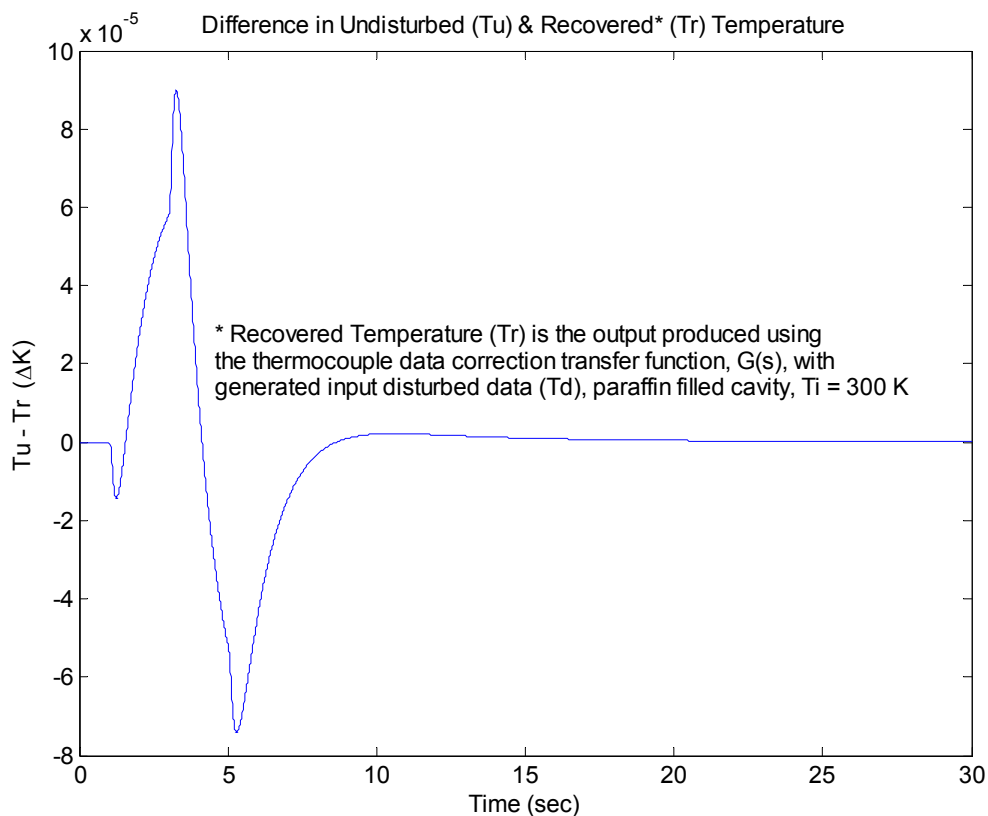
Figure 5.11 - Case 3a: Error in Recovered Temperature Response

Case 3b: Noiseless Temperature Data – Air TC Cavity Filler

In the same manner as Case 3a, Case 3b was executed for the more realistic

situation of an air filled thermocouple cavity. Figure 5.12 displays the difference

between the disturbed "measured" data for the non-moving air filled cavity and the

undisturbed temperature response. Figure 5.13 is representative of the installation error

contained in the "measured" data, or its difference from the "true" undisturbed response.

The maximum error is approximately 1 K overestimation for the current system and

boundary input. The error of the disturbed response is less for air when compared to the paraffin because the thermal diffusivity of the air is much larger than that of the paraffin wax.
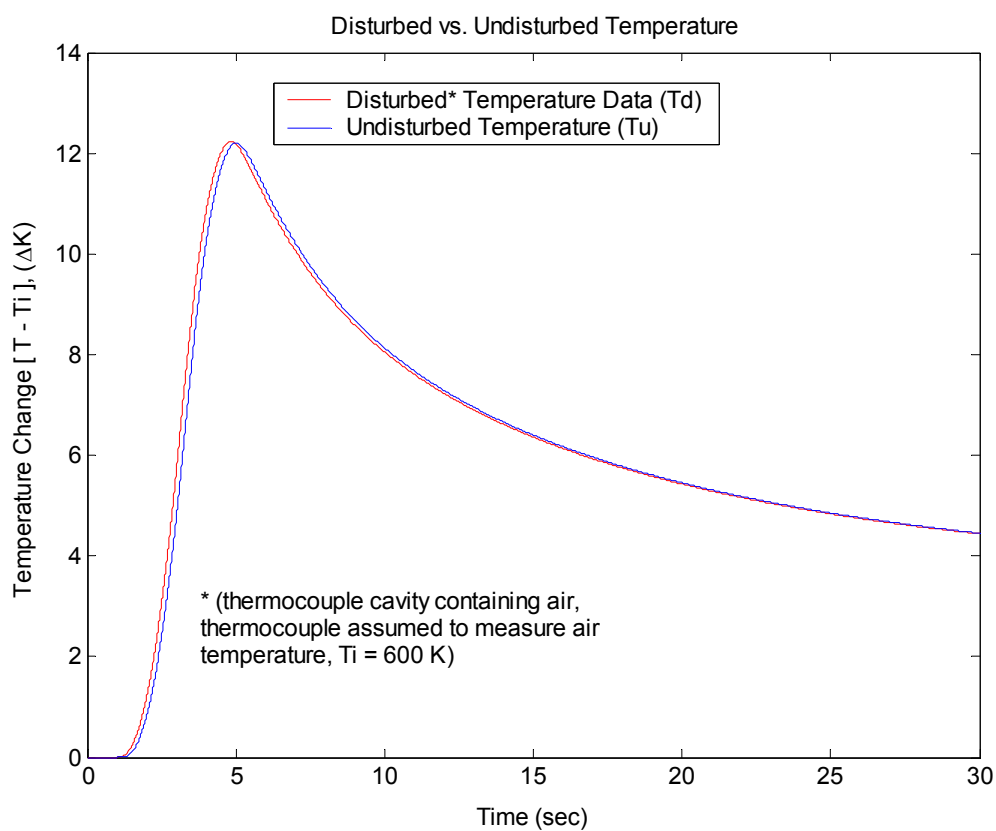

Figure 5.12 - Case 3b: Disturbed vs. Undisturbed Temperature Responses
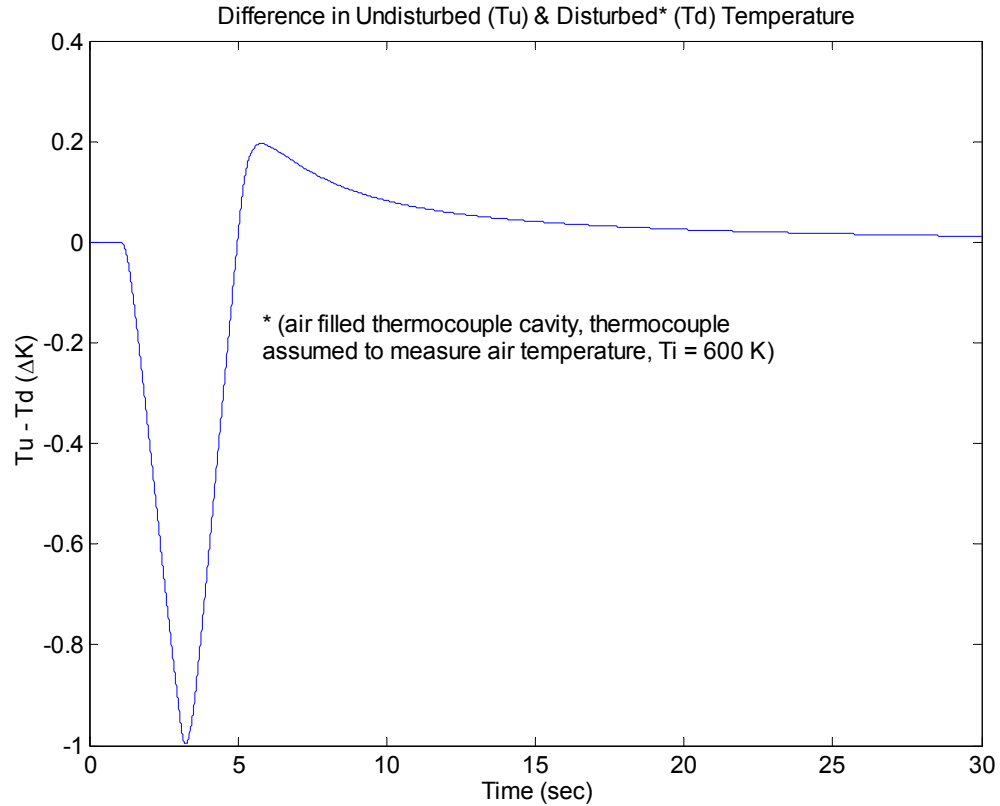
Figure 5.13 - Case 3b: Error in Disturbed Response

As was performed for Case 3a, the ETC transfer function is employed on the

disturbed "measured" data of Case 3b. Figure 5.14 shows the results of the ETC transfer

function on the "measured" data to produce a set of recovered temperature data that

closely approximates the undisturbed response. Figure 5.15 displays the error of the

reconstructed data with respect to the undisturbed response, which is once again seen to

be minimal.
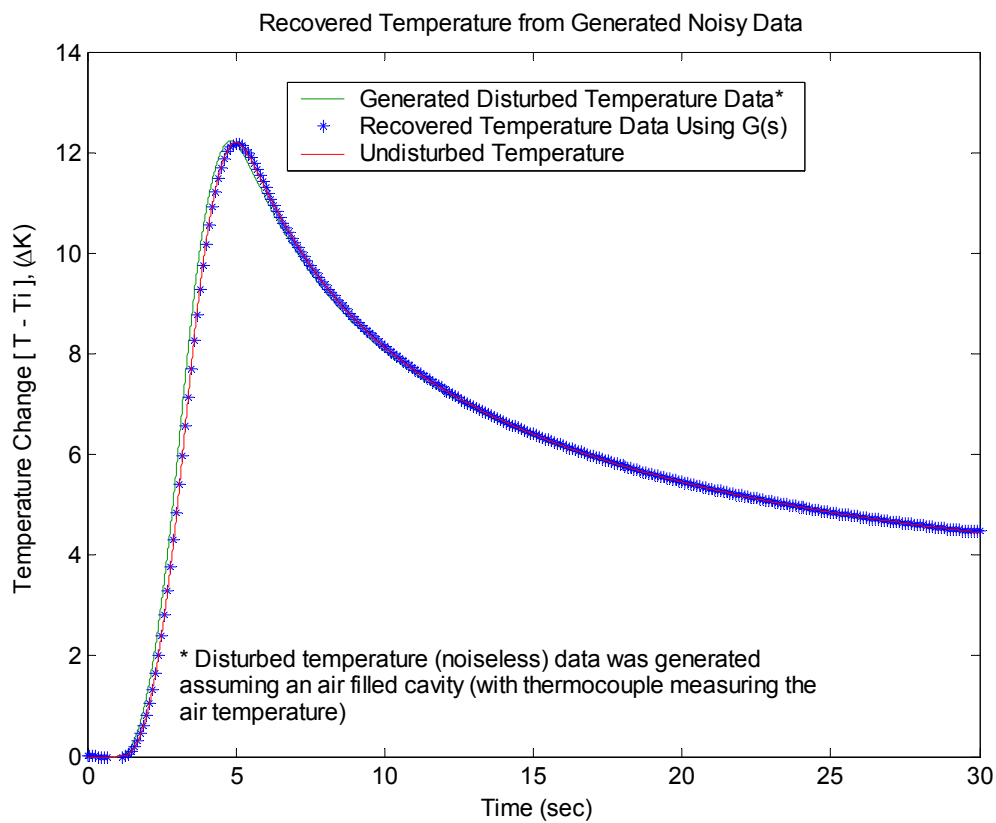
Figure 5.14 - Case 3b: Recovered Temperature Response
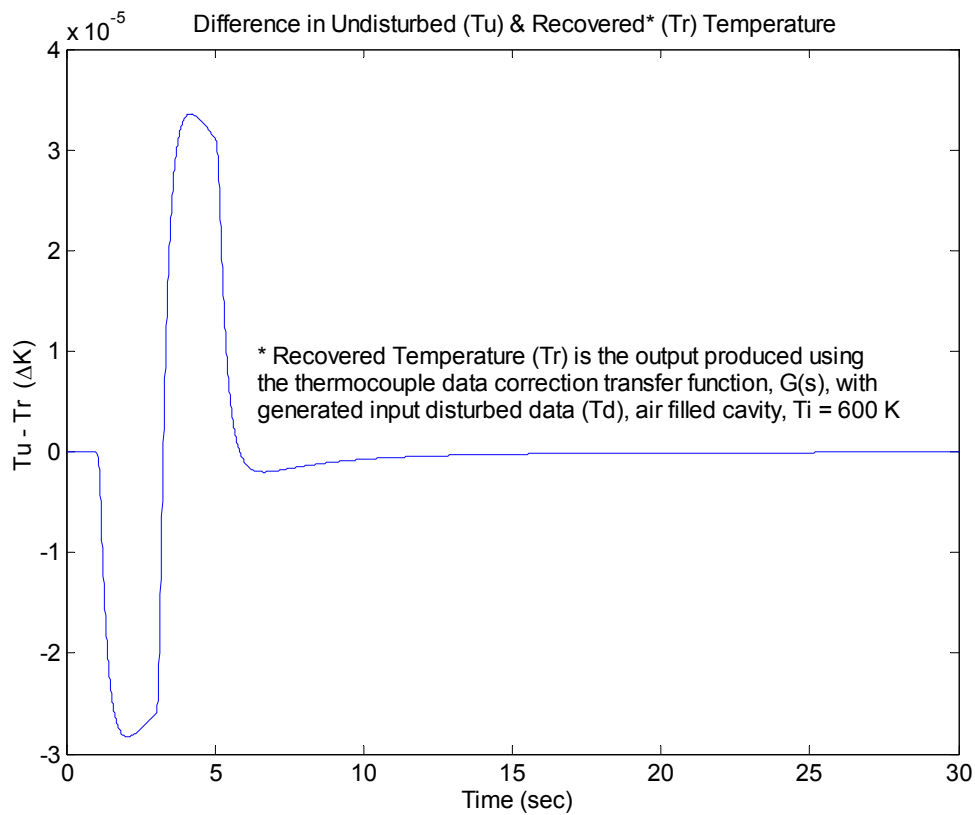
Figure 5.15 - Case 3b: Error in Recovered Temperature Response

Case 3c: Noisy (σ = 0.1 Kelvin) Temperature Data – Air TC Cavity Filler
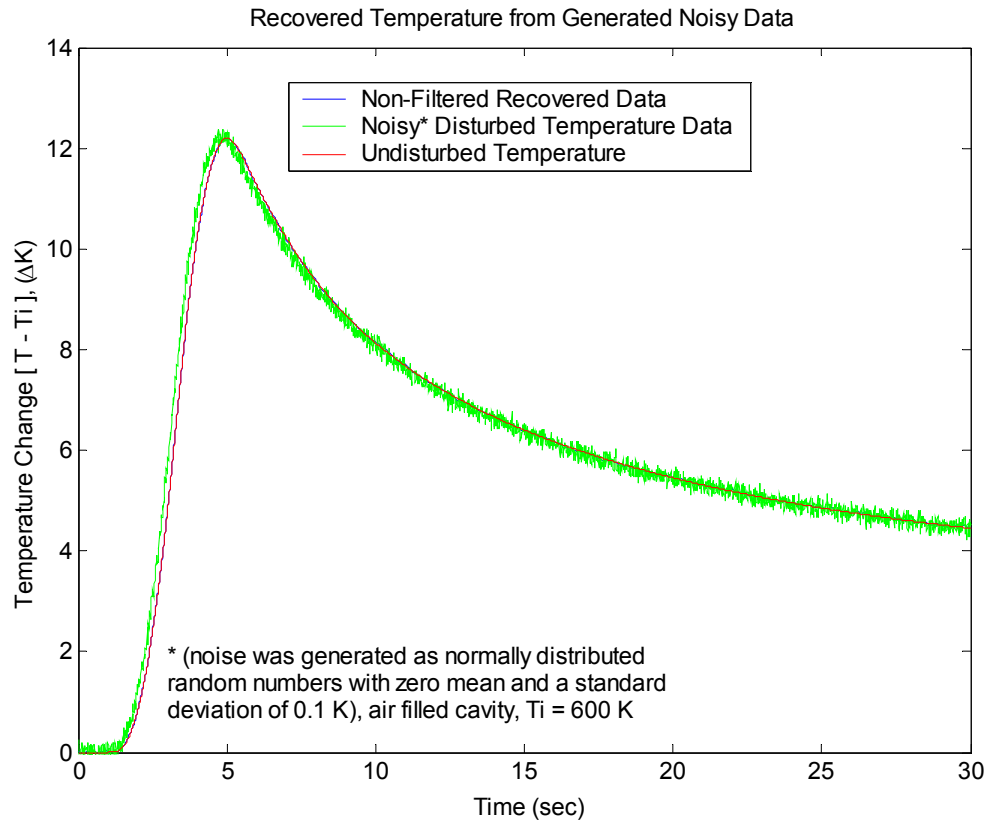
Figure 5.16 - Case 3c: Non-Filtered Recovered Temperature Response

Noise was created with a standard deviation of 0.1 Kelvin and added to the measured signal of Case 3b to produce noisy "measured" data. Figure 5.16 shows the recovered temperature data when using the noisy data as an input to ETC transfer function. Although not particularly evident, the noise is amplified (slightly in this configuration) through the recovery process, which makes the recovered temperature data unacceptable.   Therefore, a lowpass Butterworth filter was constructed in MATLAB to filter the noisy "measured" temperature data. The filtered data was then used in the ETC

transfer function temperature response recovery process. The resulting recovered

temperature data from the filtered noisy data is shown in Figure 5.17. The error

remaining in the recovered temperature data with respect to the undisturbed temperature

is shown in Figure 5.18 and is approximately at or less than the level of the injected

random noise.
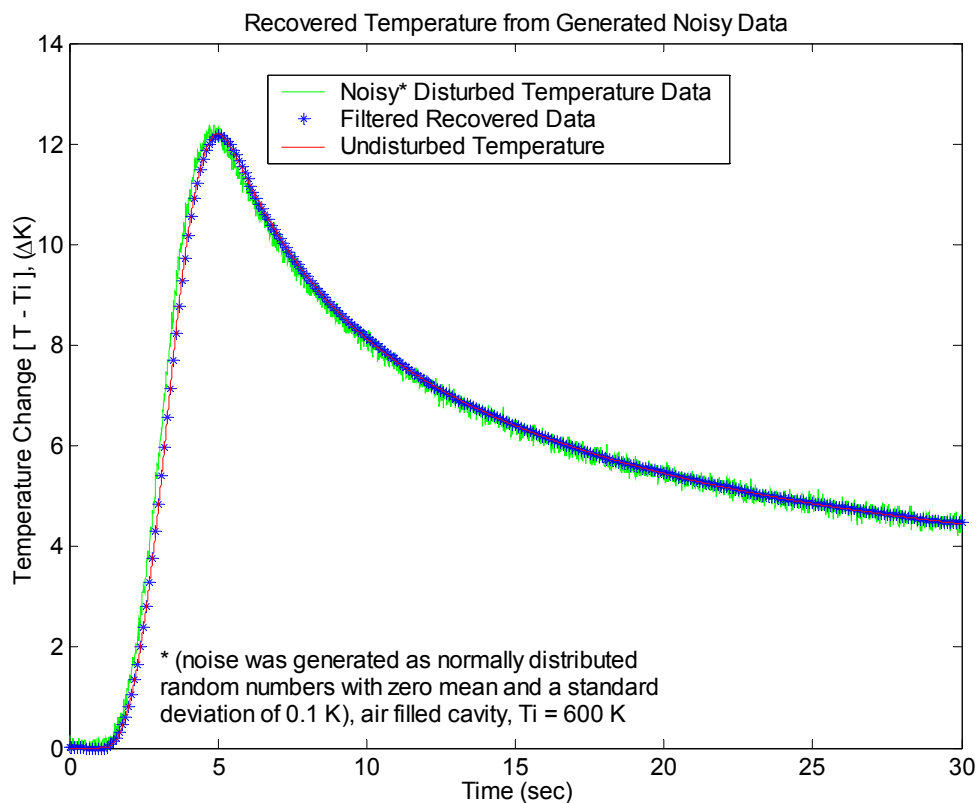
Figure 5.17 - Case 3c: Filtered Recovered Temperature Response
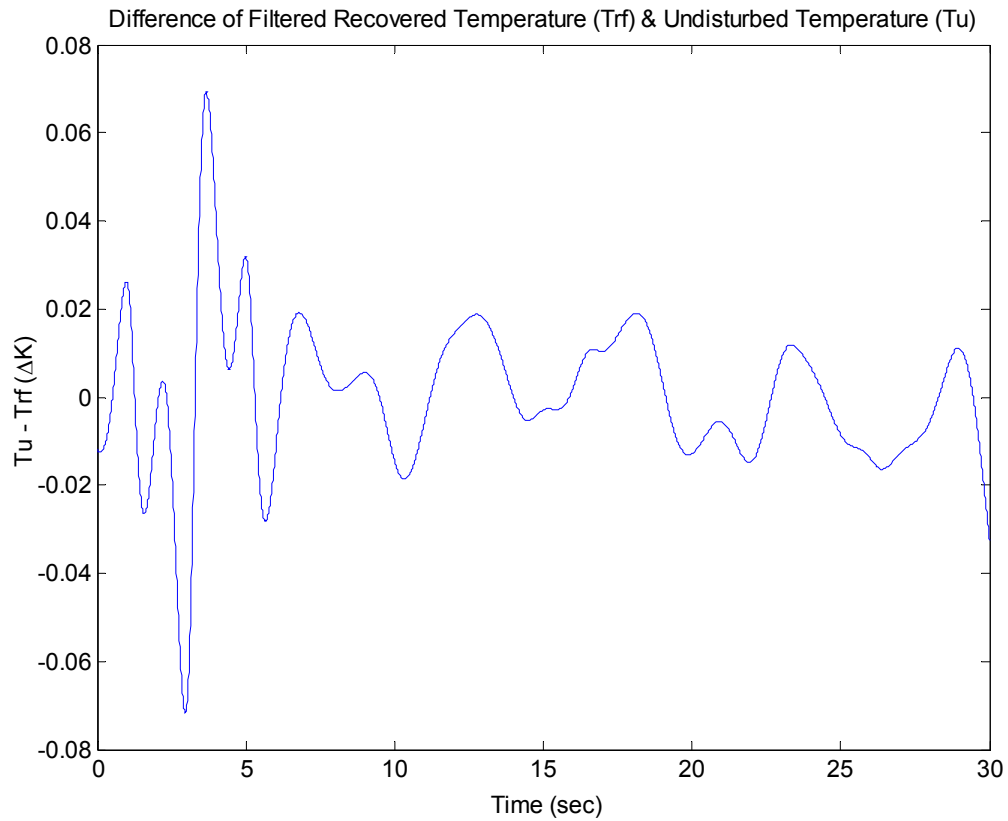
Figure 5.18 - Case 3c: Error in Filtered Recovered Temperature Response

Case 3d: Noisy ($\sigma = 0.5$ Kelvin) Temperature Data – Air TC Cavity Filler

The standard deviation for the noise was increased to 0.5 Kelvin in Case 3d. This noise was then added to the generated "measured" temperature data of Case 3b, and that noisy data was filtered. Figure 5.19 shows the temperature response recovered from the filtered noisy data. Figure 5.20 shows the error remaining in the recovered data with respect to the undisturbed response, which again is slightly less than the level of introduced random noise.

Recovered Temperature from Generated Noisy Data
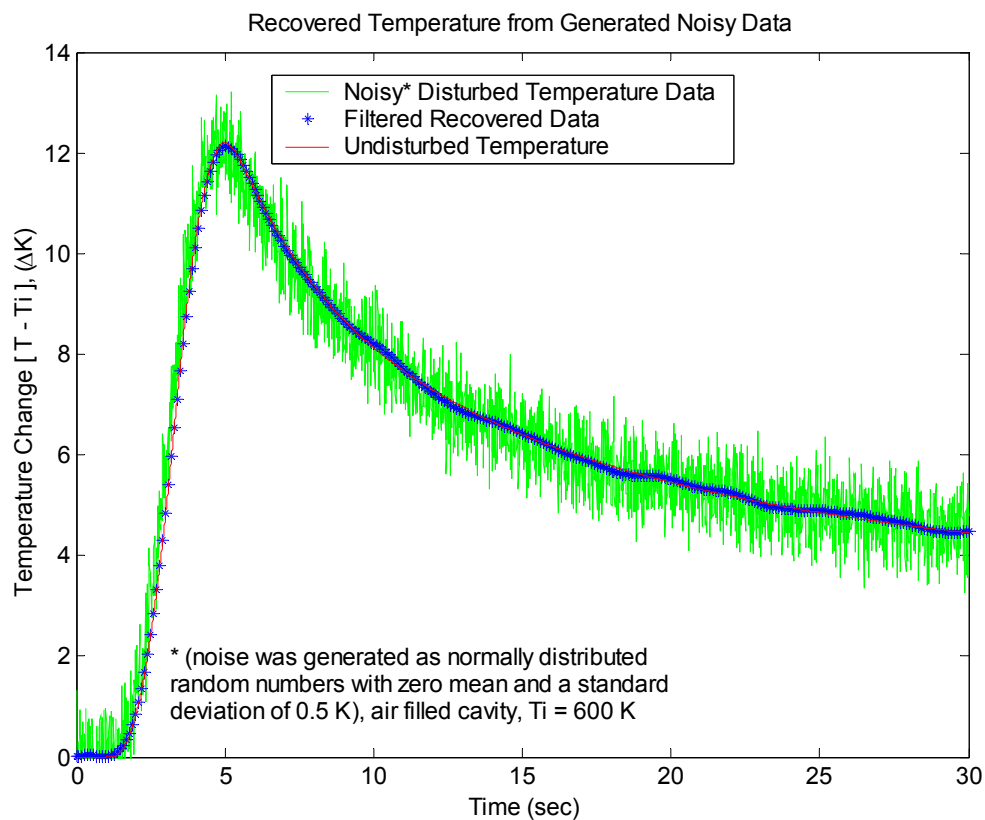
Figure 5.19 - Case 3d: Filtered Recovered Temperature Response
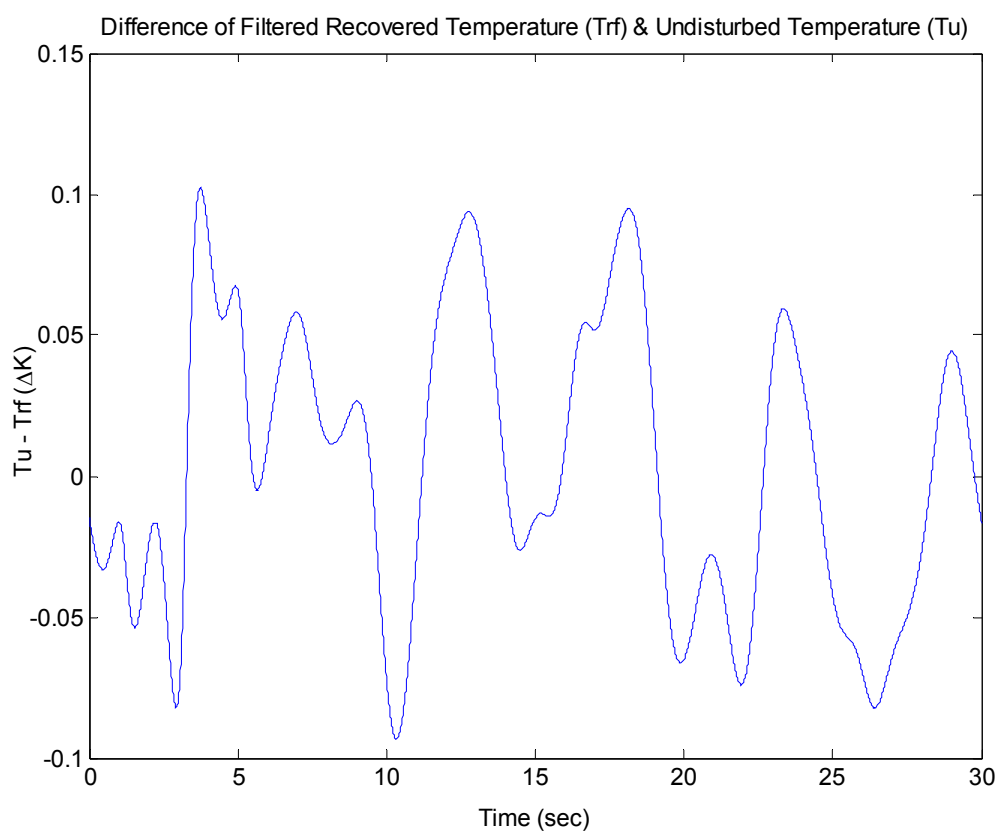
Figure 5.20 - Case 3d: Error in Filtered Recovered Temperature Response

Case 4: Inverse Heat Conduction Solution for Boundary Heat Flux

Following Shenefelt in [7, 37], the MATLAB code used to perform singular value decomposition for model reduction, an inverse conduction method, was created. As with other IHC methods, given internal temperature data input, an estimate for the applied boundary heat flux can be determined. The objective of this example is to provide evidence demonstrating that the use of the installation error biased temperature data in an inverse solution can lead to an inaccurate estimate for boundary heat flux. For this example, the generated "measured" data and non-filtered ETC recovered data for the paraffin filled ($\sigma = 0$ K) and air filled ($\sigma = 0.1$ K) thermocouple cavity systems are both presented. Since the recovered data is an estimate of the undisturbed temperature measurement, the impulse response employed for the building the Φ matrix, as described by Shenefelt, is that of the simple undisturbed system, a block of low carbon steel. The comparison of estimated boundary heat flux determined using the model reduction methods for both the generated "measured" and ETC recovered temperature responses is shown in Figure 5.21 for the paraffin filled thermocouple cavity and in Figure 5.22 for the air filled thermocouple cavity. It is obvious in the case of the low thermal diffusivity paraffin filler that the use of the uncorrected "measured" data produces an estimated boundary heat flux that is largely damped in magnitude and delayed in time. Conversely, the air filled thermocouple cavity data tends to slightly overestimate the heat flux and shift it forward in time. Nevertheless, the recovered temperature response developed with the ETC transfer function for each case approximates the boundary heat flux very effectively. Figure 5.23 and Figure 5.24 display the error of the estimated heat flux using

the ETC recovered data from the paraffin and air filler, respectively, as compared to the actual applied heat flux of Figure 5.2. The maximum error observed is slightly larger than 1% of the actual heat flux for both cases.
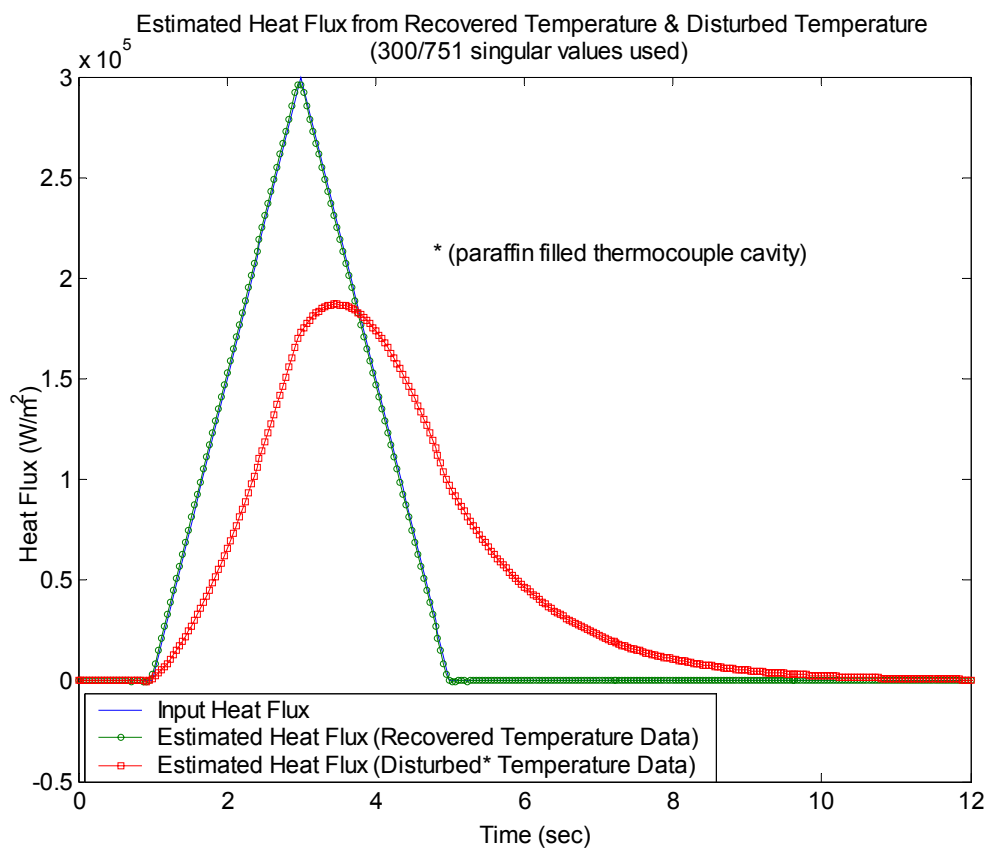

Figure 5.21 - Estimated Heat Flux Comparison (Paraffin Filler, $\sigma = 0$ K)
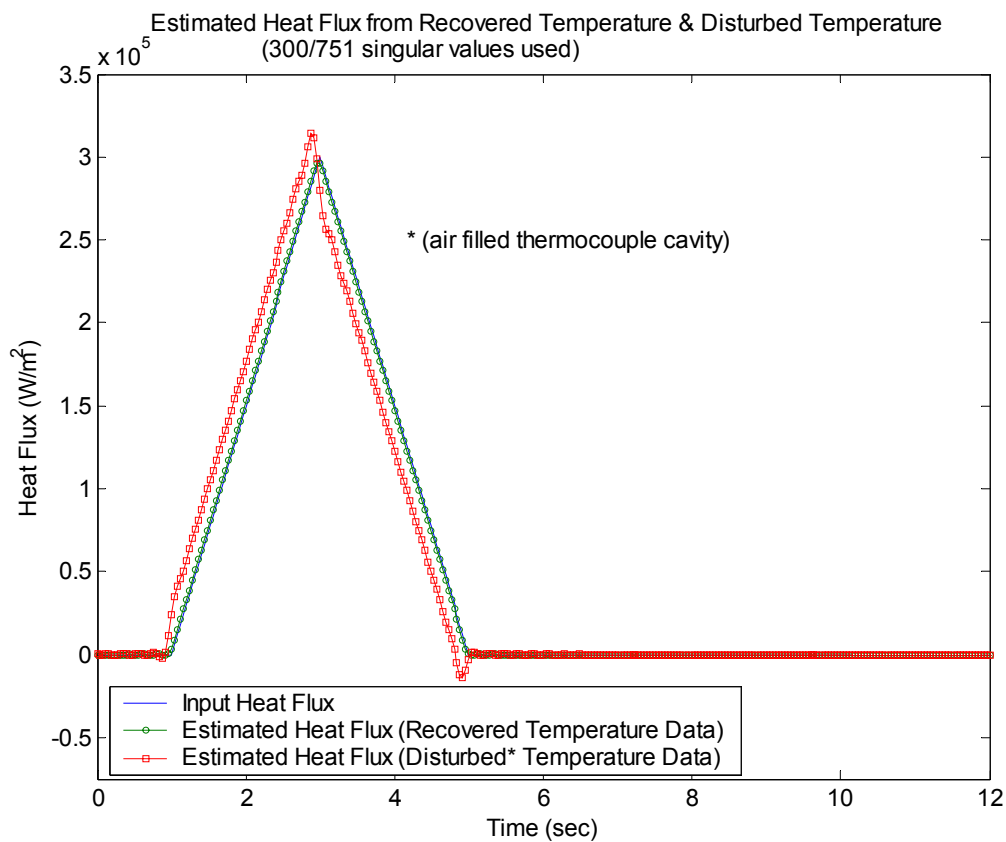
Figure 5.22 - Estimated Heat Flux Comparison (Air Filler, σ = 0.1 K)
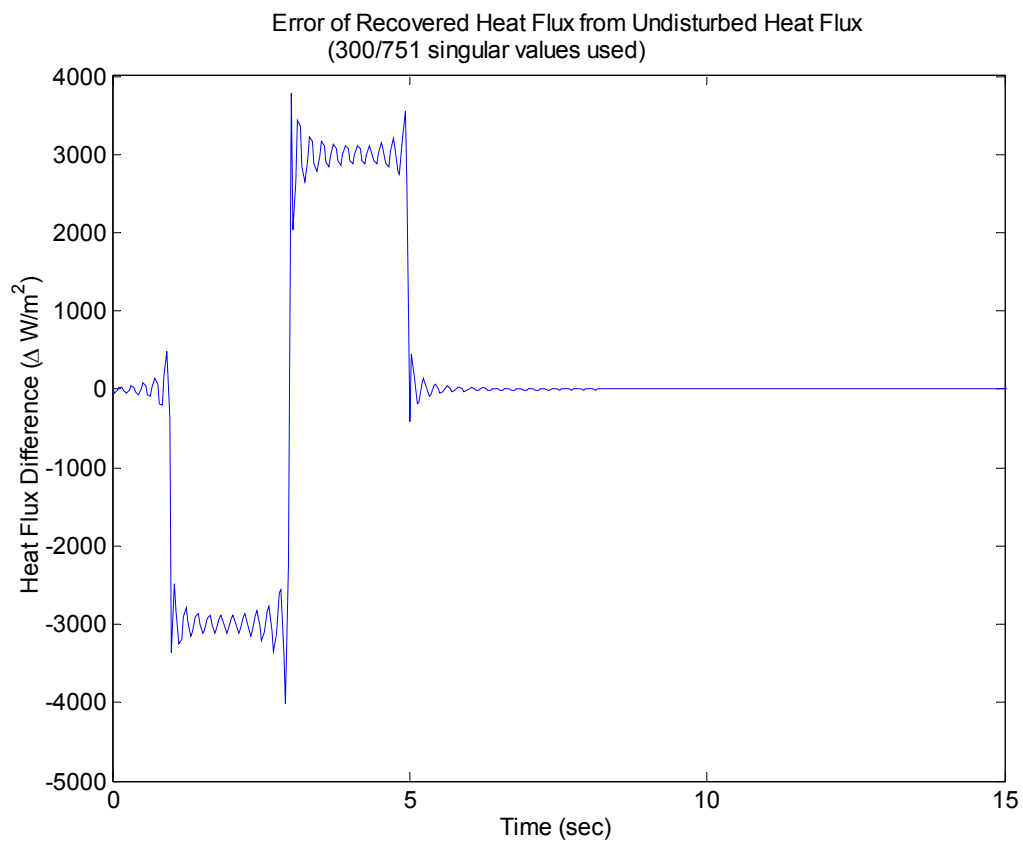
Figure 5.23 - Error of IHC Estimated Heat Flux (Paraffin Filler, $\sigma = 0$ K)
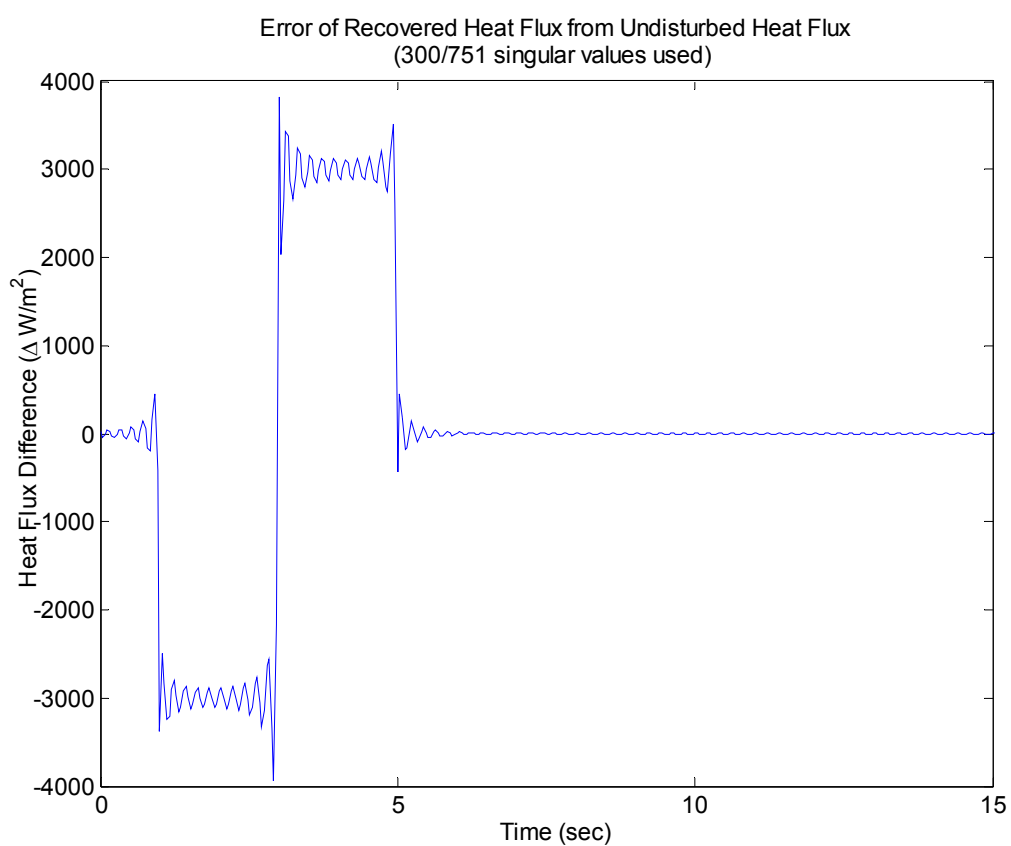
Figure 5.24 - Error of IHC Estimated Heat Flux (Air Filler, σ = 0.1 K)

Adjusting Experimentally Acquired Data with the ETC Transfer Function

As outlined in Chapter III, several experimental pourings of A356 aluminum were completed in a three-piece steel mold. During each experimental run, internal mold temperatures at several locations (Figure 3.4 in Chapter III) were collected using embedded thermocouples. The purpose for the determination of the embedded thermocouple correction (ETC) transfer function was to develop a means to recover an undisturbed temperature response, removed of the bias error due to sensor installation, from embedded thermocouple data. Therefore, a case is now presented showing the correction of a set of experimental temperature data collected from one of the metal casting runs using the ETC transfer function methods.
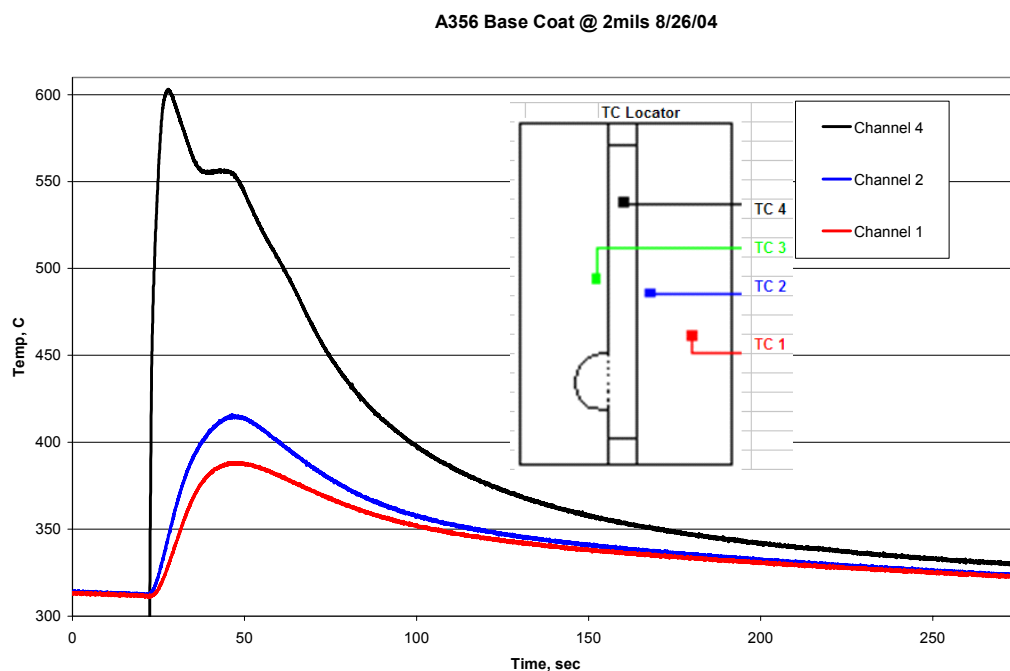
Figure 5.25 - Mold Temperature: 8/26/2004

Figure 5.25 shows a plot of the experimental internal mold temperature data collected for the run completed on August 26, 2004. Channels 1 and 2 are two separate embedded thermocouples within the mold, and channel 4 is the thermocouple within the casting. The first ninety seconds of temperature data from channel 1 (thermocouple located approximately 5 mm from interface) were imported into the MATLAB program for use in the ETC method assuming an air filled thermocouple cavity. Figure 5.26 displays the results of using the ETC transfer function with ninety seconds of experimental data, sampled at 25 Hz, as the input.
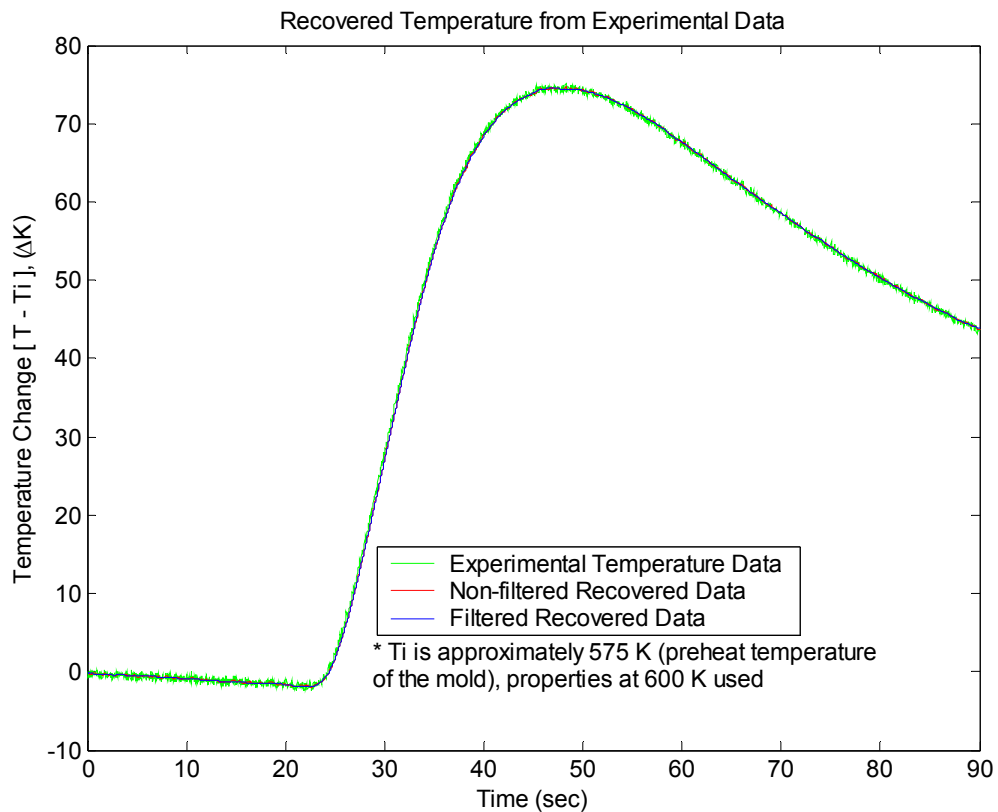
Figure 5.26 - ETC Recovered Temperature (Experimental Data)

Both the non-filtered and Butterworth filtered recovered responses are shown. The difference between the filtered recovered temperature response and the experimental data are shown by Figure 5.27. A maximum temperature difference of approximately 1 K − 1.5 K is observed. The correction made to the experimental data, as compared to some of the previous example cases, is not nearly as radical. This is most likely due to the more gradual effects of the boundary heat flux experienced in the experimental situation as compared to the sudden changes in the simulated heat flux of Figure 5.2.
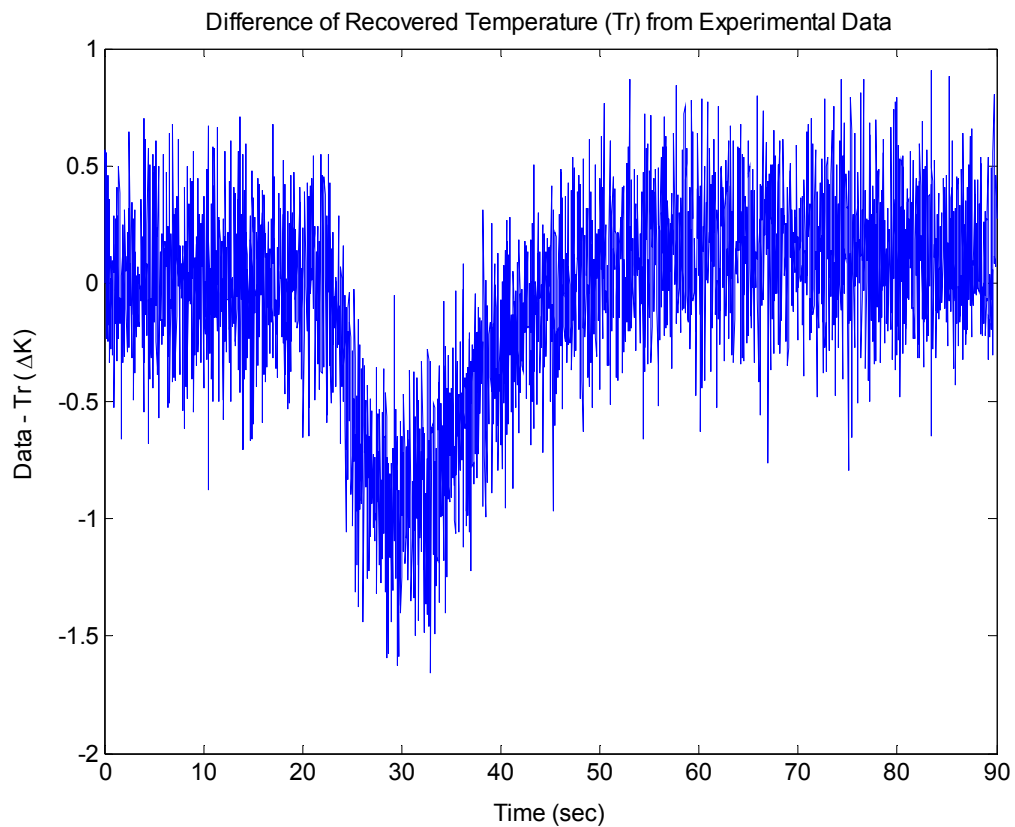
Figure 5.27 - Difference of Filtered Recovered and Experimental Temperature Data

As a closing study, the experimental data and the ETC recovered temperature response shown in Figure 5.28, were used in the IHC methods presented by Shenefelt [7, 37] to estimate unknown boundary heat flux condition experienced at the mold-metal interface in the casting experiment. Figure 5.29 is a plot comparing the estimated heat fluxes produced for both the "raw" experimental data and the non-filtered recovered ETC data. The peak value for the ETC recovered data estimated heat flux is around 377 kW/m^2, which is comparable to other values found in literature [16, 39]. As was true with the recovered temperature response and the experimental data, the estimated heat fluxes for each are not as drastically different as in the case for the generated data in Figure 5.21. This is most likely due to the higher thermal diffusivity of the air filled thermocouple cavity and because, as mentioned before, the boundary heat flux experienced in the casting process does not exhibit the sudden changes of the simulated heat flux of Figure 5.2. As seen in Figure 5.30, the maximum difference between the two estimated heat fluxes is around 12 kW/m^2, which is approximately 3 % of the peak value observed.
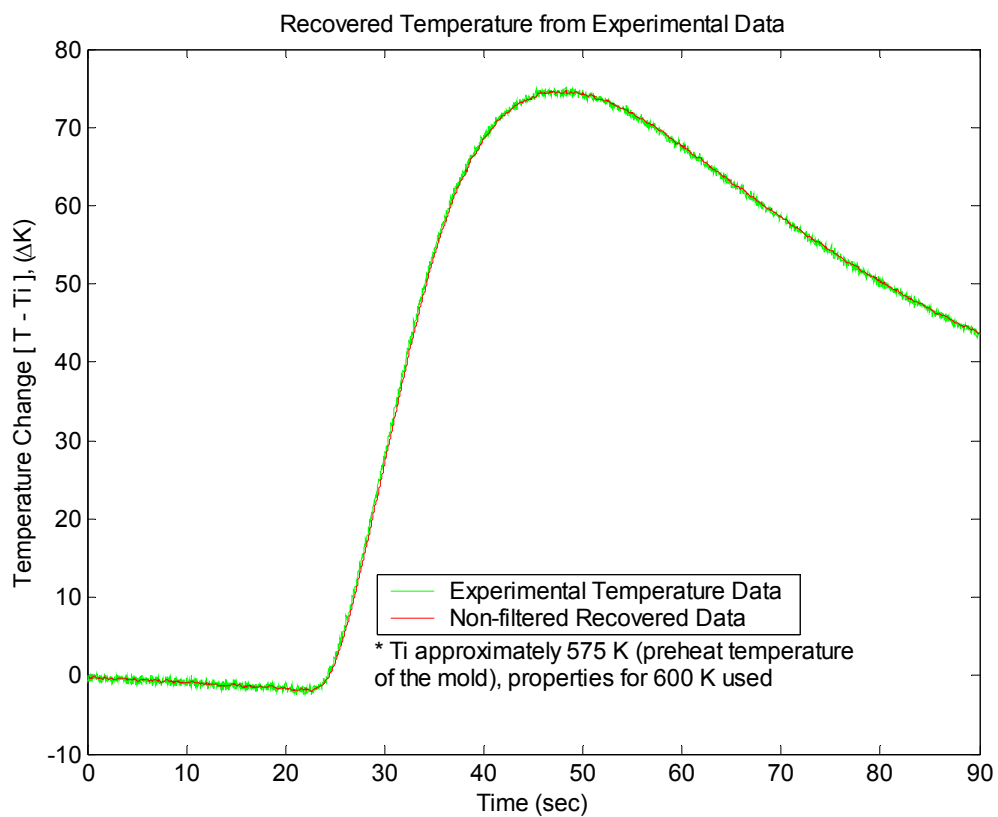
Figure 5.28 - Comparison of Non-filtered ETC Recovered Data to Experimental Data
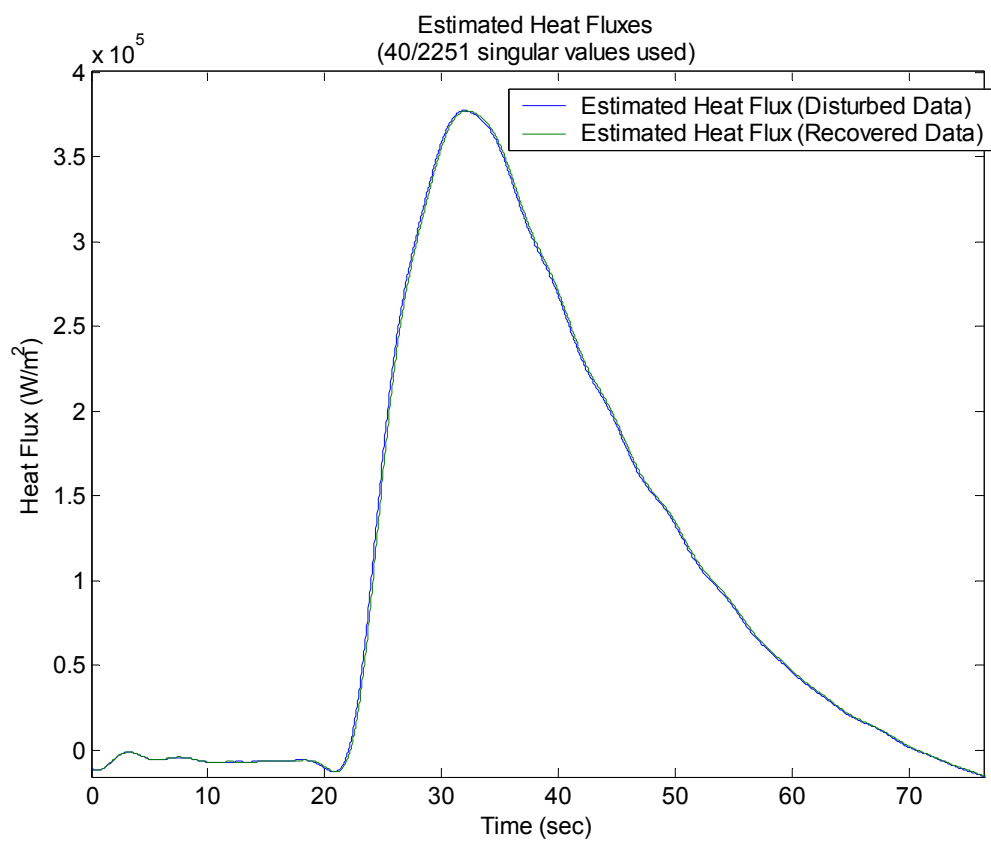
Figure 5.29 - Estimated Heat Fluxes (Experimental Data)
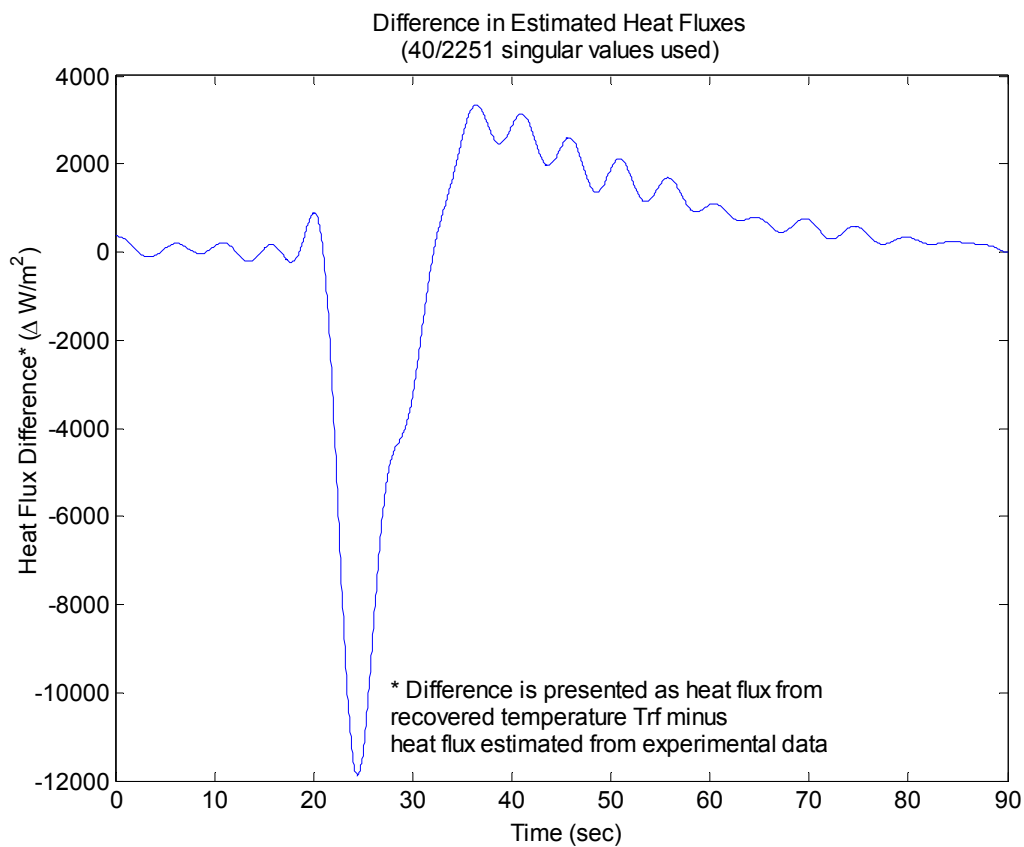
Figure 5.30 - Difference in Estimated Heat Fluxes (Experimental Data)

www.manaraa.com

CHAPTER VI

SUMMARY AND CONCLUSIONS

Solid-embedded thermocouples are utilized for a variety of industrial applications where the internal temperature of a solid is desired. Depending upon the application, the accuracy requirements for the temperature data collected may be very stringent. Inverse conduction problems, where internal temperature measurements are used to estimate boundary condition, are one such application in which very accurate temperature measurements are essential. The literature contains many discussions concerning the way in which small errors in measured temperature data can be amplified through the inversion process, resulting in large errors in estimated boundary conditions. Therefore, when considering the design of an experiment to collect temperature data for use in inverse conduction calculations, it is imperative to recognize the wide variety of sources from which error can be introduced into a temperature signal, as well as to be able to minimize their contributions.

Chapter II discussed in detail a variety of factors that can contribute error to solid-embedded thermocouple temperature measurements. Systematic and random errors were visited, with a particular focus on the inherent systematic error that is induced when a thermocouple is embedded within a solid, designated as installation error. References were cited that provide detailed studies regarding the significant errors in signal magnitude and phase due to the installation of the sensor, particularly during transient

106

measurement periods, and these installation errors were established as problems that may be too often overlooked in industry.

The practices employed during metal casting experiments, in which internal mold temperatures were collected during casting processes, were summarized in Chapter III. In these experiments, embedded thermocouples were used to collect temperature measurements for application in inverse conduction solutions to estimate the heat flux and heat transfer coefficient at the mold-metal interface. Equipment and practices utilized to minimize the random error introduced into the temperature signals through electrical noise in the testing environment were presented.

With the minimization of random errors typically managed during the experimental set up, the goals of additional error reduction led to the techniques discussed in Chapter IV for the elimination of the bias error in an embedded thermocouple temperature signal due to the presence of the sensor within the measured domain. Modeling techniques were presented to simulate transient heat conduction within the measured domain, with and without the thermocouple installation in place. Methods for determining an embedded thermocouple correction (ETC) transfer function from these models, used to correct for installation error in temperature data, were presented and a MATLAB program was constructed to automate the assembly of this transfer function based on user defined system descriptive parameters.

Chapter V provided examples demonstrating the effectiveness of the ETC transfer function in removing installation bias errors from simulated noisy embedded thermocouple data to recover estimated undistorted temperature data. A simulation was

also presented showing the inaccuracy of simulated noisy embedded thermocouple data estimated boundary heat flux, when used for an inverse conduction solution. However, the ETC transfer function recovered response, when alternatively used in same inverse conduction solution, was shown to accurately estimate the actual boundary heat flux. The ETC transfer function method was also demonstrated with a sample set of experimental temperature data collected during the casting experimentation described in Chapter III to recover an undisturbed temperature response. The differing estimates of boundary heat flux produced for the recovered and "raw" temperature data, when employed in an inverse conduction scheme, were also compared to published values and discussed. For the assumed situation of an air filled thermocouple cavity, it was observed that the amount of distortion in temperature signal and IHC estimated boundary heat flux were fairly minimal.

The ETC transfer function can effectively be considered as a filter, or a dynamic calibration tool, that can adjust a temperature response in both phase and magnitude to remove the bias error due to the sensor installation. This type of data adjustment can be very beneficial for applications in which accurate transient temperature measurement is vital, such as that of inverse conduction problems.

This thesis has investigated the use of solid-embedded thermocouples as a specific means for determining accurate transient temperature measurements within a solid. However, no cause is without its effect, and the apparent simplicity of being able to measure accurate transient temperatures within a solid by simply embedding a thermocouple does not come without cost. By installing a sensor in the solid domain, the

dynamics of the heat conduction system are changed. This can result in temperature

measurements that can potentially turn into hindrances, if the presence of installation

induced bias errors in the temperature signal are not recognized and managed in an

effective and appropriate fashion.

REFERENCES

[1]   Adeleke, J. and Muikku, A., "Inverse Analysis for Determination of Interfacial Heat Transfer Coefficient in Complex Three-Dimensional Sand Casting Processes," presented at Tenth International Conference on Modeling of Casting, Welding, and Advanced Solidification Processes, Destin, Florida, 2003.

[2]   Griffiths, W. D., "A Model of the Interfacial Heat-transfer Coefficient during Unidirectional Solidification of an Aluminum Alloy," *Metallurgical & Materials Transactions B*, vol. 31B, 2, pp. 285 - 295, 2000.

[3]   Carrol, M., Walsh, C., and Makhlouf, M., "Determination of the Effective Interfacial Heat Transfer Coefficient Between Metal Molds & Aluminum Alloy Castings," presented at CastExpo 1999, St. Louis, Missouri, 1999.

[4]   Prabhu, K. N. and Campbell, J., "Investigation of Casting/Chill Intefacial Heat Transfer during Solidification of Al-11% Si Alloy by Inverse Modelling and Real-time X-ray Imaging," *International Journal of Cast Metals Research*, vol. 12, 137 - 143, 1999.

[5]   Blum, J. and Marquardt, W., "An Optimal Solution to Inverse Heat Conduction Problems Based on Frequency-domain Interpretation and Observers," *Numerical Heat Transfer, Part B*, vol. 32, 453 - 478, 1997.

[6]   Xue, X., Luck, R., and Berry, J. T., "Comparisons and Improvements Concerning Accuracy and Robustness of Inverse Heat Conduction Algorithms," *Inverse Problems in Science and Engineering*, vol. 13, 2, pp. 177 - 199, 2005.

[7]   Shenefelt, J. R., Luck, R., Taylor, R. P., and Berry, J. T., "Solution to Inverse Heat Conduction Problems Employing Singular Value Decomposition and Model-reduction," *International Journal of Heat and Mass Transfer*, vol. 45, 67 - 74, 2002.

[8]   Woodbury, K. A. and Gupta, A., "Effect of Deterministic Thermocouple Errors on the Solution of the Inverse Heat Conduction Problem," (unpublished / to be published), University of Alabama, 2004.

[9]   Holman, J. P., *Experimental Methods for Engineers*, 7 ed: McGraw Hill, 2001.

[10]   *OMEGA Complete Temperature Measurement Handbook and Encyclopedia*, vol. MMV, 5th ed: OMEGA Inc., 2004.

[11]   Dantzig, J. A., "Improved Transient Response of Thermocouple Sensors," *Rev. Sci. Instrumentation*, vol. 56, 5, pp. 723 - 725, 1985.

[12]   Balakovskii, S. L., Baranovskii, E. F., and Sevast'yanov, P. V., "Optimization of Thermocouple Installation for Study of Intense Transient Thermal Actions on Materials," *Journal of Engineering Physics*, 805 -809, 1989.

[13]   Rabin, Y. and Rittel, D., "A Model for the Time Response of Solid-embedded Thermocouples," *Experimental Mechanics*, vol. 39, 2, pp. 1 - 5, 1999.

[14]   Chen, C. J. and Li, P., "Theoretical Error Analysis of Temperature Measurement by an Embedded Thermocouple," *Letters in Heat and Mass Transfer*, vol. 1, 2, pp. 171 - 180, 1974.

[15]   Attia, M. H., Cameron, A., and Kops, L., "Distortion in Thermal Field Around Inserted Thermocouples in Experimental Interfacial Studies, Part 4: End Effect," *Journal of Manufacturing Science and Engineering*, vol. 124, 135 -145, 2002.

[16]   Kim, T.-G., Choi, Y.-S., and Lee, Z.-H., "Heat Transfer Coefficients Between A Hollow Cylinder Casting and Metal Mold," presented at Eighth International Conference on Modeling of Casting, Welding and Advanced Solidification Processes, San Diego, California, 1998.

[17]   Griffiths, W. D., "The Heat-transfer Coefficient during the Unidirectional Solidification of an Al-Si Alloy Casting," *Metallurgical & Materials Transactions B*, vol. 30B, 3, pp. 473 - 482, 1999.

[18]   Wang, W. and Qiu, H.-H., "Interfacial Thermal Conductance in Rapid Contact Solidification Process," *International Journal of Heat and Mass Transfer*, vol. 45, 2043 - 2053, 2002.

[19]   Coleman, H. W. and Steele, W. G., *Experimentation and Uncertainty Analysis for Engineers*, 2nd ed: John Wiley & Sons, 1999.

[20]   Attia, M. H. and Kops, L., "Distortion in the Thermal Field Around Inserted Thermocouples in Experimental Interfacial Studies - Part 3: Experimental and Numerical Verification," *Journal of Engineering for Industry*, vol. 115, 444 - 449, 1993.

[21]   Attia, M. H. and Kops, L., "Distortion in the Thermal Field Around Inserted Thermocouples in Experimental Interfacial Studies - Part II: Effect of the Heat Flow Through the Thermocouple," *Journal of Engineering for Industry*, vol. 110, 7 - 14, 1988.

[22]   Attia, M. H. and Kops, L., "Distortion in Thermal Field Around Inserted Thermocouples in Experimental Interfacial Studies," *Journal of Engineering for Industry*, vol. 108, 241 - 246, 1986.

[23]   Alwang, W. G., "A Model of the Measurement Process for Estimating the Uncertainty of Time-dependent Measurements," presented at Proceedings of the 1998 44th International Instrumentation Symposium, Reno, NV, USA, 1998.

[24]   Elphick, I. G., Chen, A. M. C., and Shoukri, M., "Modelling Steady State and Transient Response of Thermocouple Assemblies in Solids," presented at American Society of Mechanical Engineers: Winter Meeting, Anaheim, CA, 1986.

[25]   Chen, C. J. and Danh, T. M., "Transient Temperature Distortion in a Slab Due to Thermocouple Cavity," *AAIA Journal*, vol. 14, 979 - 981, 1976.

[26]   Alwang, W. G., "The Analysis of Uncertainty in Transient Measurements," presented at Proceedings of the 37th International Instrumentation Symposium, 1991.

[27]   Weathers, J., Johnson, A., Luck, R., Walters, K., and Berry, J. T., "The Effects of Thermocouple Placement on Highly Transient Temperature Measurements in Mold Media for Aluminum Castings," presented at American Foundry Society Cast Expo 2005, St. Louis, MO, 2005.

[28]   Rittel, D., "Transient Temperature Measurement Using Embedded Thermocouples," *Experimental Mechanics*, vol. 38, 2, pp. 73 - 78, 1998.

[29]   Incropera, F. P. and DeWitt, D. P., *Fundamentals of Heat and Mass Transfer*, 5 ed: John Wiley & Sons, Inc., 2002.

[30]   Baker, H. D., Ryder, E. A., and Baker, N. H., *Temperature Measurement in Engineering*, vol. 1. New York: John Wiley & Sons, Inc., 1953.

[31]   Chen, C. J. and Thomsen, D. M., "On Transient Cylindrical Surface Heat Flux Predicted from Interior Temperature Response," *AAIA Journal*, vol. 13, 5, pp. 697 - 699, 1975.

[32]   Beck, J. V., "Determination of Undisturbed Temperatures from Thermocouple Measurements Using Correction Kernels," *Nuclear Engineering and Design*, vol. 7, 9 - 12, 1968.

[33]   Weathers, J., "Combining the Matrix Transform Method with Three-Dimensional Finite Element Modeling to Estimate the Interfacial Heat Transfer Coefficient Corresponding to Various Mold Coatings," M.S. Thesis: Department of Mechanical Engineering, Mississippi State University, 2005.

[34]   Chiesa, F. and Boisvert, A., "Factors Affecting Drying Conditions of Coatings Sprayed on Permanent Molds," *AFS Transactions*, vol. 104, 769 - 775, 1996.

[35]   *SCB-68 68-Pin Shielded Connector Block User Manual*: National Instruments, Co., 2002.

[36]   Patankar, S. V., *Numerical Heat Transfer and Fluid Flow*: Hemisphere Publishing Co., 1980.

[37]   Shenefelt, J. R., "Heat Flux and Thermal Contact Conductance Determination Employing Inverse Heat Conduction Using Model Reduction Through Matrix Transform," PhD. Dissertation: Department of Mechanical Engineering, Mississippi State University, 1999.

[38]   Bejan, A., *Heat Transfer*: John Wiley & Sons, Inc., 1993.

[39]   Gunasegaram, D. R., van der Touw, J., and Nguyen, T. T., "Heat Transfer at Metal-Mould Interfaces," presented at IMMA/ADCA International Conference on Casting and Solidification of Light Alloys, Gold Coast, Australia, 1995.

APPENDIX A

DAQ CARD BIT ANALYSIS

114

DAQ Card Bit Analysis --- August Johnson 8/21/2004

$$\text{Bits} := \begin{pmatrix} 12 \\ 16 \\ 32 \end{pmatrix} \qquad \text{VoltRange} := 0.1V \qquad i := 0..(\text{length}(\text{Bits}) - 1) \qquad \mu V := 10^{-6}V$$

$$MP_i := \frac{\text{VoltRange}}{2^{\text{Bits}_i}} \qquad MP = \begin{pmatrix} 24.414063 \\ 1.525879 \\ 0.000023 \end{pmatrix} \mu V \qquad \frac{MP_0}{MP_1} = 16 \qquad \frac{MP_0}{MP_2} = 1.049 \times 10^6$$

Temperature Conversion Curve (OMEGA)

$$c := \begin{pmatrix} 0 \\ 2.508355 \times 10^{-2} \\ 7.860106 \times 10^{-8} \\ -2.503131 \times 10^{-10} \\ 8.315270 \times 10^{-14} \\ -1.228034 \times 10^{-17} \\ 9.804036 \times 10^{-22} \\ -4.413030 \times 10^{-26} \\ 1.057734 \times 10^{-30} \\ -1.052755 \times 10^{-35} \end{pmatrix} \cdot 10^6 \qquad T(E) := c_0 + \sum_{i=1}^{9} c_i \cdot E^i$$
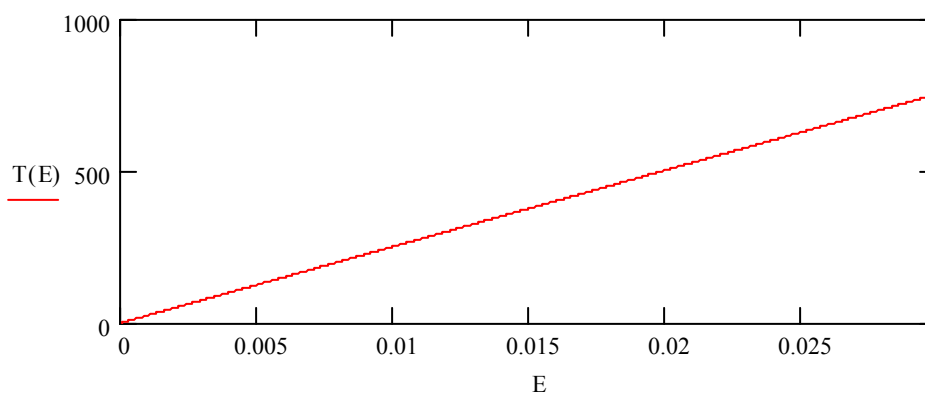
$X := 0.02$

Given

$T(X) = 500$

$T_{500} := Find(X)$

$T_{500} = 0.019933381$

$k := 0.. 100$

$Voltage_k := 0.0001993 k$

$Temp_k := T(Voltage_k)$

$Temp_0 := 0.0000000$

$$MP = \begin{pmatrix} 24.4140625 \\ 1.5258789063 \\ 0.0000232831 \end{pmatrix} \mu V$$

$$\Delta V := \frac{MP}{V}$$

$$\Delta T_{k, i} := \frac{T(Voltage_k + \Delta V_i) - T(Voltage_k - \Delta V_i)}{2}$$

$M := augment(Voltage, Temp, \Delta T)$

Machine Precision (converted to deg C)

$$\frac{T(2 \cdot \Delta V_i)}{2} =$$

0.612	12 bit
0.038	16 bit
$5.84 \cdot 10^{-7}$	32 bit

APPENDIX B

MODEL CONSTRUCTION AND SIMULATION FILES

B.1   SENSOR SUB-MODEL MATHCAD FILE

Thermocouple "Sensor" Sub-Model System Matrix Builder:

▼ CV Term Generator

$NN := 21$ Number of Nodes (including boundary nodes) in Sensor Sub-model

$i := 0..(NN - 1)$

-------------- If thermocouple cavity is to include non-parent material (use this section) --

Parent Material (Steel)   TC Cavity Filler (Air)   in $\dfrac{W}{m \cdot K}$

$K_m := 48.8$ $K_a := 0.0469$

Correcting for interface conductivities (as Patankar pg. 44 - Interface conductivity) (air -> steel in first c.v. "ring")

$$Kmn := \frac{2 \cdot (K_m \cdot K_a)}{K_m + K_a} \qquad Kmn = 0.09371$$

For $K_{filler} \ll K_{parent}$ (checks!)

$$Kmn2 := 2 \cdot K_a \qquad Kmn2 = 0.0938$$

$$k_i := K_m \cdot \frac{W}{m \cdot K}$$

Interface Conductivity Corrections (fills center c.v. and first "ring" with air):

$$k_0 := K_a \frac{W}{m \cdot K} \qquad k_1 := Kmn \frac{W}{m \cdot K} \qquad k_2 := Kmn \frac{W}{m \cdot K} \qquad k_3 := Kmn \frac{W}{m \cdot K} \qquad k_4 := Kmn \frac{W}{m \cdot K}$$

$k_i = K_m \cdot \dfrac{W}{m \cdot K}$ Used to set all c.v. in sensor sub-model back to "parent material" conductivity

Geometry for Control Volumes (set parameters for each of NN nodes):

$$\Delta r := (0 \ 1 \ 1 \ 1 \ 1 \ 1 \ 1 \ 1 \ 1 \ 1 \ 1 \ 1 \ 1 \ 1 \ 1 \ 1 \ 1 \ 0 \ 0 \ 0 \ 0)^T \cdot mm$$

$$\delta r := (1 \ 1 \ 1 \ 1 \ 1 \ 1 \ 1 \ 1 \ 1 \ 1 \ 1 \ 1 \ 1 \ 1 \ 1 \ 1 \ 1 \ 1 \ 0.5 \ 0.5 \ 0.5 \ 0.5)^T \cdot mm$$

$$r_b := (0.001 \ 1 \ 1 \ 1 \ 1 \ 2 \ 2 \ 2 \ 2 \ 3 \ 3 \ 3 \ 3 \ 4 \ 4 \ 4 \ 4 \ 4.5 \ 4.5 \ 4.5 \ 4.5)^T \cdot mm$$

118

$$r_n := \begin{pmatrix} 0 & .5 & .5 & .5 & .5 & 1.5 & 1.5 & 1.5 & 1.5 & 2.5 & 2.5 & 2.5 & 2.5 & 3.5 & 3.5 & 3.5 & 3.5 & 4.5 & 4.5 & 4.5 & 4.5 \end{pmatrix}^T \cdot mm$$

$$r_s := \begin{pmatrix} .5 & 1.5 & 1.5 & 1.5 & 1.5 & 2.5 & 2.5 & 2.5 & 2.5 & 3.5 & 3.5 & 3.5 & 3.5 & 4.5 & 4.5 & 4.5 & 4.5 & 4.5 & 4.5 & 4.5 & 4.5 \end{pmatrix}^T \cdot mm$$

$$\Delta\theta_i := 90 \cdot deg \qquad \delta\theta_i := 90 \cdot deg$$

a_N, a_S, a_E, a_W ($a_E = a_W = b$) for each of the control volumes: Volumes for CVs

$$a_{n_i} := \frac{k_i \cdot \Delta\theta_i \cdot r_{n_i}}{\delta r_i} \qquad a_{s_i} := \frac{k_i \cdot \Delta\theta_i \cdot r_{s_i}}{\delta r_i} \qquad b_i := \frac{k_i \cdot \Delta r_i}{r_{b_i} \cdot \delta\theta_i} \qquad V_i := \int_{r_{n_i}}^{r_{s_i}} \int_0^{\Delta\theta_i} r \, d\theta \, dr$$

$$a_n = \begin{pmatrix} 0 \\ 0.074 \\ 0.074 \\ 0.074 \\ 0.074 \\ 114.982 \\ 114.982 \\ 114.982 \\ 114.982 \\ 191.637 \\ 191.637 \\ 191.637 \\ 191.637 \\ 191.637 \\ 268.292 \\ 268.292 \\ 268.292 \\ 268.292 \\ 689.894 \\ 689.894 \\ 689.894 \\ 689.894 \end{pmatrix} \frac{kg\,m}{s^3 K} \quad a_s = \begin{pmatrix} 0.037 \\ 0.221 \\ 0.221 \\ 0.221 \\ 0.221 \\ 191.637 \\ 191.637 \\ 191.637 \\ 191.637 \\ 268.292 \\ 268.292 \\ 268.292 \\ 268.292 \\ 268.292 \\ 344.947 \\ 344.947 \\ 344.947 \\ 344.947 \\ 689.894 \\ 689.894 \\ 689.894 \\ 689.894 \end{pmatrix} \frac{kg\,m}{s^3 K} \quad b = \begin{pmatrix} 0 \\ 0.06 \\ 0.06 \\ 0.06 \\ 0.06 \\ 15.534 \\ 15.534 \\ 15.534 \\ 15.534 \\ 10.356 \\ 10.356 \\ 10.356 \\ 10.356 \\ 10.356 \\ 7.767 \\ 7.767 \\ 7.767 \\ 7.767 \\ 0 \\ 0 \\ 0 \\ 0 \end{pmatrix} \frac{kg\,m}{s^3 K} \quad V = \begin{pmatrix} 0.196 \\ 1.571 \\ 1.571 \\ 1.571 \\ 1.571 \\ 3.142 \\ 3.142 \\ 3.142 \\ 3.142 \\ 4.712 \\ 4.712 \\ 4.712 \\ 4.712 \\ 4.712 \\ 6.283 \\ 6.283 \\ 6.283 \\ 6.283 \\ 0 \\ 0 \\ 0 \\ 0 \end{pmatrix} mm^2$$

$$V_0 := 4 \cdot V_0 \qquad \text{*4 for center c.v.}$$

-------------------- Other Material Properties ---

$$\rho_m := 7832 \frac{kg}{m^3} \qquad c_{pm} := 559 \frac{J}{kg \cdot K} \qquad \text{for parent material} \qquad \frac{k_5}{\rho_m \cdot c_{pm}} \cdot 10^6 = 11.146 \frac{m^2}{s}$$

$$\rho_t := 0.5804 \frac{kg}{m^3} \qquad c_{pt} := 1051 \frac{J}{kg \cdot K} \qquad \text{air in hole @ 600 K} \qquad \frac{k_0}{\rho_t \cdot c_{pt}} \cdot 10^6 = 76.885 \frac{m^2}{s}$$

Parent Material Everywhere	Resets Filler Material (center c.v.)	Resets center + makes 1st ring air too
$C_i := \rho_m \cdot c_{pm} \cdot V_i$	$C_0 = \rho_t \cdot c_{pt} \cdot V_0$	$h := 0, 1 .. 4 \qquad C_h := \rho_t \cdot c_{pt} \cdot V_h$

🔺 CV Term Generator

🔽 System Matrix Builder - Sensor

1st row -- put in e & w (2 & 4) as N and S "a's" rather than b's b/c all are "north" of center CV

$$D := \begin{pmatrix} a_{n_1} + a_{n_3} + a_{n_2} + a_{n_4} \\ a_{n_5} + a_{s_0} + b_4 + b_2 \\ a_{n_6} + a_{s_0} + b_1 + b_3 \\ a_{n_7} + a_{s_0} + b_2 + b_4 \\ a_{n_8} + a_{s_0} + b_3 + b_1 \\ a_{n_9} + a_{s_1} + b_8 + b_6 \\ a_{n_{10}} + a_{s_2} + b_5 + b_7 \\ a_{n_{11}} + a_{s_3} + b_6 + b_8 \\ a_{n_{12}} + a_{s_4} + b_7 + b_5 \end{pmatrix}$$

$$A := \begin{pmatrix} \frac{-D_0}{C_0} & \frac{a_{n_1}}{C_0} & \frac{a_{n_2}}{C_0} & \frac{a_{n_3}}{C_0} & \frac{a_{n_4}}{C_0} & 0 & 0 & 0 & 0 \\ \frac{a_{s_0}}{C_1} & \frac{-D_1}{C_1} & \frac{b_2}{C_1} & 0 & \frac{b_4}{C_1} & \frac{a_{n_5}}{C_1} & 0 & 0 & 0 \\ \frac{a_{s_0}}{C_2} & \frac{b_1}{C_2} & \frac{-D_2}{C_2} & \frac{b_3}{C_2} & 0 & 0 & \frac{a_{n_6}}{C_2} & 0 & 0 \\ \frac{a_{s_0}}{C_3} & 0 & \frac{b_2}{C_3} & \frac{-D_3}{C_3} & \frac{b_4}{C_3} & 0 & 0 & \frac{a_{n_7}}{C_3} & 0 \\ \frac{a_{s_0}}{C_4} & \frac{b_1}{C_4} & 0 & \frac{b_3}{C_4} & \frac{-D_4}{C_4} & 0 & 0 & 0 & \frac{a_{n_8}}{C_4} \\ 0 & \frac{a_{s_1}}{C_5} & 0 & 0 & 0 & \frac{-D_5}{C_5} & \frac{b_6}{C_5} & 0 & \frac{b_8}{C_5} \\ 0 & 0 & \frac{a_{s_2}}{C_6} & 0 & 0 & \frac{b_5}{C_6} & \frac{-D_6}{C_6} & \frac{b_7}{C_6} & 0 \\ 0 & 0 & 0 & \frac{a_{s_3}}{C_7} & 0 & 0 & \frac{b_6}{C_7} & \frac{-D_7}{C_7} & \frac{b_8}{C_7} \\ 0 & 0 & 0 & 0 & \frac{a_{s_4}}{C_8} & \frac{b_5}{C_8} & 0 & \frac{b_7}{C_8} & \frac{-D_8}{C_8} \end{pmatrix}$$

Pattern Realized......now to shorten the process.......

Zero Padders for zero portions of total system matrix:

$$ZR := (0 \ \ 0 \ \ 0 \ \ 0)Hz \qquad ZC := (0 \ \ 0 \ \ 0 \ \ 0)^T Hz \qquad Z := identity(4) \cdot 0Hz$$

Ring 2 (partially completed above in symbolic workthrough):

$$N2 := \frac{a_{n_9}}{C_5} identity(4)$$

Ring 3:

$$D3 := \frac{-\left(a_{n_{13}} + a_{s_5} + b_{10} + b_{12}\right)}{C_9} \qquad OD3 := \frac{b_{10}}{C_9} \qquad S3 := \frac{a_{s_5}}{C_9} \cdot identity(4) \qquad N3 := \frac{a_{n_{13}}}{C_9} \cdot identity(4)$$

$$R3D := identity(4) \cdot D3 + \begin{pmatrix} 0 & 1 & 0 & 1 \\ 1 & 0 & 1 & 0 \\ 0 & 1 & 0 & 1 \\ 1 & 0 & 1 & 0 \end{pmatrix} \cdot OD3$$

Pattern for 1 Ring (containing four control volumes):

$$(S3 \ \ R3D \ \ N3) = (\{4,4\} \ \ \{4,4\} \ \ \{4,4\}) Hz$$

Ring 4:

$$D4 := \frac{-\left(a_{n_{17}} + a_{s_9} + b_{14} + b_{15}\right)}{C_{13}} \qquad OD4 := \frac{b_{14}}{C_{13}} \qquad S4 := \frac{a_{s_9}}{C_{13}} \cdot identity(4)$$

$$R4D := identity(4) \cdot D4 + \begin{pmatrix} 0 & 1 & 0 & 1 \\ 1 & 0 & 1 & 0 \\ 0 & 1 & 0 & 1 \\ 1 & 0 & 1 & 0 \end{pmatrix} \cdot OD4$$

Combining all those pieces into a SYSTEM MATRIX

$$W1 := augment(A, augment(stack(ZR, Z, N2), stack(ZR, Z, Z)))$$

$$W2 := stack(augment(ZC, Z, S3, R3D, N3), augment(ZC, Z, Z, S4, R4D)) \qquad AA := stack(W1, W2)$$

B Matrix (boundary node temperature locator matrix)

$$BC := \frac{a_{n_{17}}}{C_{13}}$$

$ZbR := identity(3) \cdot 0$

$BB := stack(ZbR, ZbR, ZbR, ZbR, ZbR, ZbR)$ $BB_{13,1} := 1$ $BB_{14,0} := 1$

$BB := submatrix(BB, 0, 16, 0, 2)$

$BB_{15,1} := 1$ $BB_{16,2} := 1$

$BB := BB \cdot BC$

▲ System Matrix Builder - Sensor _____

$A_s := AA$ $B_s := BB$

Outputs of the A_S and B_S matrices required for the system sub-model portion of the MATLAB code. (section must be expanded to see A_S and B_S)

▶ OUTPUT- Cut and Paste in MATLAB _____

▶ Various Sub-system Matrices _____

Model Linking Visual Aid

$nodes := 51$

$p := 0, 1 .. nodes$

TC Region: $g := 0, 1 .. 3$

$dx := 0.75$ mm $len := nodes \cdot dx$ mm $CVstart := 1$ $OD := 9$ mm $Rd := .5 \cdot OD$

$xb_p := dx \cdot p$ $y1_p := 0$

$n1 := (CVstart - 0.5 \cdot dx)dx$

$t := (n1 \quad n1 + Rd \quad n1 + OD)^T$ $y2 := (0.1 \quad 0.1 \quad 0.1)^T$

$len = 38.25$
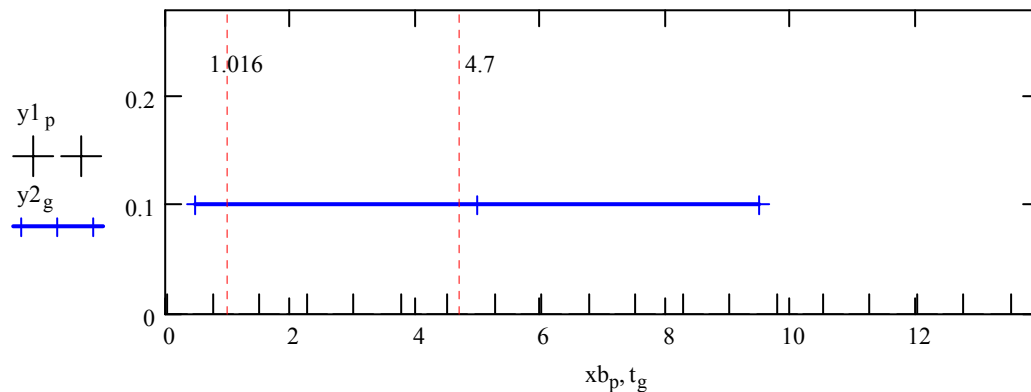
Model Notes (for determining linking, etc. for A356 casting experiment model setup)

$1.5in = 38.1mm$ Mold Half Thickness?

$0.04in = 1.016mm$ Close hole

$0.185in = 4.699mm$ Less Close hole

Linking Nodes
1, 7, 13

$.125in = 3.175mm$ Hole diameter

B.2   ETC.M MATLAB FILE

```matlab
% ------[ Created by August Johnson   4/1/2004  ]
%etc.m             *****     MODEL CONSTRUCTION FILE     *****
%
%%%%%%%%%%%%%%%%%%%%%%%%%%%%%%   UNDISTURBED MODEL CONSTRUCTION
%%%%%%%%%
%%%%% (The current properties and geometries simulate
%%%%% the heat transfer through a permanent steel mold
%%%%% half after molten A356 has been poured in it) %%%
clear;
clc;
% Quick Input of material properties & geometry for model
k=48.8;
rho=7832;
cp=559;
n=51;
Dx=0.00075;
dx=0.00075;
node=7;
nu=1;
nd=13;
a1 = k/dx;
C = rho*cp*Dx;
C1 = zeros(1,n);
C2 = zeros(1,n);
C3 = zeros(1,n);
C1(1,node) = 1;  % Observer row vector for node of interest
C2(1,nu) = 1;    % Observer row vector for upstream node
C3(1,nd) = 1;    % Observer row vector for downstream node
% Construct the A-matrix from material properties and geometry
AA=0;
for i=1:n-1;
    AA(i,i)=-2;
    AA(i+1,i)=1;
    AA(i,i+1)=1;
end;
AA(1,1)=-1;
AA(n,n)=-1;
E=(a1/C);
A=AA*(E);
% Construct B-matrix, Heat Flux Input Location Matrix
% Qin(t) and Qout(t)=0 (insulated back boundary)
B=zeros(n,1);
B(1,1)=(1/C);
%B(n,2)=(1/C1)
D = 0;
```

123

```matlab
sys1 = ss(A,B,C1,D);  % Q --> Tu
sys2 = ss(A,B,C2,D);  % Q --> Tup
sys3 = ss(A,B,C3,D);  % Q --> Tdwn
% Obtaining Transfer function data for the three systems above
[num,den] = tfdata(sys1,'v');
G1=tf(num,den);     % Gu - undisturbed temperature TF
[num2,den2] = tfdata(sys2,'v');
G2=tf(num2,den2);  % Gup
[num3,den3] = tfdata(sys3,'v');
G3=tf(num3,den3);  % Gdwn
%%%%%%%%%%%%%%%%%%%%%%%%%%   SENSOR SUB-MODEL CONSTRUCTION
%%%%%%%%%%%%%
%%%%% Thermocouple is assumed to measure center node
%%%%% of the sensor sub-model%%%%%
ntc=17;     %Number of Control Volumes for TC Model%%
% Import the System Matrix, A,
% for sensor sub-model from MathCAD Matrix Builder
% (the A2 below has adjusted thermal conductivities at the dissimalar
mat.
% interface --- see patankar pg. 46)

A2=[-614.491       153.623      153.623      153.623      153.623      0
      0      0     0     0     0     0     0     0     0     0     0
38.443      -120162.886 62.261     0      62.261      119999.921  0
      0     0     0     0     0     0     0     0     0
38.443      62.261      -120162.886 62.261      0      0      119999.921
      0     0     0     0     0     0     0     0     0
38.443      0      62.261      -120162.886 62.261      0      0
      119999.921 0     0     0     0     0     0     0     0     0
38.443      62.261      0      62.261      -120162.886 0      0      0
      119999.921 0     0     0     0     0     0     0     0     0
0      0.016 0      0      0      -16.208      1.129 0      1.129 13.933
      0      0      0      0      0      0      0
0      0      0.016 0      0      1.129 -16.208      1.129 0      0
      13.933      0      0      0      0      0      0
0      0      0      0.016 0      0      1.129 -16.208      1.129 0      0
      13.933      0      0      0      0      0
0      0      0      0      0.016 1.129 0      1.129 -16.208      0      0
      0      13.933      0      0      0      0
0      0      0      0      0      9.289 0      0      0      -23.297      0.502
      0      0.502 13.004      0      0      0
0      0      0      0      0      0      9.289 0      0      0.502 -23.297
      0.502 0      0      13.004      0      0
0      0      0      0      0      0      0      9.289 0      0      0.502 -
23.297      0.502 0      0      13.004      0
0      0      0      0      0      0      0      0      9.289 0.502 0      0.502
      -23.297      0      0      0      13.004
0      0      0      0      0      0      0      0      0      9.753 0      0
      0      -35.397      0.282 0      0.282
0      0      0      0      0      0      0      0      0      0      9.753 0
      0      0.282 -35.397      0.282 0
0      0      0      0      0      0      0      0      0      0      0      9.753
      0      0      0.282 -35.397      0.282
```

```
0       0     0      0       0       0     0      0       0       0     0      0
      9.753 0.282 0     0.282 -35.397];

% Import the Temperature Input Location Matrix, B,
% for sensor sub-model from MathCAD Matrix Builder
B2 = [0      0     0
0       0     0
0       0     0
0       0     0
0       0     0
0       0     0
0       0     0
0       0     0
0       0     0
0       0     0
0       0     0
0       0     0
0       0     0
0       25.079     0
25.079      0      0
0       25.079     0
0       0      25.079];

C4 = zeros(1,ntc);    % Observer row vector for thermacouple node, Node
1 (Gup = Gdwn)
C4(1,1) = 1;
C5 = zeros(1,ntc);    % Observer row vector for thermacouple node, Node
1 (Gm)
C5(1,1) = 1;
sys4 = ss(A2,B2(:,1),C4,D);       % Sys4 --> Gup = Gdwn
sys5 = ss(A2,B2(:,2),C5,D);       % Sys5 --> Gm
[num4,den4] = tfdata(sys4,'v');  % Obtaining TF data from SS
G4=tf(num4,den4);                 % Gup & Gdwn (Gup = Gdwn)
[num5,den5] = tfdata(sys5,'v');  % Obtaining TF data from SS
G5=tf(num5,den5);                 % Gm
%
%%%%%%%%%%%%%%   Determination of TOTAL TRANSFER FUNCTION for Tu/Td
%%%%%%
%
Gund=G1; %vThe UNDISTURBED system TF ---> Gu
%
%%%%%%%%   Intermediate TFs to develop the DISTURBED TF
GG1=G2*G4;
[nnum1,dden1] = tfdata(GG1,'v');
GG2=G1*G5;
[nnum2,dden2] = tfdata(GG2,'v');
GG3=G3*G4;
[nnum3,dden3] = tfdata(GG3,'v');
a=nnum1;
b=nnum2;
c=nnum3;
% Statement written to padd numerators of TFs with zeros so they can be
added
if length(b)>=length(a) & length(b)>=length(c)
```

```matlab
    N=length(b);
    a=[zeros(1,N-length(a)),a];
    c=[zeros(1,N-length(c)),c];
elseif (length(c)>=length(a) & length(c)>=length(b))
    N=length(c);
    a=[zeros(1,N-length(a)),a];
    b=[zeros(1,N-length(b)),b];
else
    N=length(a);
    b=[zeros(1,N-length(b)),b];
    c=[zeros(1,N-length(c)),c];
end
nnumT=a+b+c;  % addition of the coeffiecients of the numerator
polynomials
ddenT=dden1;  % Obtaining denominator -- ddenT = dden1 = dden2 = dden3
Gdis=tf(nnumT,ddenT); % Assembling the TF represntation of the
DISTURBED TF, Gd
GT=(Gund/Gdis);        % Creating the Embedded TC Correction TF, GT

%% Adjusting smallest zero and pole values that were
%% causing numerical problems --->  new discrete GT
[z,p,kk] = zpkdata(GT,'v');
[rz,cz]=size(z);
[rp,cp]=size(p);
kk=kk*z(rz)/p(rp);
z=z(1:rz-1,1);
p=p(1:rp-1,1);
GT = zpk(z,p,kk);
```

B.3   SEMI.M MATLAB FILE

```matlab
% ------[ Created by August Johnson    4/1/2004   ]
%semi.m     Semi-infinite Analytical Solution Maker
alpha = k/(rho*cp);  % Material properties
xx=0.005;   % point of interest
Qi=30000;   % heat flux
Tend=30;
delt=0.01;
Ti=0;
%xx = input('X location: (m)  ');
%Qi = input('Input Constant Heat Flux: (W/m^2-K)  ');
%Tend = input('End Time: (s)  ');
%delt = input('Delta Time: (s)  ');
%Ti = input('Initial Cond: (K)  ');
tt=0:delt:Tend;
tt=tt';
warning off MATLAB:divideByZero;
for i=1:length(tt);
T1(i) = 2*(Qi/k)*(alpha*tt(i)/pi)^(1/2)*exp(-xx^2/(4*alpha*tt(i)));
T2(i) = (-Qi*xx/k)*erfc(xx/(2*(alpha*tt(i))^(1/2)));
Tsi(i)= Ti + T1(i) + T2(i);
end
plot(tt,Tsi)
clear alpha xx Tend Ti Qi delt T1 T2;
warning on MATLAB:divideByZero;
```

127

B.4   HEAT FLUX GENERATOR MATLAB FILE

```matlab
% ------[ Created by August Johnson   4/1/2004  ]
%Heat Flux Input Maker
%t's are time, y's are heat flux profiles
ti=0:.01:20;
t=[0 0.0999 0.1 0.2 0.201 20];
Y=[0 0 300000 300000 0 0];
yi = interp1(t,Y,ti);
ti2=0:.01:30;
t2=[0 1 3 5 30];
Y2=[0 0 300000 0 0];
yi2 = interp1(t2,Y2,ti2);
ti3=0:.1:10;
t3=[0 0.5 2.5 4.5 10];
Y3=[0 0 5000 0 0];
yi3 = interp1(t3,Y3,ti3);
ti4=0:.01:30;
t4=[0 30];
Y4=[30000 30000];
yi4 = interp1(t4,Y4,ti4);
ti5=0:0.05:30;
t5=[0 0.5 0.1 0.15 0.2 30];
Y5=[0 0 1 1 0 0];
yi5 = interp1(t5,Y5,ti5);
```

B.5 EXAMPLE.M MATLAB FILE

```matlab
% ------[ Created by August Johnson   4/1/2004  ]
%% example.m %%
etc; %<------------Insert Model Construction Program  Here   %%%%
%  Heat Flux Input (yi2)  %
Tf=30;
deltati2=0.01;
ti2=0:deltati2:Tf;
t2=[0 1 3 5 Tf];
Y2=[0 0 300000 0 0];
yi2 = interp1(t2,Y2,ti2);  %%%%  Heat Flux Input Created  %%%%
% Obtaining Various Temperature Responses from Models  %
[yu tt]=lsim(Gund,yi2,ti2);   % Undisturbed ("True") Response
[yd tt]=lsim(Gdis,yi2,ti2);   % Disturbed Response (no noise)
[yr tt]=lsim(GT,yd,tt);        % Recovered Response (no noise in
Disturbed)
% Creation of Random Noise to inject into Disturbed Response  %
stdev=0.1;   % Standard Deviation of Noise (degree Kelvin)
randn('state',21);   % Set "seed" as 21 for randn for reproducible
noise
noise = stdev*randn(size(tt));  %Creation of zero mean noise
ydn = yd + noise;    % Addition of noise to Disturbed Response
[yrn tt]=lsim(GT,ydn,tt);  % Recovered Temperature (from noisy
Disturbed)
% Creating a Lowpass Butterworth filter
Ny=(1/deltati2)/2;  % Half the sampling frequency
Cf=0.5;             % Cut-off frequency desired
Ord=3;              % Filter Order
[b,a]=butter(Ord,Cf/Ny);  % Butterworth filter construction
yrf = filtfilt(b,a,yrn);  % Filter noisy data




%%%%%%%%%%%%%% FIGURES    %%%%%%%%%%%%%%%
figure(1),
plot(tt,yu - yrf),xlabel('Time (sec)'),ylabel('Temperature (delta
K)')...
    ,title('Difference of Filtered Recovered Temperature & Undisturbed
Temperature')
```

129

```
figure(2),
plot(tt,yrn,'b',tt,ydn,'g',tt,yu,'r')...
    ,xlabel('Time (sec)'),ylabel('Temperature (K)')...
    ,title('Recovered Temperature from Generated Noisy Data')...
    ,legend('Non-Filtered Recovered Data','Noisy* Disturbed Temperature
Data',...
    'Undisturbed Temperature')
figure(3),
plot(tt,ydn,'g',tt(1:10:end),yrf(1:10:end),'*',tt,yu,'r')...
    ,xlabel('Time (sec)'),ylabel('Temperature (K)')...
    ,title('Recovered Temperature from Generated Noisy Data')...
    ,legend('Noisy* Disturbed Temperature Data','Filtered Recovered
Data',...
    'Undisturbed Temperature')
```

B.6 ICEXAMPLE.M MATLAB FILE

```matlab
% ------[ Created by August Johnson   4/1/2004  ]
%icexample.m     Inverse Conduction Example w/ Generated Data
etc; %<-------------Insert Model Construction Program  Here   %%%%
%  Heat Flux Input (yi2)  %
Tf=30;
deltati2=0.04;
ti2=0:deltati2:Tf;
t2=[0 1 3 5 Tf];
Y2=[0 0 300000 0 0];
yi2 = interp1(t2,Y2,ti2);  %%%%  Heat Flux Input Created  %%%%
% Obtaining Various Temperature Responses from Models  %
[yu tt]=lsim(Gund,yi2,ti2);   % Undisturbed ("True") Response
[yd tt]=lsim(Gdis,yi2,ti2);   % Disturbed Response (no noise)
[yr tt]=lsim(GT,yd,tt);       % Recovered Response (no noise in
Disturbed)
% Creation of Random Noise to inject into Disturbed Response  %
stdev=0.1;   % Standard Deviation of Noise (degree Kelvin)
randn('state',21);   % Set "seed" as 21 for randn for reproducible
noise
noise = stdev*randn(size(tt));  %Creation of zero mean noise
ydn = yd + noise;    % Addition of noise to Disturbed Response
[yrn tt]=lsim(GT,ydn,tt);  % Recovered Temperature (from noisy
Disturbed)
% Creating a Lowpass Butterworth filter
Ny=(1/deltati2)/2;  % Half the sampling frequency
Cf=0.5;             % Cut-off frequency desired
Ord=3;              % Filter Order
[b,a]=butter(Ord,Cf/Ny);  % Butterworth filter construction
yrf = filtfilt(b,a,yrn);  % Filter noisy data

sys1d = c2d(sys1,deltati2);
%[ad,bd,cd,dd,Ts] = ssdata(sys1d);
[I tt]=impulse(sys1d,ti2);  %discrete impulse response for Undisturbed
Model

NN=length(I);
phi=zeros(NN,NN);
for i=1:NN;
    phi(i:NN,i)=I(1:NN-i+1);
end;
newphi=phi(1:NN,1:NN);
[U,S,V]=svd(newphi);
['There are ',num2str(NN),' singular values.']
svdselect;
```

131

B.7   SVDSELECT.M MATLAB FILE

```matlab
% ------[ Created by August Johnson   4/1/2004  ]
%svdselect.m     Inverse Conduction Example w/ Generated Data
%%  USED TO RE-SELECT NUMBER OF SINGULAR VALUES
%%  IN icexample.m and RE-GENERATE PLOTS
nsv = input('Select the number of singular values to retain (integer)
');
Vr=V(:,1:nsv);
Sr=S(1:nsv,1:nsv);
Ur=U(:,1:nsv);

estTu=inv(Sr)*Ur'*yu(1:NN);
estQu=Vr*estTu;

estTd=inv(Sr)*Ur'*yd(1:NN);
estQd=Vr*estTd;

estTrf=inv(Sr)*Ur'*yrf(1:NN);
estQrf=Vr*estTrf;

estTr=inv(Sr)*Ur'*yr(1:NN);
estQr=Vr*estTr;

figure(1),
plot(tt(1:10:end),yrf(1:10:end),'*',tt,yu,'r',tt,ydn,'g')...
    ,xlabel('Time (sec)'),ylabel('Temperature (K)')...
    ,title('Comparison of Recovered Temperature from Disturbed w/
Noise')
figure(2),
plot(ti2,yi2,ti2,estQr,ti2,estQd);
,xlabel('Time (sec)'),ylabel('Heat Flux (W/m^2)')...
,title([' Recovered Heat Flux vs. Undisturbed Heat Flux:
(',int2str(nsv),'/',int2str(NN),' singular values used)'])
figure(3),
plot(ti2,yi2'-estQr,'b');
,xlabel('Time (sec)'),ylabel('Heat Flux Difference (delta W/m^2)')...
,title([' Error of Recovered Heat Flux from Undisturbed Heat Flux:
(',int2str(nsv),'/',int2str(NN),' singular values used)'])
```

132

B.8 EXAMPLE2.M MATLAB FILE

```matlab
% ------[ Created by August Johnson   4/1/2004  ]
%% example2.m %% FOR USE WITH EXPERIMENTALLY OBTAINED EMBEDDED  %%%
           %% THERMOCOUPLE DATA                          %%%


etc;  %<-------------Insert Model Construction Program  Here   %%%%

datafile;    %<-------put time and temperature data in this file
ti2=DTA(:,1);     %<------time first column
data=DTA(:,2);    %<------temperature second column
sr=25;            %<---  Sampling Rate (Hz)

[yrn tt]=lsim(GT,data,ti2);  % Recovered Temperature (from experimental
data)

% Creating a Lowpass Butterworth filter
Ny=sr/2;  % Half the sampling frequency
Cf=0.5;              % Cut-off frequency desired
Ord=3;               % Filter Order
[b,a]=butter(Ord,Cf/Ny);  % Butterworth filter construction
yrf = filtfilt(b,a,yrn);  % Filter noisy data, Filtered Recovered Data

%%%%%%%%%%%%%%%%  FIGURES    %%%%%%%%%%%%%%%%%
figure(1),
plot(tt,yrn,'b',tt,data,'g',tt,yrf,'r')...
    ,xlabel('Time (sec)'),ylabel('Temperature (K)')...
    ,title('Recovered Temperature from Experimental Data')...
    ,legend('Non-Filtered Recovered Data','Experimental Temperature
Data',...
    'Filtered Recovered Temperature Data')
figure(2),
plot(tt,data-yrf,'b')...
    ,xlabel('Time (sec)'),ylabel('Temperature (delta K)')...
    ,title('Difference of Filtered Recovered Temperature & Experimental
Temperature')
figure(3),
plot(tt,data,'g',tt,yrf,'r')...
    ,xlabel('Time (sec)'),ylabel('Temperature (K)')...
    ,title('Recovered Temperature from Experimental Data')...
    ,legend('Experimental Temperature Data','Filtered Recovered
Temperature Data')
```

133

B.9   ICEXAMPLE2.M MATLAB FILE

```matlab
% ------[ Created by August Johnson   4/1/2004  ]
%icexample2.m     Inverse Conduction Example w/ Real Data
etc; %<------------Insert Model Construction Program  Here   %%%%

datafile;    %<-------put time and temperature data in this file
ti2=DTA(:,1);      %<------time first column
data=DTA(:,2);     %<------temperature second column
sr=25;             %<---  Sampling Rate (Hz)

[yr tt]=lsim(GT,data,ti2);  % Recovered Temperature (from experimental
data)

% Creating a Lowpass Butterworth filter
Ny=sr/2;  % Half the sampling frequency
Cf=0.5;               % Cut-off frequency desired
Ord=3;               % Filter Order
[b,a]=butter(Ord,Cf/Ny);  % Butterworth filter construction
yrf = filtfilt(b,a,yr);  % Filter noisy data, Filtered Recovered Data

sys1d = c2d(sys1,1/sr);
%[ad,bd,cd,dd,Ts] = ssdata(sys1d);
[I tt]=impulse(sys1d,ti2);  %discrete impulse response for Undisturbed
Model
NN=length(I);
phi=zeros(NN,NN);
for i=1:NN;
    phi(i:NN,i)=I(1:NN-i+1);
end;
newphi=phi(1:NN,1:NN);
[U,S,V]=svd(newphi);
['There are ',num2str(NN),' singular values.']
svdselect2;
```

134

B.10   SVDSELECT2.M MATLAB FILE

```matlab
% ------[ Created by August Johnson   4/1/2004  ]
%svdselect2.m     Inverse Conduction Example w/ Real Data
%%  USED TO RE-SELECT NUMBER OF SINGULAR VALUES
%%  IN icexample2.m and RE-GENERATE PLOTS
nsv = input('Select the number of singular values to retain (integer)
');
Vr=V(:,1:nsv);
Sr=S(1:nsv,1:nsv);
Ur=U(:,1:nsv);

estTd=inv(Sr)*Ur'*data(1:NN);
estQd=Vr*estTd;

estTrf=inv(Sr)*Ur'*yrf(1:NN);
estQrf=Vr*estTrf;

estTr=inv(Sr)*Ur'*yr(1:NN);
estQr=Vr*estTr;

estyr=newphi*estQr;

figure(1),
plot(tt,data,'g',tt,yr,'r',tt,yrf,'b')...
    ,xlabel('Time (sec)'),ylabel('Temperature (K)')...
    ,title('Comparison of Recovered Temperature to Experimental Data')
figure(2),
plot(tt,data,'g',tt,estyr,'r')...
    ,xlabel('Time (sec)'),ylabel('Temperature (K)')...
    ,title('Comparison of Matrix Transform Filtered Recovered
Temperature to Experimental Data')
figure(3),
plot(ti2,estQd,ti2,estQr)...
,xlabel('Time (sec)'),ylabel('Heat Flux (W/m^2)')...
,title(['Recovered Heat Fluxes: (',int2str(nsv),'/',int2str(NN),'
singular values used)'])
figure(4),
plot(ti2,estQr-estQd,'b')...
,xlabel('Time (sec)'),ylabel('Heat Flux Difference (delta W/m^2)')...
,title(['Difference in Recovered Heat Fluxes:
(',int2str(nsv),'/',int2str(NN),' singular values used)'])
figure(5),
plot(tt,yrf-data)...
    ,xlabel('Time (sec)'),ylabel('Temperature (K)')...
    ,title('Comparison of Recovered Temperature to Experimental Data')
```

135